

Volume 29 Number 1 June 1998

ISSN 0046-5828

GEOTECHNICAL

ENGINEERING

Journal of
SOUTHEAST ASIAN GEOTECHNICAL SOCIETY

Sponsored by
ASIAN INSTITUTE OF TECHNOLOGY



GEOTECHNICAL ENGINEERING

CONTENTS

Photographic Feature:

Geological Features Influencing Slope Stability of Volcanic Rock in Hong Kong Island <i>by C.A.M. Franks, S.D.G. Campbell and N.P. Koor</i>	i
---	---

Main Papers:

X-Ray Diffraction and Microstructural Studies of Lime-Marine Clay Reaction Products <i>by G. Rajasekaran and S.N. Rao</i>	1
Strength and Stiffness of Hong Kong Marine Deposits Mixed with Cement <i>by J.H. Yin and C.K. Lai</i>	29
Hyperbolic Model Parameters for Mechanical Behavior of Reclamation Soils <i>by L.K. Chien and Y.N. Oh</i>	45
A Simple Analysis of Piles in Raft Foundations <i>by C. Anagnostopoulos and M. Georgiadis</i>	71
Rock Slope Stabilization Along Railroad at Fushun Mine <i>by M.S. Wang, X.L. Wu and M.C. Wang</i>	85
PVD Improvement of Soft Bangkok Clay with Combined Vacuum and Reduced Sand Embankment Preloading <i>by D.T. Bergado, J.C. Chai, N. Miura and A.S. Balasubramaniam</i>	95

PHOTOGRAPHIC FEATURE

Geological Features that Influence Slope Stability in Fine-Ash Eutaxitic Volcanic Rocks in Hong Kong Island

by C.A.M. Franks, S.D.G. Campbell, and N.P. Koor¹

A major landslide causing one death and one injury occurred in a cut slope at Fei Tsui Road, Chai Wan, Hong Kong Island on the 13 August 1995 (Fig. 1) following a period of intense rainfall associated with Typhoon Helen. The landslide was an unusual cut slope failure in terms of its large size (about 14,000 m³) and large travel distance (70 m) of the debris (Fig. 2). The subsequent forensic investigation (GEO, 1996) highlighted various geological features that influenced the stability of the slope. At the landslide site, the rock type was a eutaxitic, fine-ash crystal tuff, and the features included :

1. moderately wide to wide (> 60 mm) laterally persistent (> 4 m) concentrations of white to buff-colored kaolin in impermeable and weak layers within the rock mass (Fig. 3),
2. completely and highly decomposed and variably kaolinized tuff (Grades V and IV) forming rough planar seams that sit on slightly and moderately decomposed tuff (Grades II and III) which dip directly, or obliquely outward from the rock slope face (Fig. 4), and,
3. persistent (> 4 m), closely to medium-spaced, tight and rough, planar, steep (dip > 60°) joint sets that could form release surfaces.

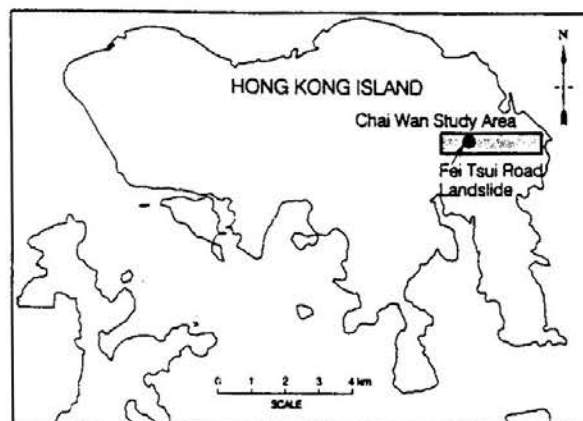


Fig. 1 Location Map of the Fei Tsui Road Landslide Site and the Chai Wan Study Area

¹ Geotechnical Engineering Office, 101 Princess Margaret Road, Homantin, Kowloon, Hong Kong.

Note: Discussion is open until 1 September 1998. This feature is part of the *Geotechnical Engineering Journal*, Vol. 29, No. 1, June 1998. Published by the Southeast Asian Geotechnical Society, ISSN 0046-5828.

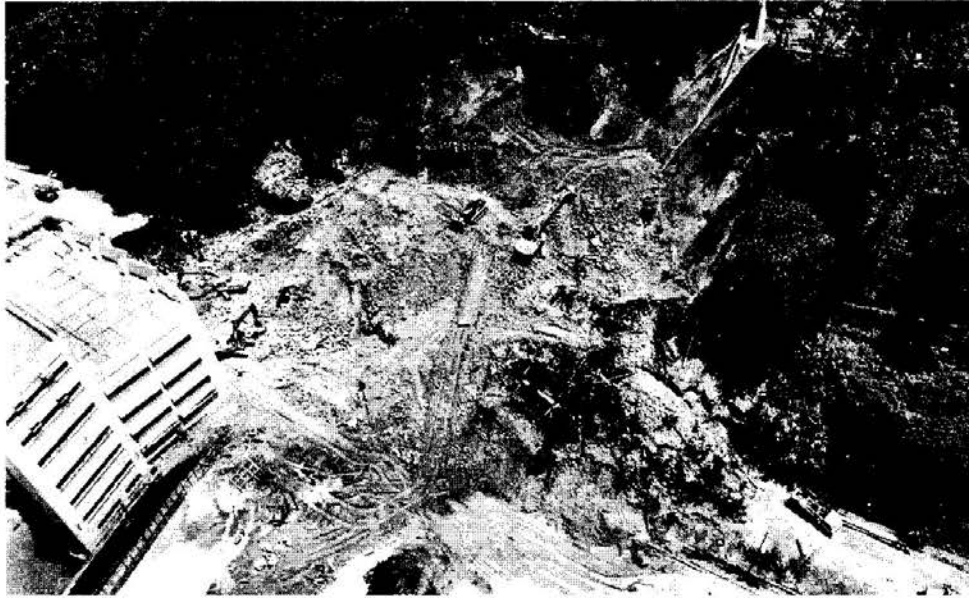


Fig. 2 Large Debris Run Out Distance at the Fei Tsui Road Landslide Site



Fig. 3 Development of White and Buff Colored Kaolin Veins Within Completely and Highly Decomposed Tuff

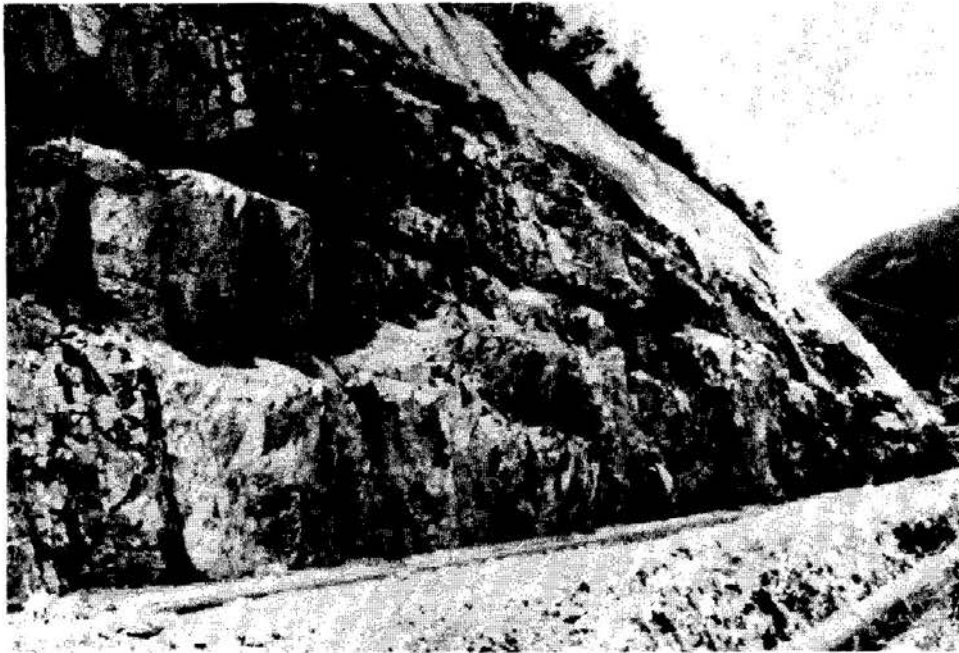


Fig. 4 Cut Slope at Fei Tsui Road after Site Formation in 1977

In addition, prior to failure and in association with these features, the slope was notable for the following conditions :

4. adverse orientation of stratification (as indicated by eutaxitic foliation) which is sub-parallel to the main kaolinized layer,
5. zones of continuous seepage, and
6. clusters of previous small-scale slope failures (Knill, 1996).

These conditions if found elsewhere may indicate the presence of such features in similar rocks. The detection of such conditions and appropriate preventive actions will lead to significant improvements in slope safety.

Follow-up investigations in the Chai Wan area (Campbell, et al., 1997) identified only a very few slopes containing similar geological conditions to those in the Fei Tsui Road slope. More commonly, slopes in the area contain abrupt, planar, shallowly-inclined (5° - 20°) discontinuities at the weathering front. Such slopes are typically sites for kaolin concentration (up to tens of millimeters thick) that can be laterally continuous and associated with localized seepage, and hence could be similar to the main geological conditions at the Fei Tsui Road landslide site.

Integrated studies are ongoing to identify existing or proposed slopes that may contain the above features. Such studies involve aerial photograph interpretation (API),

a desk study of all available records and geological survey of the slope, and subsequent ground investigation to confirm suspect conditions. The API and desk study is focused on establishing histories of past failures (including the mechanism and type of failure) and persistent seepage, and where site formation photographs are available, of significant planar discontinuities. The geological survey is concentrated on establishing whether the orientation of bedding, bedding-parallel structures (e.g., eutaxitic foliation) or laterally continuous discontinuities is adverse, and identifying any kaolin accumulations, especially where infilling adversely-orientated discontinuities or accumulated along the weathering front. Subsequent ground investigations are focused on examining and logging the saprolite profile in detail, with emphasis placed on identifying the fabric, relict features and presence of adversely-oriented low strength clay seams in the vicinity of, and up to 5 metres below, the weathering front.

Further studies of the type outlined above are currently in progress in a wider range of rock types to determine the recognition criteria and nature of similar geological conditions that may influence slope stability.

ACKNOWLEDGEMENT

The permission of the Director of Civil Engineering, Hong Kong Special Administrative Region Government to publish this feature is acknowledged. The authors also acknowledge the earlier contribution to this study by P.A. Kirk and W.L. Shum.

REFERENCES

- CAMPBELL, S.D.G.; KOOR, N.P.; FRANKS, C.A.M. and SHUM, W.L. (1997). Geological Assessment of Slopes in Areas Close to Major Landslides in Hong Kong Island. *Proceedings of the HKIE Geotechnical Division Annual Seminar 1996-97, Slope Engineering in Hong Kong*, (in press).
- GEOTECHNICAL CONTROL OFFICE (1988). *Guide to Rock and Soil Descriptions, Geoguide 3*. Hong Kong: Geotechnical Control Office, Civil Engineering Services Department, Hong Kong Government, 189p.
- GEOTECHNICAL ENGINEERING OFFICE (1996). *Report on the Fei Tsui Road Landslide of 13 August 1995, Volume 2, Findings of the Landslide Investigation*. Hong Kong: Geotechnical Engineering Office, Civil Engineering Department, Hong Kong Government, 68p.
- KNILL, J. (1996). *Report on the Fei Tsui Road Landslide of 13 August 1995, Volume 1, Independent Review of the Investigation by the Geotechnical Engineering Office*. Hong Kong: Geotechnical Engineering Office, Civil Engineering Department, Hong Kong Government, 13p.

X-RAY DIFFRACTION AND MICROSTRUCTURAL STUDIES OF LIME-MARINE CLAY REACTION PRODUCTS

G. Rajasekaran¹ and S. Narasimha Rao²

ABSTRACT

Soft clays of low strength and high compressibility are located in many coastal and offshore areas, and they cause several foundation problems for the structures resting on these marine deposits. The necessity to construct engineering structures on these deposits is a challenging task for the civil engineers and there is a need to improve the engineering behavior of these clays. The present investigation deals with an experimental work carried out in the laboratory using lime column and lime injection techniques to stabilize a marine clay. The formation of new reaction products due to soil-lime reactions was studied using XRD and SEM techniques. The results indicated the formation of cementitious compounds such as calcium silicate hydrate (CSH) and calcium aluminate hydrate (CAH) in different lime treated soil systems and it has been observed that their formation was not affected by the presence of sea water. There is a considerable improvement in the physical properties of the lime treated soil systems, and the test results have established that both the lime column and lime injection techniques can be successfully used to improve the behavior of soft marine clayey deposits.

INTRODUCTION

Weak clay deposits are encountered along the coastal regions of the world and they are imposing severe foundation problems to the structures resting on them due to their high compressibility and low shear strength behavior (Bjerrum, 1973). It is widely in practice that lime can be used to improve the engineering properties of fine grained deposits and it is now being extended at deep in-situ level either in the form of lime column or lime injection techniques (Broms and Boman, 1975 and Okumara and Terashi, 1975). The changes occurred in the lime treated soils are attributed to the cementation of the soil particles due to soil-lime reactions, and attempts were made to identify the new reaction products formed (Kawamura and Diamond, 1975; Lee, et al., 1983; and Transportation Research Board, 1987).

1 Professional Officer, Department of Civil Engineering, National University of Singapore, Singapore 119260. Former Research Scholar, Ocean Engineering Center, Indian Institute of Technology, Madras 600 036, India.

2 Professor, Ocean Engineering Center and Department of Civil Engineering, Indian Institute of Technology, Madras 600 036, India.

Note: Discussion is open until 1 September 1998. This paper is part of the *Geotechnical Engineering Journal*, Vol. 29, No. 1, June 1998. Published by the Southeast Asian Geotechnical Society, ISSN 0046-5828.

It is helpful to identify the constituent minerals present in the soil before any chemical method of stabilization is taken up (Ingles and Metcalf, 1994 and Rajasekaran, 1994). From the earlier investigations it was clear that the reaction products like calcium silicate hydrate (CSH) and calcium aluminate hydrate (CAH) were formed in lime treated soils (Eades, et al., 1962; Wang, et al., 1963; and Joshi, et al., 1981). Even though several investigators brought out the beneficial effects of lime stabilization on land based clays, only a limited literature is available on the studies of reaction products formed in marine clays. Hence there is a need to study the formation of various reaction products due to soil-lime reactions, and their stability in the marine environment. In the present investigation an attempt has been made to study the nature of reaction products formed in an Indian marine clay using lime in the form of lime column or lime slurry injection techniques. A testing program has been carried out to investigate the mineralogical and microstructural changes occurring in the lime treated soil systems using x-ray diffraction (XRD) and scanning electron micrograph (SEM) techniques.

TEST PROGRAM

Soil and Chemicals Used

The soil used was a marine clay procured from the coast of Madras, India (Lat. 13.04°N and Long. 80.17°E). The clay was formed under shallow coastal sea water conditions and the soil samples were taken at a depth of 1 m to 2 m below the seabed. The excavation was carried out using an open trench excavation during low tide period and the properties of the untreated soil are given in Table 1. In first set of experiments quicklime with additives such as calcium chloride, calcium sulphate and sodium sulphate were used as column filling materials along with quicklime in 1:1 ratio. These above compounds are usually present in the marine environment. To bring out the differences in the hydration characteristics of lime, calcium hydroxide was tried as a column filling material and in another case a mixture of quicklime and sand was used. The penetration of lime and their consequent changes on the mineralogical and microfabric features in the surrounding soil were observed. In the second set-up hydrated lime slurry of 40% concentration (by dry weight) was injected at a few locations in the clay bed.

Experimental Methodology

Basically there were two experimental setups used in the present investigation. The details of the experimental setups used are shown in Figs. 1 and 2.

X-RAY DIFFRACTION AND MICROSTRUCTURAL STUDIES

Table 1 Untreated Soil Properties

S.No	Physical and chemical properties	Test results	
		Fresh water system	Sea water system
1.	Liquid limit (%)	88	85
2.	Plastic limit (%)	33	32
3.	Plasticity Index	55	53
4.	pH	7.06	7.3
5.	Organic content (%)	1.36	1.41
6.	Sulphates (%)	0.02	0.20
7.	Chlorides (%)	0.05	1.8
8.	Cation exchange capacity (m.eq/100 g of the soil)	38	42
9.	Lime content (%)	0.19	0.21
10.	Shear strength of the soil (kN/m ²)	16	18
11.	Compression Index (C _c)	0.87	0.85

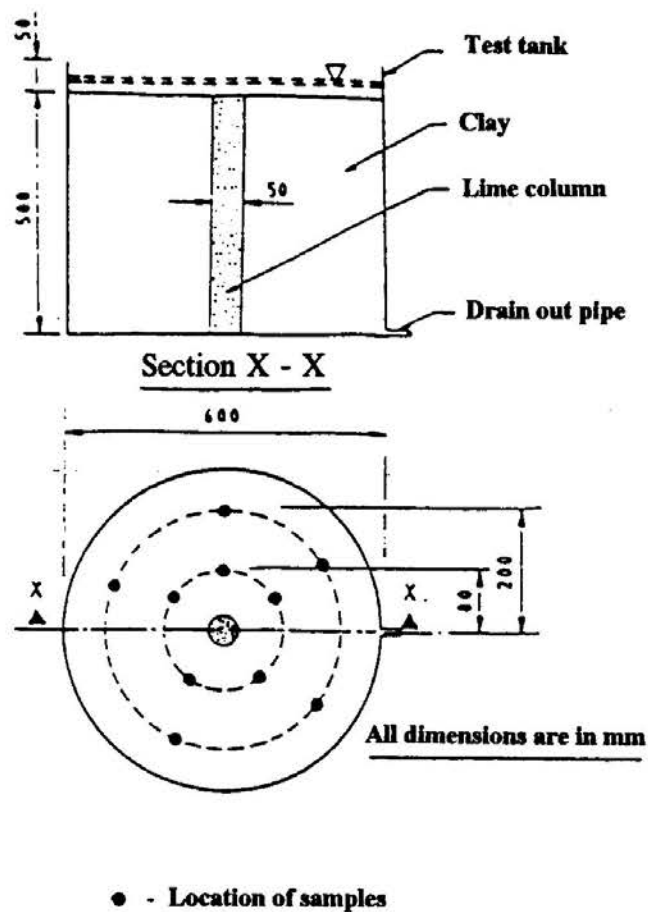


Fig. 1 Details of Experimental Setups Used for Lime Column Work

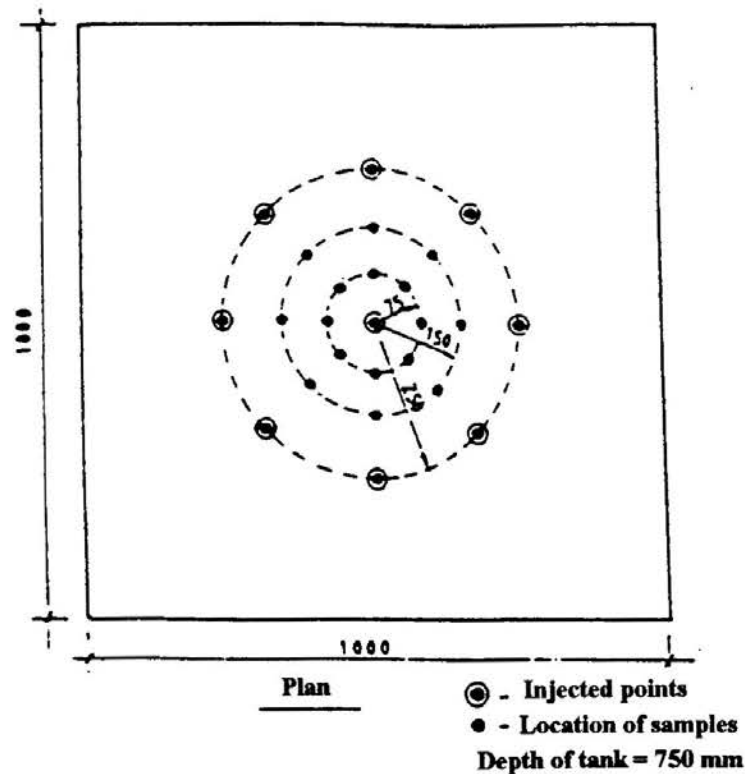


Fig. 2 Details of Experimental Setups Used for Lime Injection Work

Test Tank 1

The lime column work was carried out in a circular tank of diameter 600 mm and 550 mm height (Fig. 1). Fully saturated soil was placed in the test tank in layers of 30 mm to 50 mm thick of soft to medium stiff consistency. Each layer was first hand-packed and then pressed with a wooden template to remove the entrapped air and to ensure homogeneous packing. As per this procedure the soil bed was prepared to the required thickness of 500 mm. Because of the high water content used, there was no difficulty in forming a homogeneous soil bed. This was checked by measuring the strength using a vane shear apparatus similar to the one described by ASTM D 2573-73 (1989) and these were conducted at different depths. Further a few samples were taken for moisture contents. All these confirmed the homogeneity of the test bed. In all tests of this series, lime columns of 50 mm diameter and 500 mm height were installed at the center of the soil bed. Lime columns were formed using quicklime or calcium hydroxide as column filling materials. In most of the series, sea water was used for mixing with soil but in one series the soil bed was formed under fresh water conditions to bring out the differences in the soil behavior due to large variations in exchangeable sodium ions present in the marine environment. The excess sodium ions were removed in the fresh water setup using leaching procedure by washing with excess distilled water.

X-RAY DIFFRACTION AND MICROSTRUCTURAL STUDIES

Test Tank 2

The lime injection work was carried out in a tank of size, 1000 mm x 1000 mm x 750 mm filled with a soft marine clay (Fig. 2). The soil bed was prepared up to a thickness of 700 mm as per the procedures adopted in the Test Tank 1. The lime injection was carried out in three stages using a steel injection pipe of inner diameter 18 mm and of length 1250 mm. The pipe had 40 perforations over a length of 300 mm to 400 mm in the bottom portion and lime slurry was forced through the pipe into the soil bed at a pressure of 0.2 to 0.3 N/mm². The pipe was then slowly withdrawn in stages and the slurry was injected to the middle and top layers of 200 mm height in two stages. Samples were collected at various radial distances in different lime treated soil systems and these samples were air dried, powdered and used for XRD analysis. Samples were taken at different time intervals to study the lime induced changes that occurred in the soil system. The details of the experimental setups used are given in Table 2 and the sampling locations are shown in Figs. 1 and 2.

Table 2 Details of Experimental Setups Used

S.No	Test Programme		Water used for mixing and curing of the soil
	Lime column work (Setup 1)	Lime injection work (Setup 2)	
	Column filling material used	Injection material used	
1.	Quicklime	-	Fresh water
2.	Quicklime	-	Sea water
3.	Hydrated lime	-	Sea water
4.	Quicklime-Sand	-	Sea water
5.	Quicklime-Calcium Sulphate	-	Sea water
6.	Quicklime-Calcium Chloride	-	Sea water
7.	Quicklime-Sodium Sulphate	-	Sea water
8.	-	Hydrated Lime Slurry	Sea water

Setup 1 - Circular tank of diameter, 600 mm and height, 550 mm.

Setup 2 - Rectangular tank of size, 1000 mm x 1000 mm x 750 mm.

RESULTS AND DISCUSSION

X-ray Diffraction Analysis

The XRD analysis was carried out using a Philips X-ray diffractometer and XRD patterns were obtained using $Cu\text{-}k\alpha$ ($\lambda = 1.5148 \text{ \AA}$, nickel filter) with an input voltage of 34 kV and a current of 24 mA. A scan speed of 3° per minute was generally used and air-dried powdered samples were used for the XRD analysis of both untreated and treated samples.

The XRD patterns of untreated soil samples are shown in Fig. 3. The mineralogical analysis of the soil was carried out by comparing the obtained XRD patterns with Brown (1961) and the standard ASTM powder diffraction files (1991), and the same was used for the identification of various reaction products. The XRD pattern of the untreated bulk sample (without removing any fraction) indicates the presence of minerals such as montmorillonite, kaolinite, quartz and chlorite-vermiculite-montmorillonite (Fig. 3a). The XRD analysis of the glycerol treated sample indicate the presence of swelling mineral, montmorillonite (Fig. 3b).

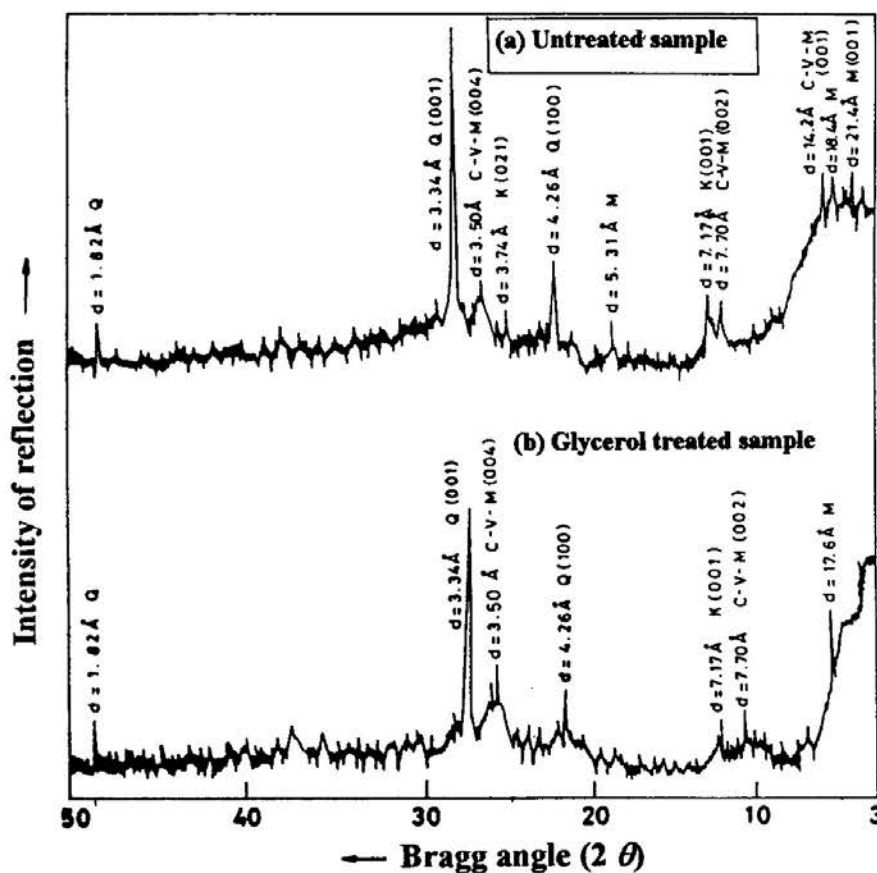


Fig. 3 XRD Patterns of Untreated Soil Samples

X-RAY DIFFRACTION AND MICROSTRUCTURAL STUDIES

It has been reported by earlier investigators that the seeped lime had induced several beneficial changes in the soil system including the formation of various products due to soil-lime reactions (Willoughby, et al., 1968; Somayazulu, 1987; and Locat, et al., 1990).

The diffractograms obtained for the samples collected at a radial distance of 200 mm from the installed quicklime column in fresh water setup are shown in Fig. 4. The appearance of several new peaks in these XRD patterns indicates the formation of new reaction products that are of moderate to strong intensity due to soil-lime reactions. These compounds are identified as calcium silicate hydrate (CSH), calcium aluminate hydrate (CAH) and stratling compound (CASH), and the test results indicated that there is an improvement in the intensities of the reaction compounds. The poor crystalline variety of CSH (1.99 \AA^0) formed at an early stage gradually develops to a more orderly structure with time. The test results indicated that the effective penetration of lime into the soil is up to a radial distance of 4 times the diameter of the lime column. The XRD patterns of the quicklime column treated soil samples in sea water taken at a radial distance of 200 mm are also shown in Fig. 5. An improvement in the intensities of various compounds such as CSH and CAH can be seen in all the XRD patterns of treated systems, and the test results indicated that the formation of cementation compounds is not affected by the presence of sea water.

Fig. 6 shows the XRD patterns of samples collected from hydrated lime column setup with sea water at a radial distance of 200 mm. The formation of various new peaks of CSH and CAH can be seen after 45 days of treatment. The increase in the intensity of CAH (2.41 \AA^0) indicates that with time, this compound is slowly converted to the well crystalline phase from an initial gel state. These compounds might have been formed due to the soil-lime reactions between lime and hydrous aluminate of the soil.

Fig. 7 indicates the XRD patterns of the quicklime-sand column treated samples taken at a radial distance of 200 mm from the column. This indicates the formation of similar compounds such as CAH as in the case of previous lime treated soil systems, and there are no changes in the type of compounds formed when compared with the XRD patterns of other lime treated soil systems. The test results indicated that lime-sand mixture can be used as an effective column filler material to achieve the lime induced beneficial changes in the soil system.

The addition of calcium sulphate (gypsum) with quicklime (Fig. 8) also resulted in the formation of similar reaction products as reported in the other lime treated soil systems. The formation of metastable CAH phase is seen at few locations of XRD patterns indicating a better formation of this compound. There is a reduction in the intensity of montmorillonite peak with time and this indicated a vigorous action of lime with soil. An increase in the intensities of few XRD peaks of CSH (2.97 \AA^0) and CASH (4.18 \AA^0 and 4.40 \AA^0) can be seen in the quicklime-calcium chloride column

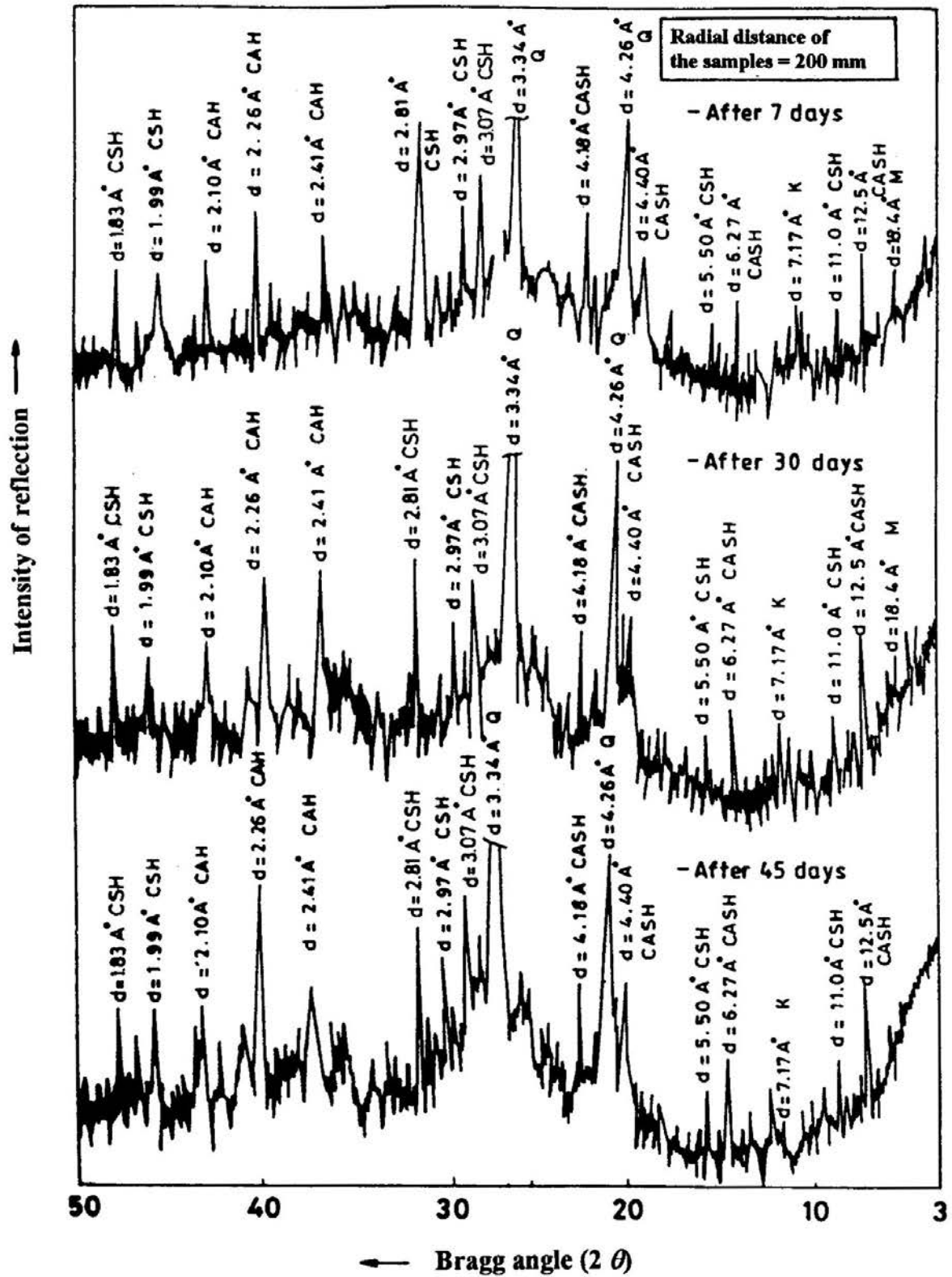


Fig. 4 XRD Patterns of Quicklime Column Treated Soil Samples in Fresh Water Set-up

X-RAY DIFFRACTION AND MICROSTRUCTURAL STUDIES

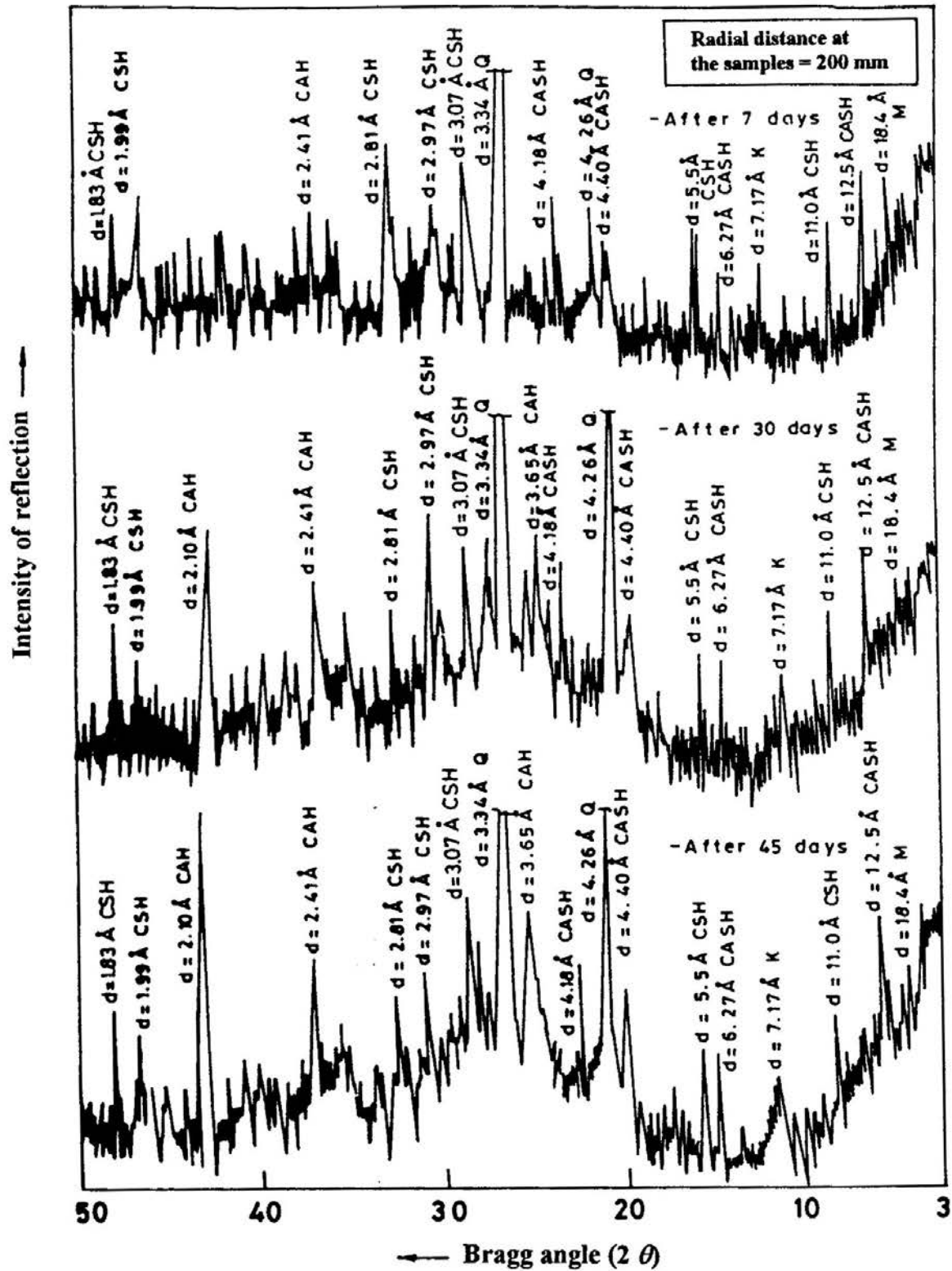


Fig. 5 XRD Patterns of Quicklime Column Treated Soil Samples in Sea Water Set-up

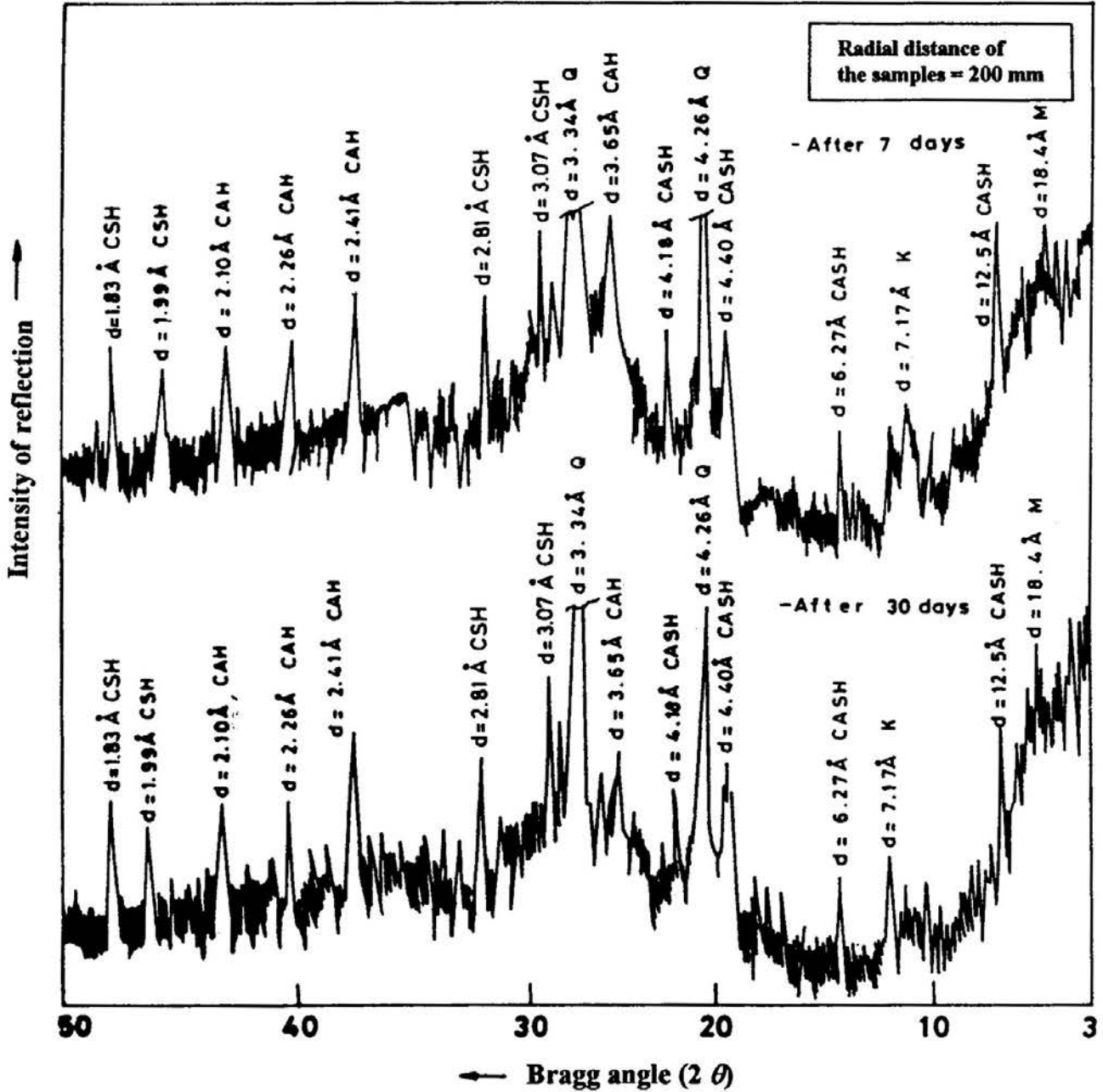


Fig. 6 XRD Patterns of Hydrated Lime Column Treated Soil Samples in Sea Water Set-up

X-RAY DIFFRACTION AND MICROSTRUCTURAL STUDIES

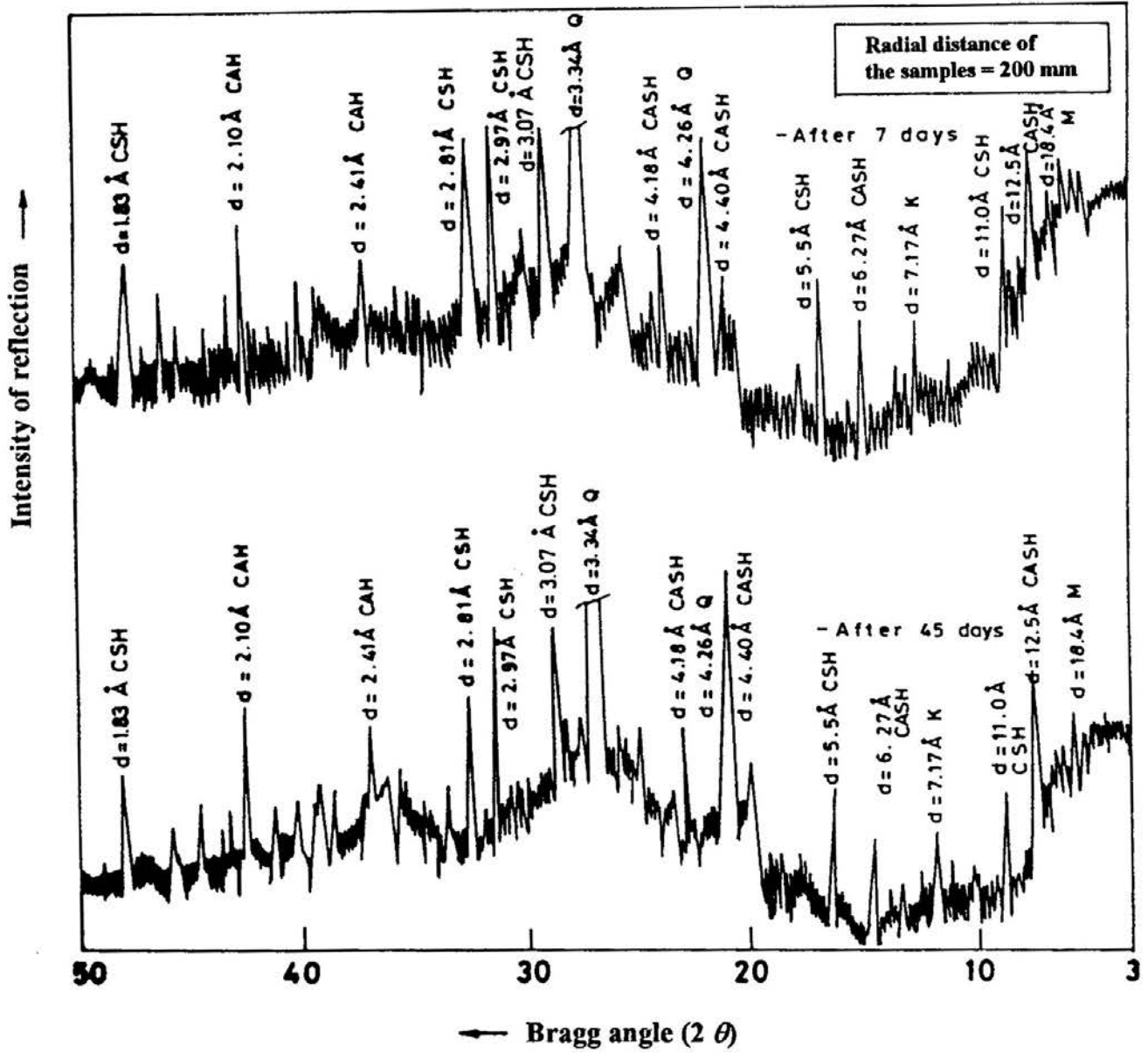


Fig. 7 XRD Patterns of Quicklime-Sand Column Treated Soil Samples in Sea Water Set-up

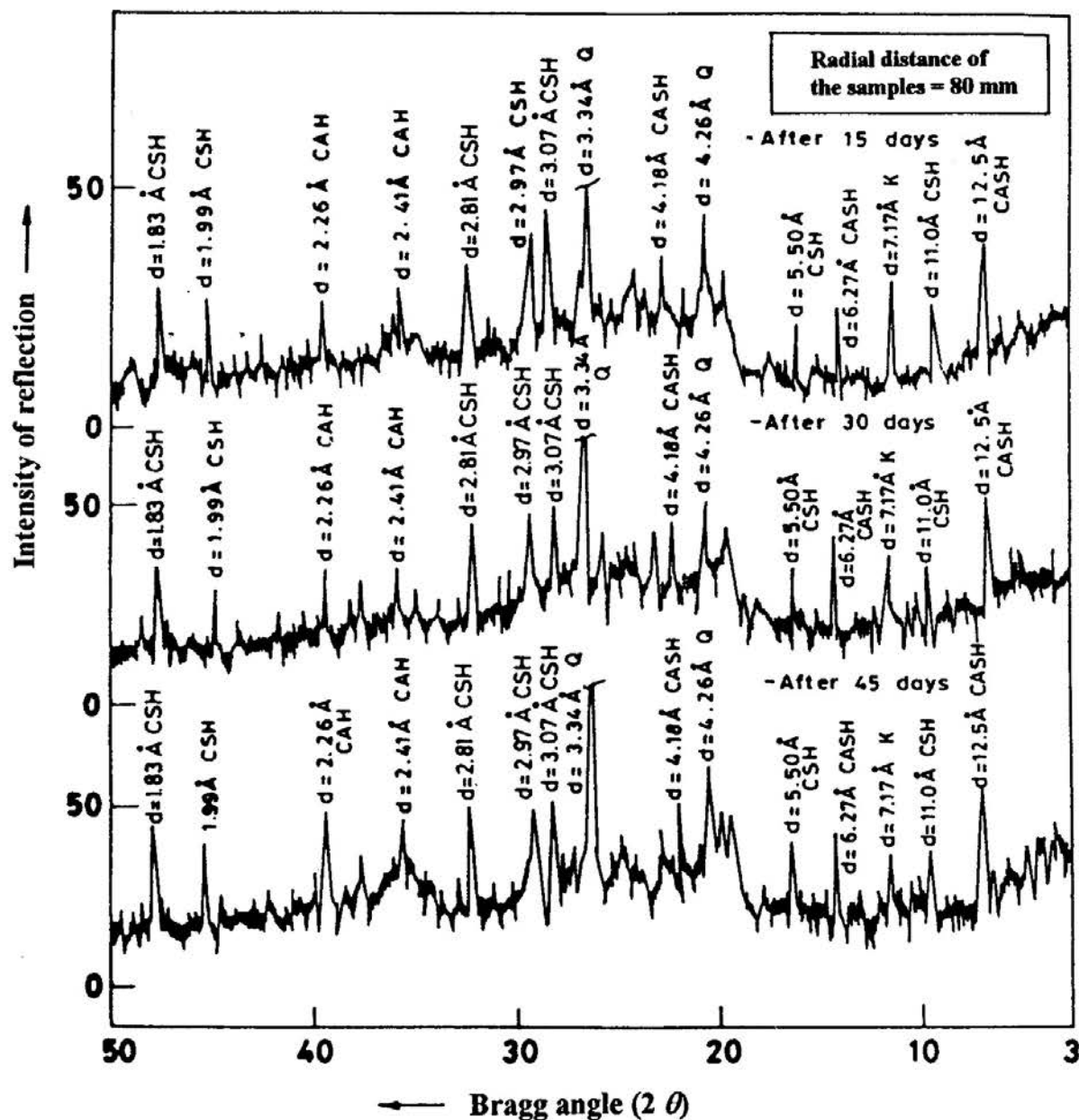


Fig. 8 XRD Patterns of Quicklime-Calcium Sulphate Column Treated Soil Samples in Sea Water Set-up

X-RAY DIFFRACTION AND MICROSTRUCTURAL STUDIES

treated soil system in sea water setup (Fig. 9). In this case also, new peaks corresponding to CAH as observed in other systems are noticed.

Fig. 10 shows the quicklime-sodium sulphate column treated soil system in sea water. With respect to time, there is a formation of the cementation compounds like CAH, CSH and CASH peaks, and these compounds are slowly crystallized with time. There is not much improvement in the peak intensities of the new compounds formed when compared with the results of earlier setups. The appearance of peaks corresponding to ettringite (calcium sulphoaluminate) mineral can be seen at a few places of XRD (9.73 \AA^0 , 5.60 \AA^0 , 3.88 \AA^0 and 2.62 \AA^0). This compound is believed to be formed due to the reaction of quicklime with sulphate in the presence of predominant sodium ions environment. Under certain conditions, these compounds have large affinity to water and expand with time due to the growth of crystals, and the formation of these compounds and their adverse effects in the soil system have been discussed in detail by few investigators (Kujala, 1983; Mitchell, 1986; and Hunter, 1988). Since the underwater deposits are already in fully saturated condition, there is no problem in the swell pressure mobilization due to the intake of water. The formation of these compounds poses problems due to increased compressibility in the submarine soils.

Fig. 11 indicates the XRD patterns of lime injection treated samples taken at a radial distance of 200 mm from the injected points and the presence of CSH (1.99 \AA^0), CAH (2.41 \AA^0) and CASH (4.18 \AA^0 and 4.40 \AA^0) peaks can be seen as in the case of previous lime treated soil systems, and the appearance of typical hydrogarnet along with traces of CSH is also seen. This indicates that lime injection technique can be successfully used in improving the behavior of the marine clays.

From the above diffractograms, it is observed that several new peaks of weak to moderate intensity are formed in the lime treated soil system due to soil-lime reactions. The various clay minerals and quartz present in the untreated soil can react with lime and form new cementation compounds, and the diffused lime attacks the clay particles and their edges to form CSH and CAH compounds. It has been noted that the formation of new reaction products in different lime treated systems are usually of CSH, CAH and CASH but in the case of quicklime-sodium sulphate treated system the formation of ettringite has been observed. The increase in the diffracted intensities of the compounds indicates that these products are gradually converted into the crystalline state from an initial gel phase. The qualitative view of these compounds and their effect on the particles at microlevel due to lime attack can be seen using SEM as explained in the following sections.

SEM Studies

Fig.12 shows the micrographic details of untreated soil in fresh water system which shows the presence of montmorillonite (M) in crystalline form with quartz (Q),

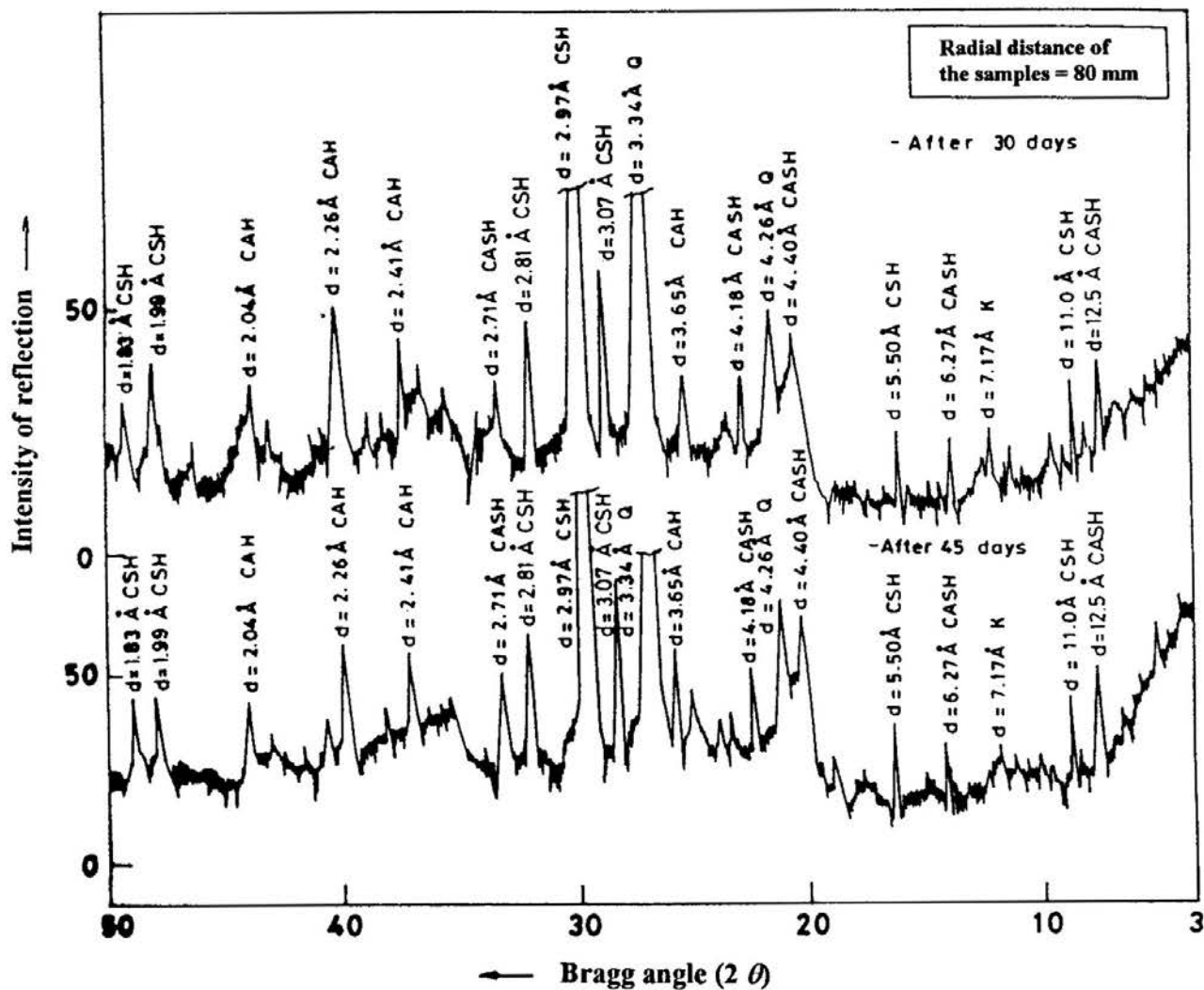


Fig. 9 XRD Patterns of Quicklime-Calcium Chloride Column Treated Soil Samples in Sea Water Set-up

X-RAY DIFFRACTION AND MICROSTRUCTURAL STUDIES

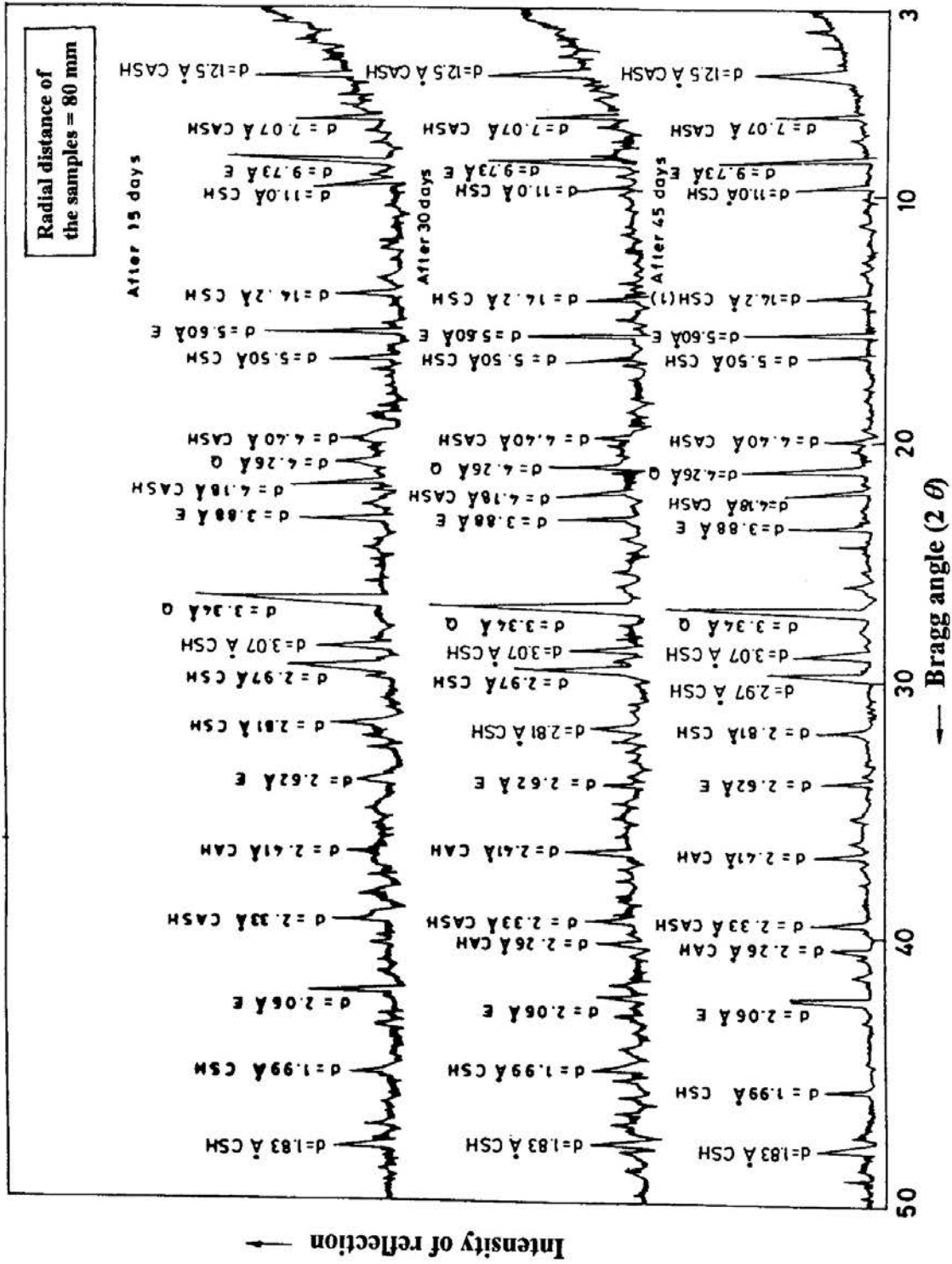


Fig. 10 XRD Patterns of Quicklime-Sodium Sulphate Column Treated Soil Samples in Sea Water Set-up

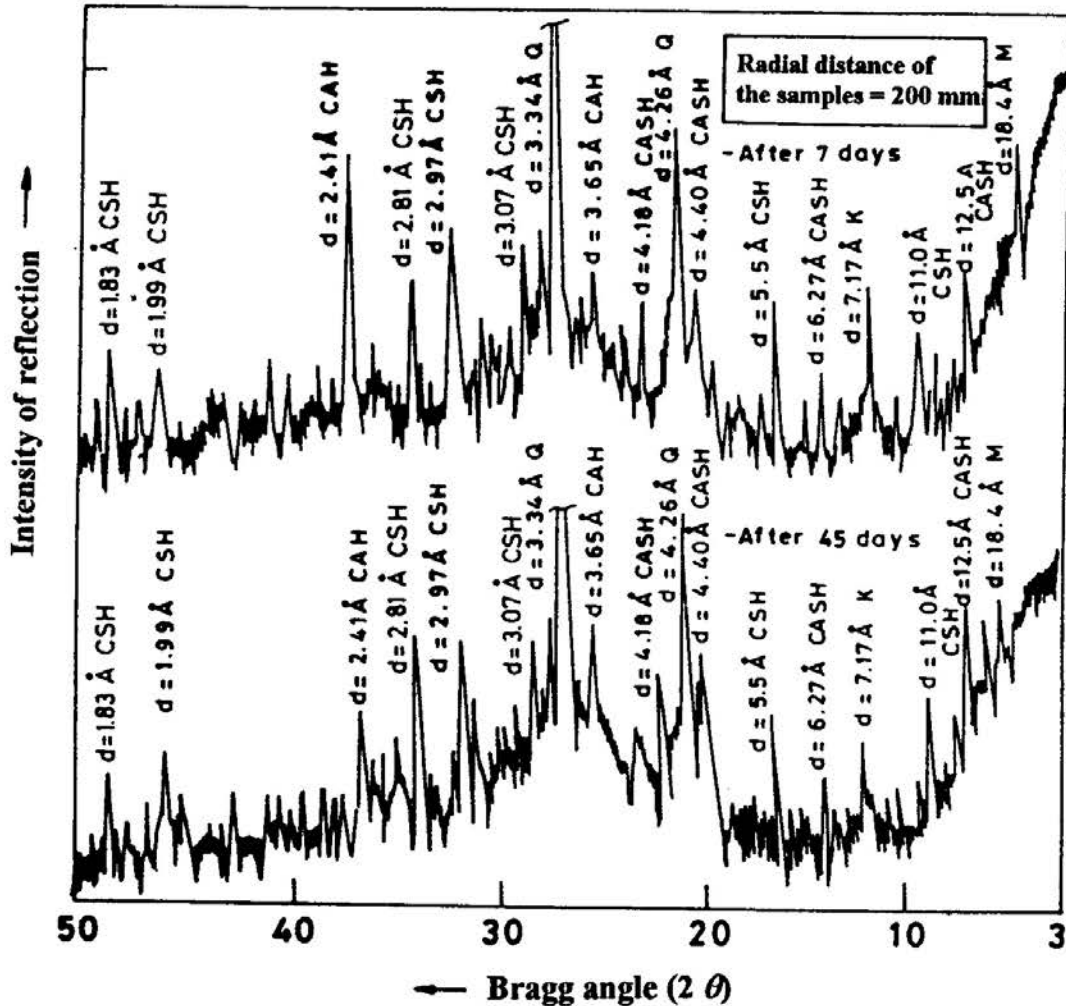


Fig. 11 XRD Patterns of Lime Injection Treated Soil Samples in Sea Water Set-up

and this type of dispersed arrangement of soil particles can be seen in the fresh water sediments. The central portion of the micrograph of Fig. 13 shows the curved plates resembling that of montmorillonite (M) in the sea water sedimented clay and on the left hand side the massive quartz (Q) particle can be seen.

The formation of massive clay aggregates (A) of the micrograph with gel coatings at the bottom due to soil-lime reactions can be seen in Fig. 14 of the quicklime column treated soil system in fresh water setup after 30 days of treatment. The XRD

X-RAY DIFFRACTION AND MICROSTRUCTURAL STUDIES

patterns of the corresponding sample (Fig. 4) indicate the formation of various new cementation products due to soil-lime reactions such as calcium silicate hydrate (CSH) and calcium aluminate hydrate (CAH). The micrograph of the quicklime column treated sample in seawater after 30 days can be seen in Fig. 15. This indicates the gel coated cementation aggregates (A) with a spongy appearance due to the lime attack on soil particles. Fig. 16 corresponds to the sample taken from the hydrated lime column treated system in sea water after 45 days of treatment and one can see a well masked aggregates (A) at several places of the micrograph. The micrograph of the Fig. 17 shows the formation of coarse aggregates (A) with porous network and this belongs to the sample taken from the quicklime-sand column treated sample in sea water. Fig. 18 shows the severe lime attack on the edges of soil particles in the quicklime-calcium sulphate treated soil system in sea water after 45 days of treatment which result in the formation of well developed aggregates. This micrograph indicates the presence of platy calcium aluminium silicate (CASH) at the center of the micrograph.

Figs. 19 and 20 show the microscopic features of quicklime-calcium chloride column treated soil system after 45 days of treatment. The formation of CSH and CASH as reported by Kawamura and Diamond (1975); Locat, et al. (1990); and Berube, et al. (1990) can be seen in the above micrograph and the XRD analysis also show the strong peaks of CSH and CASH. The presence of kaolinite (K) particles in between the clay aggregates (A) in the aggregated booklet form can be seen in the above micrographs. Fig. 21 correspond to the sample taken at a radial distance of 200 mm after 45 days treatment from the above lime treated system, and the effect of calcium chloride is severe in forming small aggregates (A) of uniform size and they are mostly of CSH products as explained in the earlier micrographs.

The presence of platy CASH and reticular CSH can be seen in the above micrographs and they are mainly responsible for the long term strength development of lime treated soil system as reported (Locat, et al., 1990). This results in the reduction of shrinkage and swell, and improves workability of the soil system. The above micrographs show the formation of various cementation products such as CSH and CAH (as confirmed by XRD studies) in different lime treated soil systems. The studies on reaction products acting as a gluing matrix with non-clay minerals show the effects of flocculation, aggregation and possibly cementation due to lime treatment. The addition of calcium sulphate and calcium chloride with quicklime induce the formation of well fused aggregates due to soil-lime reactions. The various new compounds formed induce aggregation effect on soil particles and bind them together to form crumbs of clay clusters. The addition of admixtures like calcium chloride along with quicklime increases the crowding of calcium ions on the clay particles resulting in the formation of cementation compounds, which bind the clay particles together to form aggregates of different sizes. The formation of the above reaction products result in the particle growth of soil particles with time.

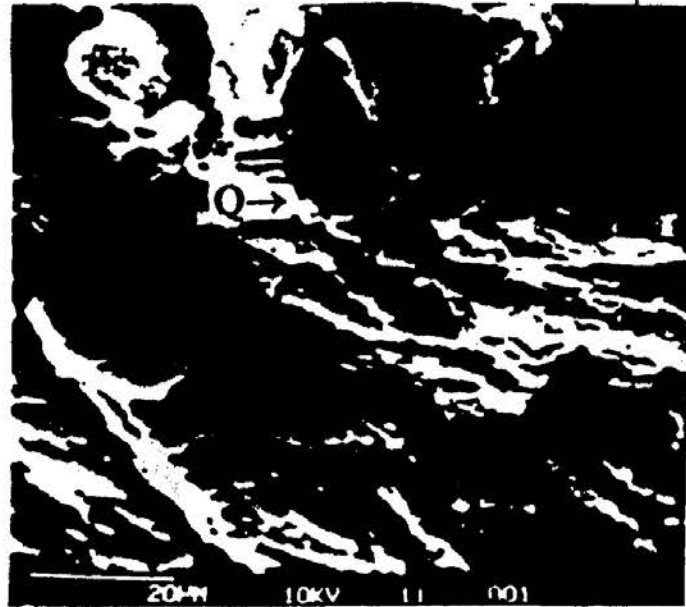


Fig. 12 Scanning Electron Micrograph of Untreated Soil in Fresh Water Set-up

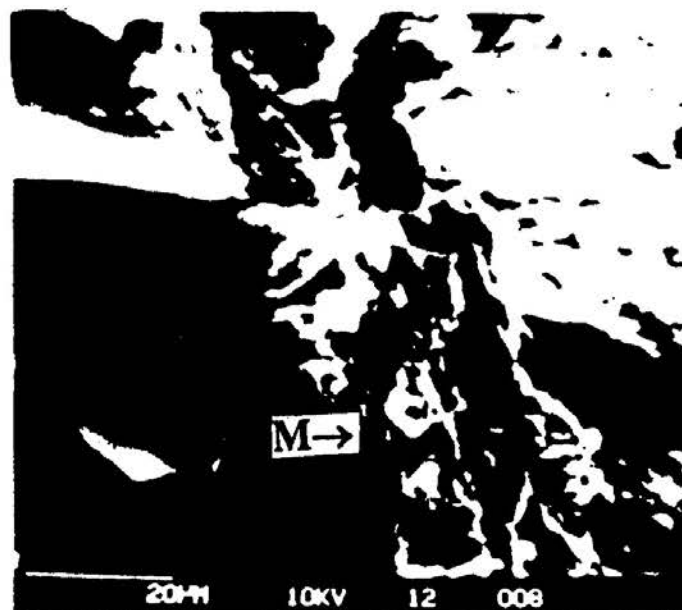


Fig. 13 Scanning Electron Micrograph of Untreated Soil in Sea Water Set-up

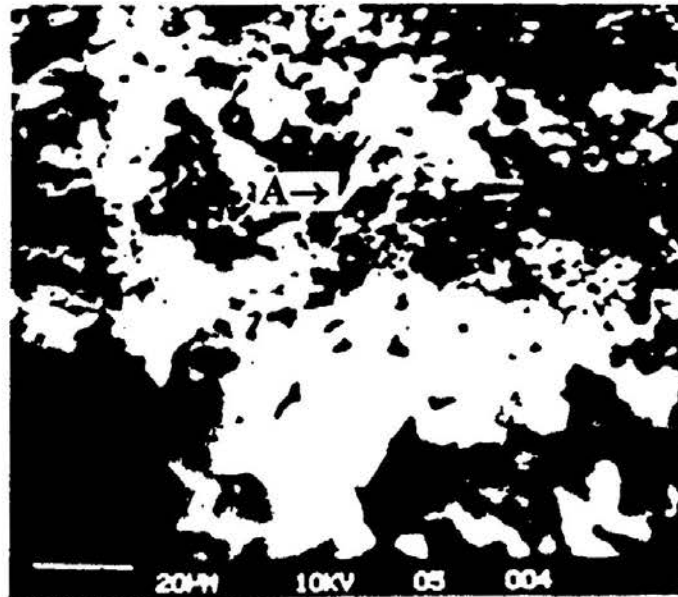


Fig. 14 Scanning Electron Micrograph of Quicklime Column Treated Sample in Fresh Water Set-up After 30 Days Treatment (Radial Distance of the Sample = 80 mm)

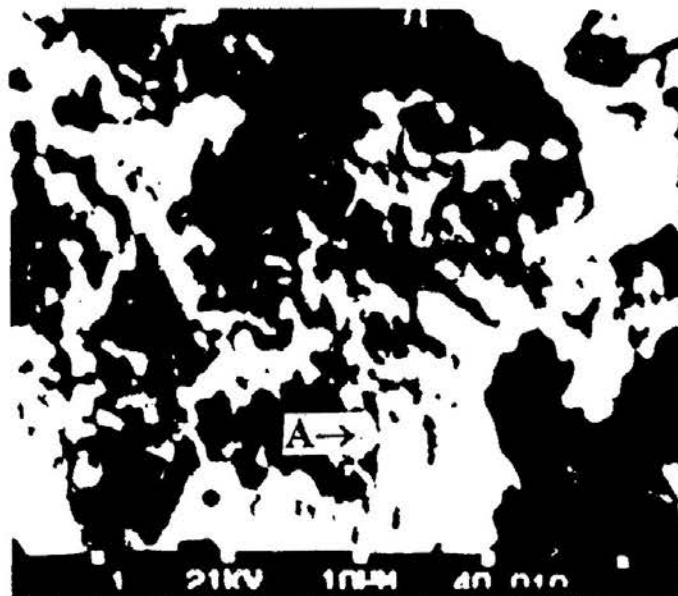


Fig. 15 Scanning Electron Micrograph of Quicklime Column Treated Sample in Sea Water Set-up After 30 Days Treatment (Radial Distance of the Sample = 80 mm)

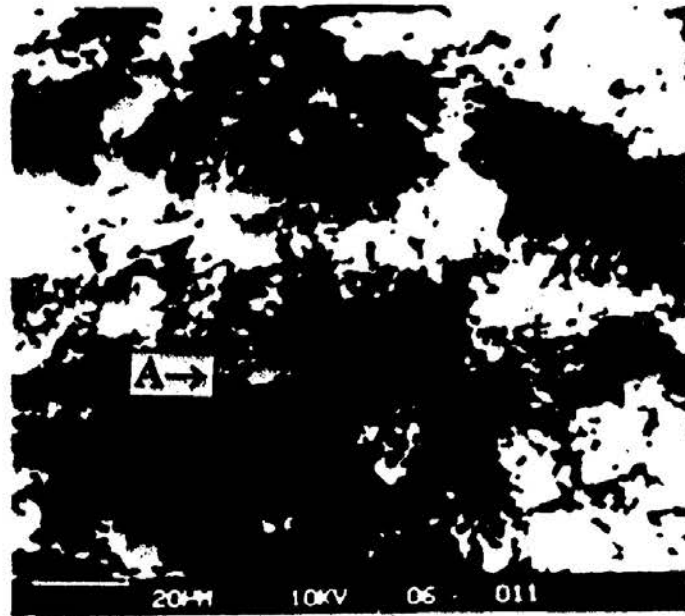


Fig. 16 Scanning Electron Micrograph of Hydrated Lime Column Treated Sample in Sea Water Set-up After 45 Days Treatment (Radial Distance of the Sample = 200 mm)

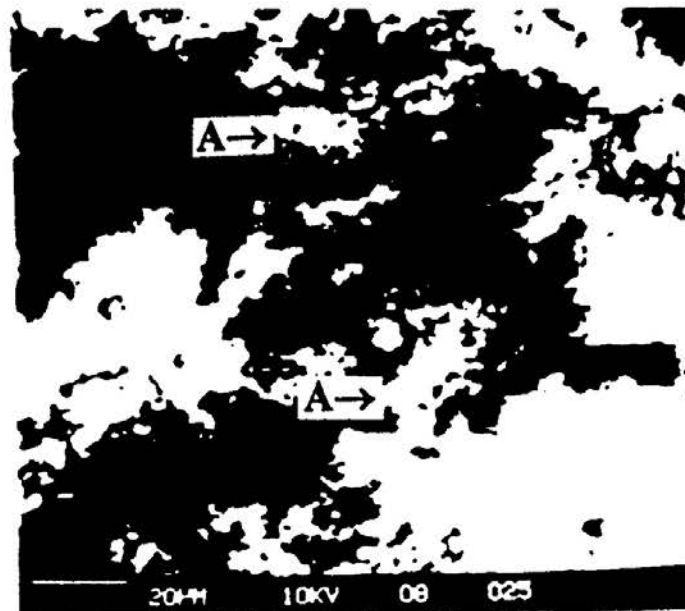


Fig. 17 Scanning Electron Micrograph of Quicklime-Sand Column Treated Sample in Sea Water Set-up After 45 Days Treatment (Radial Distance of the Sample = 200 mm)

X-RAY DIFFRACTION AND MICROSTRUCTURAL STUDIES

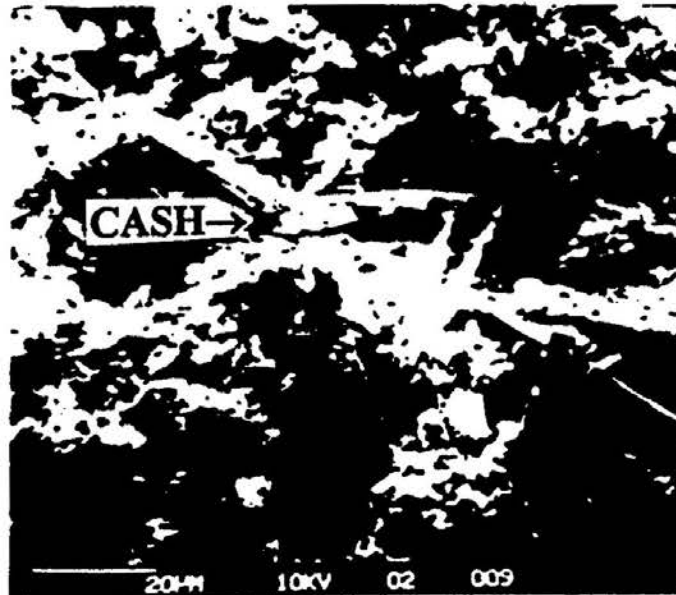


Fig. 18 Scanning Electron Micrograph of Quicklime-Calcium Sulphate Column Treated Sample in Sea Water Set-up After 45 Days Treatment (Radial Distance of the Sample = 200 mm)

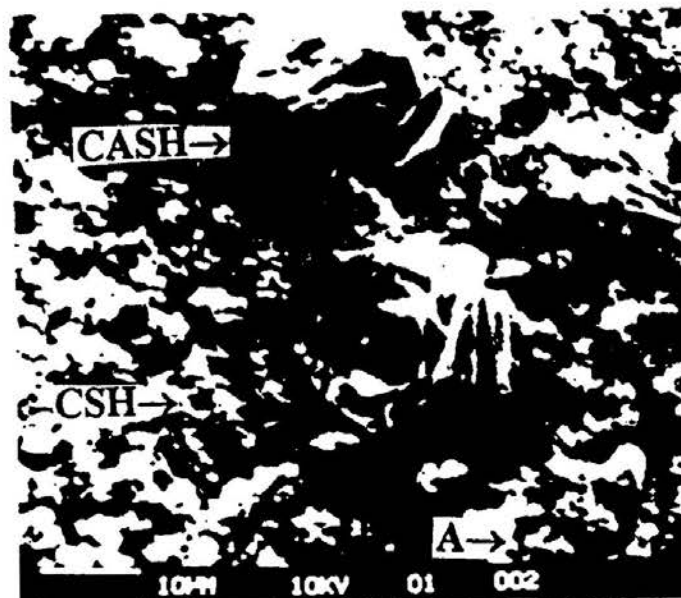


Fig. 19 Scanning Electron Micrograph of Quicklime-Calcium Chloride Column Treated Sample in Sea Water Set-up After 45 Days Treatment (Radial Distance of the Sample = 200 mm)

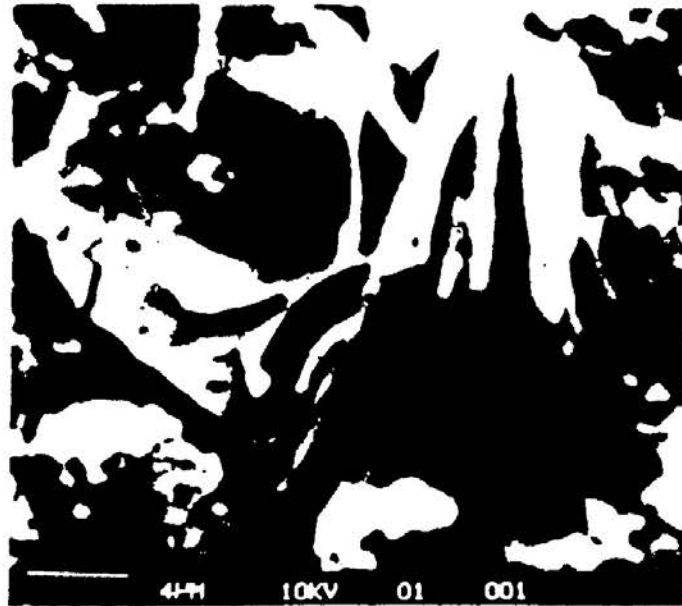


Fig. 20 Scanning Electron Micrograph of Quicklime-Calcium Chloride Column Treated Sample in Sea Water Set-up After 45 Days Treatment (Radial Distance of the Sample = 80 mm)

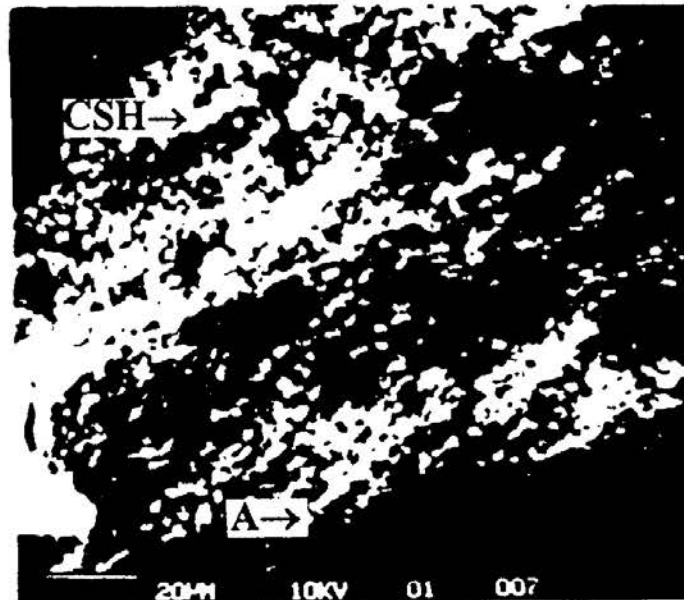


Fig. 21 Scanning Electron Micrograph of Quicklime-Calcium Chloride Column Treated Sample in Sea Water Set-up After 45 Days Treatment (Radial Distance of the Sample = 80 mm)

X-RAY DIFFRACTION AND MICROSTRUCTURAL STUDIES

The grain size distribution of the untreated soil in sea water setup and different lime treated soil systems indicate that the clay content of the untreated soil is reduced after 45 days of treatment, and the same has been converted to silt/fine sand size due to lime treatment (Fig. 22). It can be also observed that the use of quicklime-sand as column filling material has improved the aggregation effect better than other lime treated soil systems, and it indicates that sand is acting as a drainage material in seeping lime well into the soil system. The aggregation effect in the lime injection treated soil system is not severe compared to other lime treated soil systems whereas there are not much changes that occurred in the particle size distribution of the untreated and quicklime-sodium sulphate treated soil system. This may be due to the domination of sodium ions which results in the formation of ettringite in the quicklime-sodium sulphate treated soil system as explained earlier.

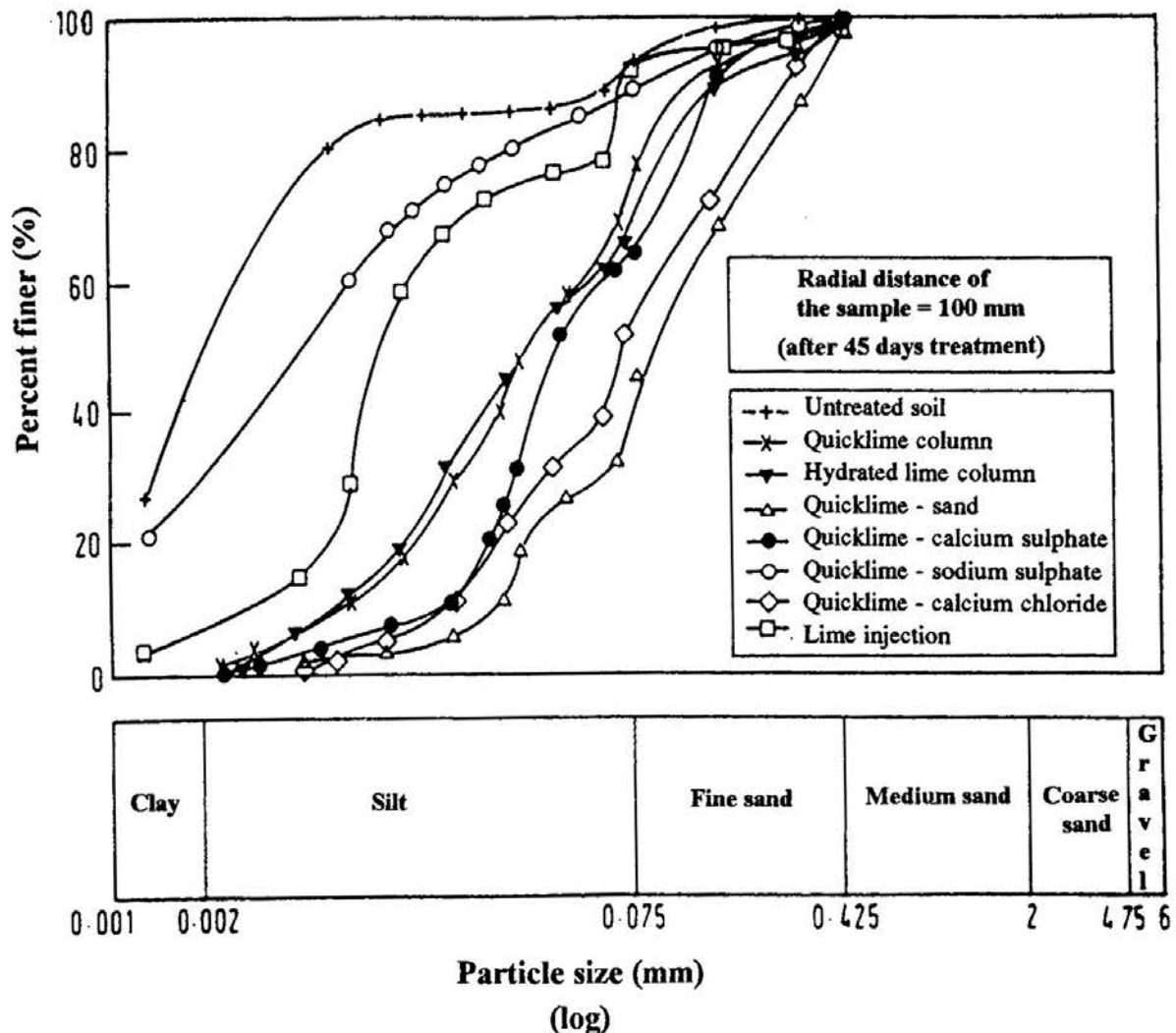


Fig. 22 Grain Size Distribution of Different Lime Treated Soil Systems

Physical and Engineering Properties of the Soil

The physical changes that occurred in the soil system due to lime treatment can change the index and engineering properties of the soil. The index tests were carried out mainly to bring out the changes that occurred in the plasticity characteristics of the soil and these tests were carried out as per the standard procedures (ASTM D 4318-24, 1989). The liquid limit and the plasticity index values of the treated soil systems after 45 days of treatment are given in Table 3. The test results indicate that there is a considerable decrease in the values of liquid limit and plasticity index values with time, and in general there is a reduction in the plasticity index values from 53 to 30 (%) after 45 days treatment. The possible changes in base exchange and the associated changes in the fabric of soil particles are expected to take place in a short interval of time. The aggregation and the formation of new compounds as a result of migration of lime into the soil system are known to take place over a long period. The changes occurred in the strength and deformation behavior of different lime treated soil systems after 45 days of treatment are given in Table 3. The above mentioned physical changes have resulted in an increase in the strength of the soil system by 8 to 10 times of the untreated soil with a corresponding decrease in the compression index (C_c) values from 0.85 to 0.36. Both the immediate and long term effects combine together to reduce the liquid limit and plasticity index, and improve the engineering behavior of the soil up to a radial distance of 4 to 6 times that of the diameter of the lime column. The addition of lime induces aggregation and cementation effects on soil particles and as a result of which, there is a considerable reduction in C_c and increase in the strength values.

CONCLUSIONS

The following conclusions were drawn from the above experimental program. The formation of various new cementation compounds such as CAH, CSH and CASH due to the soil-lime reactions can be seen in all lime treated soil systems. The presence of these compounds in the various lime treated systems have been confirmed using XRD and SEM techniques. The presence of sea water has not affected the formation of the cementation compounds and there is a considerable improvement in the physical and engineering properties of the soil due to soil-lime reactions. Thus both the lime column and lime injection techniques can be conveniently used to improve the behavior of soft marine clay deposits.

REFERENCES

ASTM (1991). *Index to the Powder Diffraction File*. Philadelphia: Joint Committee on Power Diffraction Standards, Pennsylvania.

Table 3 Variation in the Physical and Engineering Properties of Different Lime Treated Soil Systems

S.No	Type of treatment	Liquid limit (%)		Plasticity Index (%)		Shear strength of the soil (kN/m ²)		Compression Index (C _c)	
		Radial distance of the sample = 80 mm	Radial distance of the sample = 200 mm	Radial distance of the sample = 80 mm	Radial distance of the sample = 200 mm	Radial distance of the sample = 80 mm	Radial distance of the sample = 200 mm	Radial distance of the sample = 80 mm	Radial distance of the sample = 200 mm
1.	Quicklime column in fresh water setup	68	69	32	35	135	124	0.51	0.62
2.	Quicklime column in sea water setup	66	73	32	36	120	104	0.58	0.63
3.	Hydrated lime column in sea water setup	71	75	34	34	106	81	0.63	0.65
4.	Quicklime-Sand column in sea water setup	70	77	32	33	135	98	0.57	0.68
5.	Quicklime-Calcium Sulphate column in sea water setup	65	67	27	29	142	121	0.44	0.54
6.	Quicklime-Calcium Chloride column in sea water setup	65	67	27	30	163	162	0.42	0.53
7.	Quicklime -Sodium Sulphate column in sea water setup	80	88	49	54	86	57	0.84	0.83
8.	Hydrated lime injection in sea water setup	71	77	34	35	92	63	0.63	0.72

RAJASEKARAN AND NARASIMHA RAO

- ASTM D 4318-84. (1989). Standard test method for liquid limit, plastic limit and plasticity index of soils. *Annual Book of ASTM Standards*, Vol. 04.08, pp. 579-589.
- ASTM D 2573-73. (1989). Standard test method for field vane shear test in cohesive soil. *Annual Book of ASTM Standards*, Vol. 04.08, pp. 308-310.
- BERUBE, M. A.; CHOQUETTE, M.; and LOCAT, J. (1990). Effects of lime on common soil and rock forming minerals. *Applied Clay Science*, Vol. 5, pp. 145-163.
- BJERRUM, L. (1973). Geotechnical problems involved in foundation of structures in North Sea. *Geotechnique*, Vol. 23, pp. 319-358.
- BROMS, B. and BOMAN, P. (1975). Lime stabilized columns. *Proceedings of the Fifth Asian Regional Conference on Soil Mechanics and Foundation Engineering Bangalore, India*, Vol. 1, pp. 227- 234.
- BROWN, G. (1961). *The X-ray Identification and Crystal Structures of Clay Minerals*. London: Mineralogical Society (Clay Minerals Group).
- EADES, J.L.; NICHOLS, F.P, Jr.; and GRIM, R.E. (1962). Formation of new minerals with stabilization as proven by field experiments in Virginia. *Highway Research Record Bulletin. No.335*, Washington, D.C., pp. 31-39.
- HUNTER, D. (1988). Lime-induced heave in sulphate bearing soils. *Journal of Soil Mechanics and Foundation, Proceedings of ASCE*, Vol 114, No. 2, pp. 150-167.
- INGLES, O. G. and METCLAF, J. B. (1972). *Soil Stabilization*. Melbourne: Butterworths.
- JOSHI, R.C.; NATT, G.S.; and WRIGHT, P.J. (1981). Soil improvement by lime-fly ash slurry injection. *Proceedings of the Tenth International Conference on Soil Mechanics and Foundation Engineering*, Stockholm, Vol. 103, pp. 707-712.
- KAWAMURA, M. and DIAMOND, S. (1975). Stabilization of clay soils against erosion loss. *Clays and Clay Minerals*, Vol. 33, pp. 161-172.
- KUJALA, K. (1983). The long-term performance of lime and gypsum lime columns. *Proceedings of Eighth European Conference on Soil Mechanics and Foundation Engineering.*, Finnish Geotechnical Society, pp. 1309-1310.

X-RAY DIFFRACTION AND MICROSTRUCTURAL STUDIES

- LEE, G.; ABDELKADAR, M.O.; and HAMDANI, S.K. (1983). Effect of the clay fraction on some mechanical properties of lime-soil mixtures, *Journal of Institute of Highways Engineering*, Vol. 29, 2-9.
- LOCAT, J.; BERUBE, M.A.; and CHOQUETTE, M. (1990). Laboratory investigations on the lime stabilization of sensitive clays: shear strength development. *Canadian Geotechnical Journal*. Vol. 27, No. 3, pp. 294-304.
- MITCHELL, J.K (1986). Practical problems from surprising soil behavior. *Journal of Geotechnical Engineering, Proceedings of ASCE*, Vol. 112, No. SM3, pp. 259-289.
- OKUMARA, T. and TERASHI, M. (1975). Deep lime mixing method of stabilization for marine clay. *Proceedings of the Fifth Asian Regional Conference on Soil Mechanics and Foundation Engineering*, Bangalore, India, Vol. 1, pp. 69-75.
- RAJASEKARAN, G. (1994). Physico-Chemical Behavior of Lime Treated Marine Clay. Ph.D. Thesis, Indian Institute of Technology, Madras, India.
- SOMAYAZULU, J.R. (1987). Experimental Studies of Lime Columns in Soils. Ph.D. Thesis, Indian Institute of Technology, Madras, India.
- TRANSPORTATION RESEARCH BOARD. (1987). State of the art report 5: Lime stabilization: Reaction, properties, design, and construction, *Transportation Research Board*, N.A.S., Washington.
- WANG, J.W.H.; MATEOS, M.; and DAVIDSON, D.T. (1963). Comparative effects of hydraulic, calcitic and dolomitic limes and cement in soil stabilization. *Highway Research Record Bulletin No.59*, Washington, D.C., pp. 42-54.
- WILLOUGHBY, D.R.; GROSS, K.A.; INGLES, O.G.; SILVA, S.R.; and VERONICA, M.S. (1968). The identification of reaction products in alkali stabilized clay by electron microscopy, x-ray and electron diffraction, Paper No.430, *Report from the Proceedings of the Fourth Conference of Australian Board 4, Part 2*, pp. 1386-1408.

STRENGTH AND STIFFNESS OF HONG KONG MARINE DEPOSITS MIXED WITH CEMENT

J.H. Yin¹ and C.K. Lai¹

ABSTRACT

In this paper, test results of cement treated soft marine deposits (M.D.) from a Hong Kong coastal site are presented and analysed. The M.D. was mixed with Portland cement at different cement/soil ratio (A_w) in dry mass and at different initial water content (w_i) of the soil. Unconfined compression tests and consolidated undrained triaxial tests were conducted. Stress-strain-strength characteristics of the cement treated M.D. are investigated. Useful relationships are obtained for peak strength (q_{peak}), residual strength (q_{res}), cohesion and friction angle (c' , ϕ') and Young's modulus (E_{50}) as related to A_w and w_i . The effectiveness of the cement treatment is investigated. Conclusions are drawn on (a) the specific application of the improvement of Hong Kong marine deposits using cement, (b) the general trends of the stress-strain-strength characteristics of cement treated soft soils and (c) the effectiveness of soil improvement using cement treatment.

INTRODUCTION

The development of infrastructures and civil projects demands more and more marine reclamation in Hong Kong coastal waters. Most marine deposits (M.D.) encountered in Hong Kong coastal waters are silty clay or clayey silt with an undrained shear strength below 30 kPa. The thickness of the M.D. may vary from a few meters to more than 20 m. The low strength and high compressibility of the M.D. may cause excessive settlement/deformation and bearing capacity failure of reclamation and/or civil structures. A number of techniques may be used to improve and strengthen soft marine deposits, such as using vertical drains and preloading, sand columns, soil replacement, and deep cement/soil mixing.

The deep cement/soil mixing method (DM method) has been practised widely in many countries. Using this method, cement slurry or dry cement powder is supplied and mixed in-situ with soft soil by machine with rotating blades. Kawasaki, et al., (1981) investigated the use of DM method in relation to improved properties of marine soft soils mixed with cement slurry. Kamaluddin and Balasubramaniam (1995) studied

¹ Department of Civil and Structural Engineering, Hong Kong Polytechnic University, Hong Kong.
Note: Discussion is open until 1 September 1998. This paper is part of the *Geotechnical Engineering Journal*, Vol. 29, No. 1, June 1998. Published by the Southeast Asian Geotechnical Society, ISSN 0046-5828.

YIN AND LAI

the overconsolidated behavior of cement-treated Bangkok soft clay based on triaxial and odometer test results. Feng (1997) reported the time-dependent strength gain of Taiwan clay mixed with cement.

A feasibility study was carried out on the use of deep cement/soil mixing methods for improving marine deposits for construction of seawalls in Hong Kong (Aas and Engen, 1993). However, data on properties and behavior of Hong Kong marine deposits mixed with cement are not available. The effectiveness of the cement improvement on the strength and stiffness of Hong Kong M.D. has not been investigated previously. The composition and properties of Hong Kong marine deposits may not be the same as the soils studied in other countries. The relationships and correlation for other regional soils treated with cement cannot be used directly for the cement-treatment of Hong Kong marine deposits.

This paper will not discuss the field application of the deep cement/soil mixing technique, but rather focus on the strength and stiffness characteristics of Hong Kong marine deposits improved by using cement. The stress-strain-strength characteristics are investigated and useful correlation is obtained for design reference. The effectiveness of the soil improvement using cement is evaluated.

METHODOLOGY OF SAMPLE PREPARATION AND TESTING

Marine deposits were obtained from seabed in a coastal area near Tai Kowk Tsui Harbour in Hong Kong. The natural marine deposits contained rubbish, sea shells and occasionally large size gravel. In order to obtain uniform marine deposits for consistent testing, the natural marine deposits were diluted in water and then passed through a sieve with 150 μm opening size. The particles passed through the sieve were settled in a tank and later transferred to a specially designed cylinder container for dead-weight consolidation to reduce the M.D. water content to a certain value. The initial water content of the M.D. before mixing with cement was controlled at 60%, 80% or 100%.

The wet-sieved and preconsolidated marine deposits were then mixed with dry Portland cement powder at four different mass ratios ($A_w = M_{\text{cement}}/M_{\text{soil}}$), that is, 5%, 10%, 15% and 20%. The mixing process was done using a laboratory size conventional concrete mixer. After thorough mixing, an aluminium cylindrical pipe with an inside diameter of 35 mm and length of 70 mm was pushed into a batch of the cement-mixed marine deposits. The inside surface of the cylinder pipe was coated with a special sticky oil used to separate soil from aluminium surface. The cement-mixed M.D. in the cylindrical pipe was vibrated on a laboratory size vibration table to reduce air voids. If

STRENGTH AND STIFFNESS OF HONGKONG MARINE DEPOSITS

necessary, a palette knife was used to compress and trim the soil and expel air bubbles trapped. All cylindrical pipes with cement mixed M.D. were placed on smooth glass plates. All M.D. specimens in the pipes were covered up by a piece of plastic membrane and cured in air for 1 to 2 days depending on the rate of strength developed in the specimens. After 1 to 2 days of curing in air, specimens were extracted by an extractor and placed in a water tank to be cured for 28 days under a constant temperature of 25°C.

After 28 days of curing, the cement mixed M.D. specimens were weighed and the dimensions were measured. Some specimens were used for unconfined compression (UC) testing and some for consolidated undrained (CU) triaxial testing at effective cell pressures of 100 kPa, 200 kPa, and 400 kPa.

Plastic and liquid limit tests, hydrometer tests for size distribution and pH value tests were conducted. In UC testing, the speed of vertical compression test was 0.1 mm/min (equivalent to a strain rate of 0.14%/min). A UC test was stopped when the peak strength of the specimen was reached. In CU testing, a back pressure of 200 kPa was applied to ensure that the degree of saturation of the specimen was higher than 95% by checking B-value. Side filter paper strips were placed on the cylindrical surface of the soil specimen to speed up consolidation. The isotropic consolidation conducted in a triaxial cell at a given effective cell pressure lasted from 12 to 24 hours. The speed of vertical compression was 0.2 mm/min (equivalent to a strain rate of 0.28%/min). A CU test normally was stopped after an axial strain larger than 15% was reached. Effective cell pressures used in CU tests were 100 kPa, 200 kPa, and 400 kPa. After testing, the weight and water content of the specimen were measured. From the measured triaxial shear test data, the stress-strain relations of deviator stress ($q = \sigma'_1 - \sigma'_3$) and pore water pressure (u) against axial strain (ϵ) were obtained and plotted. Strength and stiffness parameters were also calculated for analysis.

PHYSICAL PROPERTIES AND TYPICAL STRESS-STRAIN CURVES

The basic properties of the marine deposits were obtained from relevant tests and are presented in Table 1. For the controlled initial water contents of $w_i = 60\%$, 80% and 100% of the M.D., the initial void ratios e_i were 1.6, 2.1, and 2.7, respectively. As a reference, the same marine deposits with a bulk density $\rho = 1.7 \text{ Mg/m}^3$, dry density $\rho_d = 1.2 \text{ Mg/m}^3$ and initial water content $w_i = 42\%$ without cement treatment had a cohesion $c' = 0$ and a friction angle $\phi' = 28^\circ$, obtained from triaxial shear tests, in normally consolidated condition. The average Young's modulus E_{50} measured from CU tests was 1.92 MPa, 13.0 MPa, 21.7 MPa, respectively for confining stress $\sigma_3 = 100 \text{ kPa}$, 200 kPa and 400 kPa, respectively. The definition of E_{50} will be discussed in the following section.

YIN AND LAI

The particle size distribution of the wet-sieved marine deposits was obtained from a hydrometer test and is as shown in Fig.1. The marine deposits contained 28% clay ($d < 0.002\text{mm}$), 46% silt ($0.002\text{mm} < d < 0.06\text{mm}$) and 26% fine sand ($0.06\text{mm} < d < 0.15\text{mm}$).

Table 1 Basic Properties of Marine Deposits

Liquid Limit	62 %
Plastic Limit	30 %
Plasticity Index	32%
Specific Gravity	2.67
pH value	8

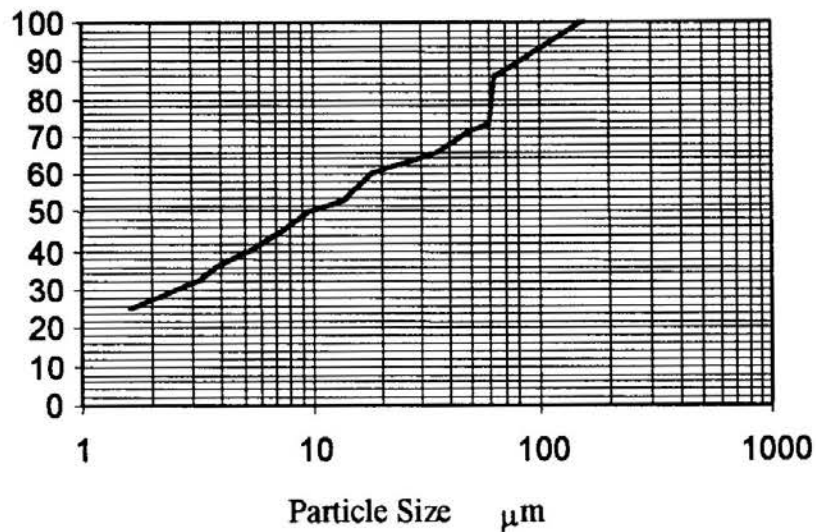


Fig. 1 Particle Size Distribution Curve Obtained from Hydrometer Test

Fig. 2 shows the curve of axial stress vs. axial strain of cement treated M.D. at $A_w = 5\%$ (cement/soil ratio in dry mass) and $w_i = 60\%$ (initial M.D. water content) from unconfined compression (UC) test. Fig. 3 shows the curve of axial stress vs. axial strain of cement treated M.D. at $A_w = 5\%$ and $w_i = 100\%$ from UC test. It is seen that peak strength occurred at a small strain value of approximately 1% for soil with a lower initial water content of $w_i = 60\%$, exhibiting brittle behaviour. At a higher initial water content $w_i = 100\%$ and for the same $A_w = 5\%$ as in Fig. 3, the peak strength occurred at a much larger strain (6.5%) indicating typical ductile behavior as shown in Fig. 3.

STRENGTH AND STIFFNESS OF HONGKONG MARINE DEPOSITS

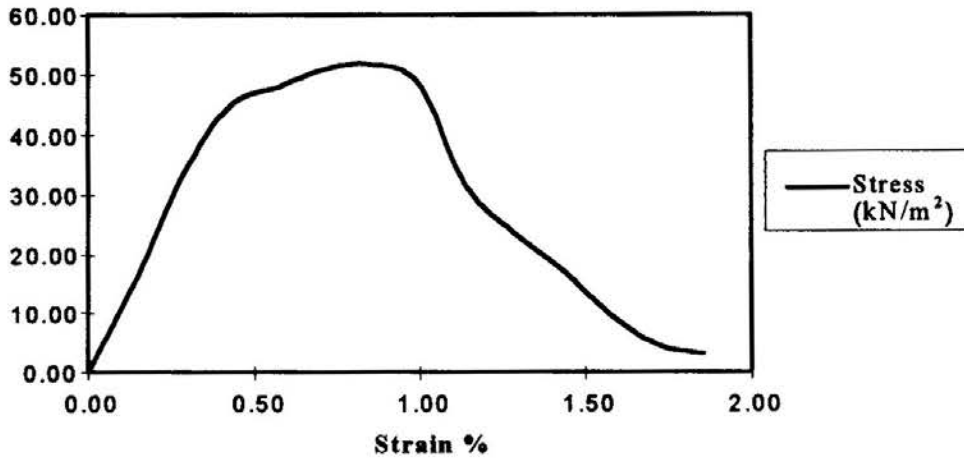


Fig. 2 Axial Stress - Axial Strain Curve at $A_w = 5\%$ $w_i = 60\%$ from UC Test

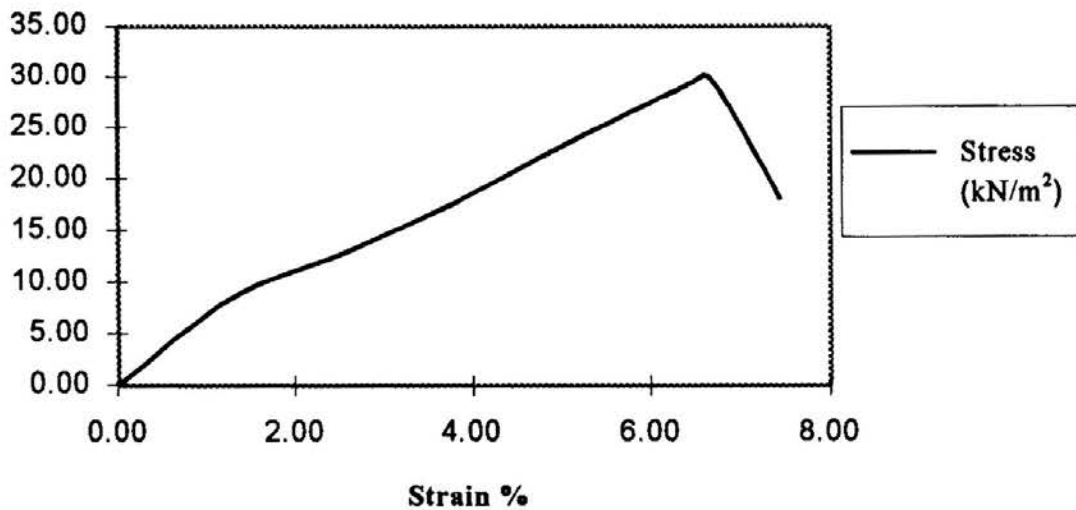


Fig. 3 Axial Stress - Axial Strain Curve at $A_w = 5\%$ $w_i = 100\%$ from UC test

Relationships of deviator stress (q) and porewater pressure (u) vs. axial strain at the same effective confining stress $\sigma_3 = 100$ kPa are shown in Fig. 4 for $A_w = 5\%$ and $w_i = 100\%$, in Fig. 5 for $A_w = 20\%$ and $w_i = 100\%$, and in Fig. 6 for $A_w = 20\%$ and $w_i = 60\%$ from results of consolidated undrained (CU) triaxial tests.

At a lower cement/soil ratio A_w and a lower initial water content w_i , the stress-strain behavior was similar to that of a normally consolidated clay with ductile behavior as shown in Fig. 4. No peak deviator stress was observed and large porewater pressure was induced. When the initial water content was the same, the increase in

cement/soil ratio caused the soil to behave like overconsolidated clay as shown in Fig. 5. In Fig. 5, a peak deviator stress is observed and the pore water pressure generated is relatively small. When the cement/soil ratio was the same, the decrease in initial water content made the soil stiffer, stronger and more overconsolidated as shown in Fig. 6 when compared to Fig. 5. In Fig. 6, a distinct peak of deviator stress-strain curve is observed. As shown in Fig. 6 the induced pore water pressure is very small and is slightly negative at large strain. Similar characteristics were reported by Kamaluddin and Balasubramaniam (1995).

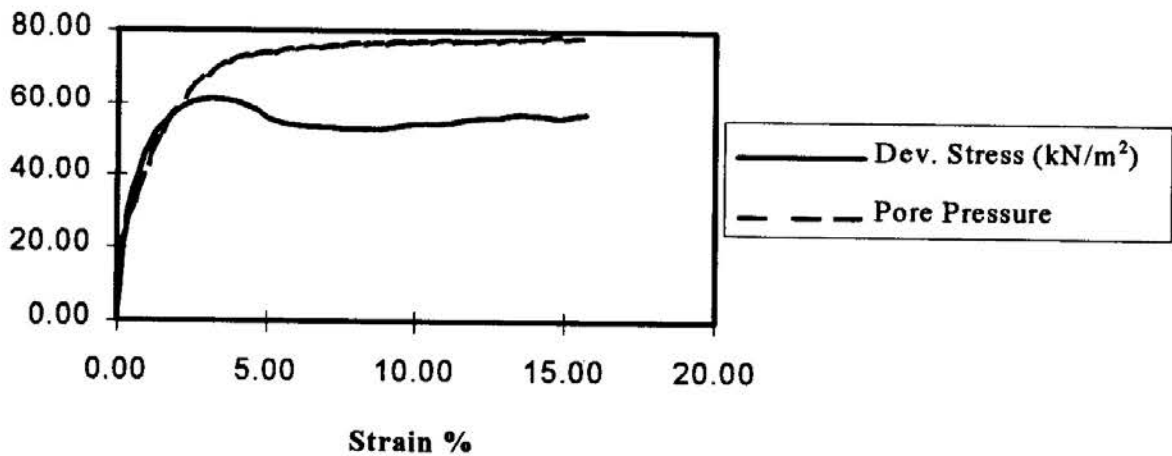


Fig. 4 Deviator Stress and Porewater Pressure vs. Axial Strain at $A_w = 5\%$, $w_i = 100\%$ and $\sigma_3 = 100$ kPa from CU test

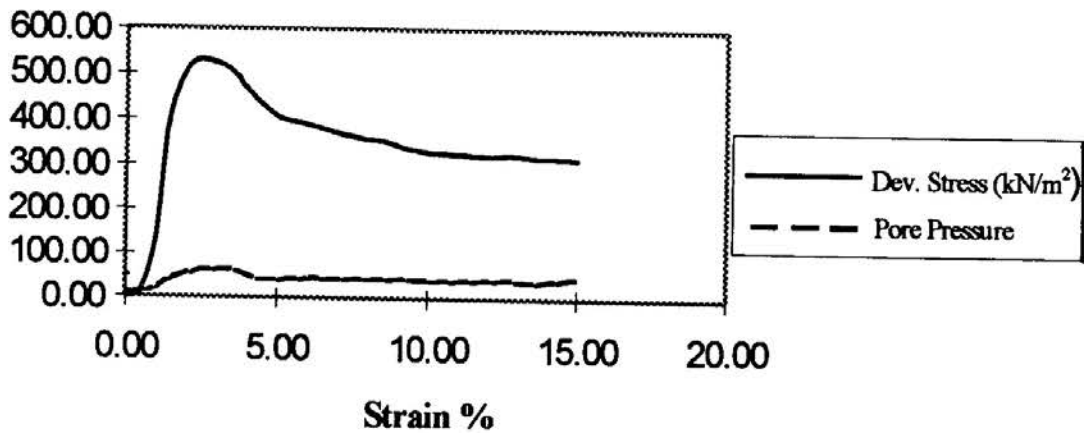


Fig. 5 Deviator Stress and Porewater Pressure vs. Axial Strain at $A_w = 20\%$, $w_i = 100\%$ and $\sigma_3 = 100$ kPa from CU test

STRENGTH AND STIFFNESS OF HONGKONG MARINE DEPOSITS

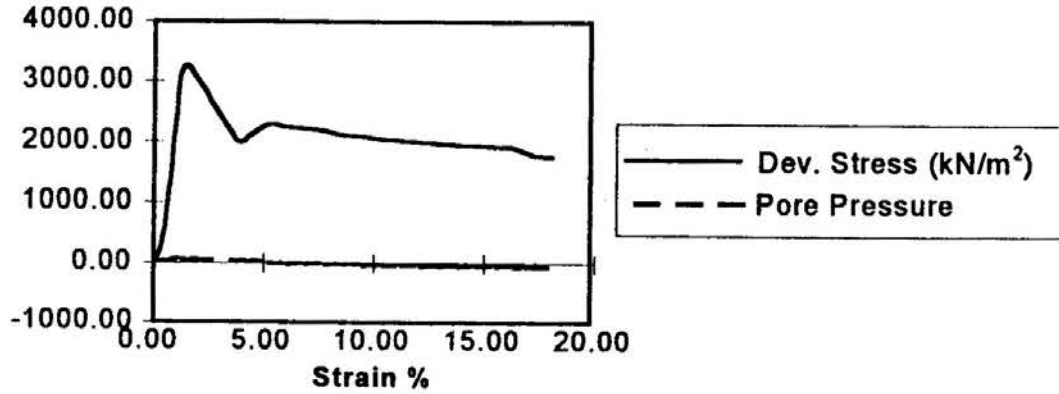


Fig. 6 Deviator Stress and Porewater Pressure vs. Axial Strain at $A_w = 20\%$, $w_i = 60\%$ and $\sigma_3 = 100$ kPa from CU test

ENHANCED STRENGTH AND STIFFNESS

As discussed in the preceding section, the initial water content of the marine deposits affects the stress-strain behavior of cement/soil mixture. The water content in the cement/soil mixture after mixing is normally smaller than the initial water content, depending on cement/soil ratio applied. The water reduction in specimens tested varied from 7% to 31%. Higher values of A_w and w_i lead to relatively higher reduction of water content after cementation. The reduction in water content is due to (a) addition of dry mass of cement and (b) hydration reaction. Higher initial water content means more free water for hydration reaction. Fig. 7 shows the relationships between water content (w) in cement/soil mixture measured after 28 days of cementation and the cement/soil ratio (A_w) and the initial water content (w_i) of the marine deposits.

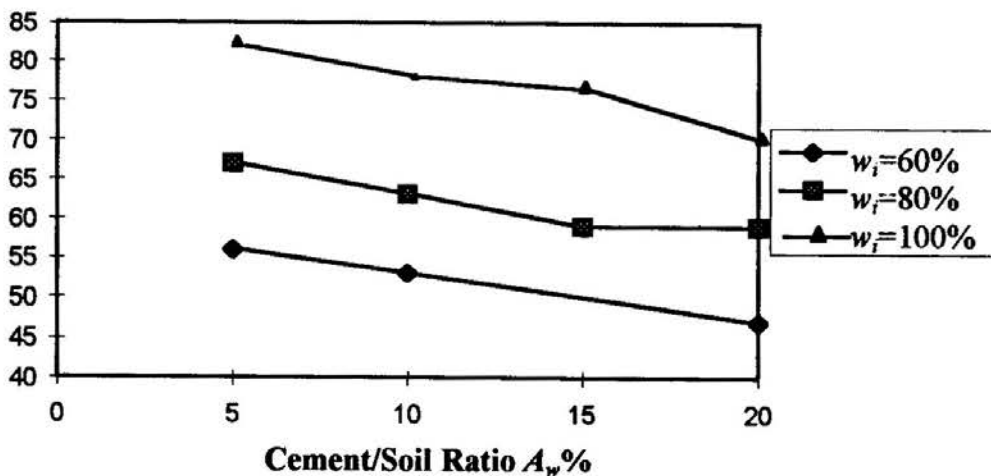


Fig. 7 Water Content of Cement Mixed M.D. after 28 Days

Test data from unconfined compression tests (UC) and consolidated undrained (CU) triaxial tests were used to derive undrained shear strength and Young's modulus as related to cement/soil ratio (A_w) and initial water content (w_i). Fig. 8 shows the relationship between peak deviator stress q_{peak} and cement/soil ratio (A_w) and initial water content (w_i). It is found that mixing only 5% ($A_w = 5\%$) cement with the marine deposits does not cause any significant increase of the peak strength. From this finding, a cement/soil ratio larger than 5%, for example 10% to 20% shall be used in order to make significant improvement of the soft Hong Kong marine deposits. It is seen in Fig. 8 that the peak deviator stress (q_{peak}) increases with the increase in cement/soil ratio (A_w) and the decrease in initial water content (w_i).

Figures 9, 10, 11 show relationships between the peak deviator stress (q_{peak}) and the cement/soil ratio (A_w) and initial water content (w_i) at effective confining stress $\sigma_3 = 100$ kPa, 200 kPa, and 400 kPa respectively from consolidated undrained (CU) triaxial tests. In general, the peak deviator stress q_{peak} increases with the increase in cement/soil ratio (A_w), decrease in the initial water content (w_i), and the confining stress (σ_3).

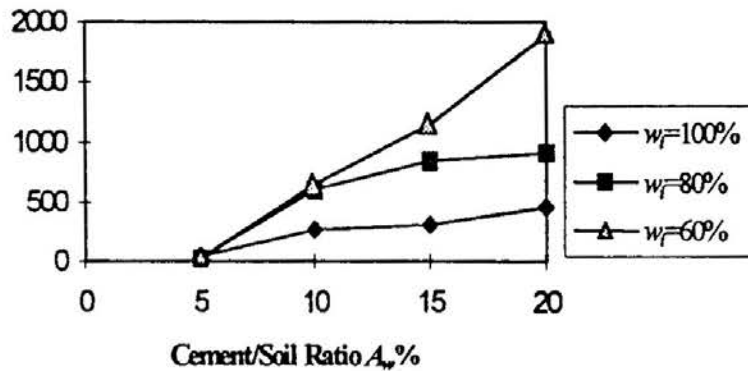


Fig. 8 Peak Deviator Stress q_{peak} vs. A_w and w_i from UC Tests

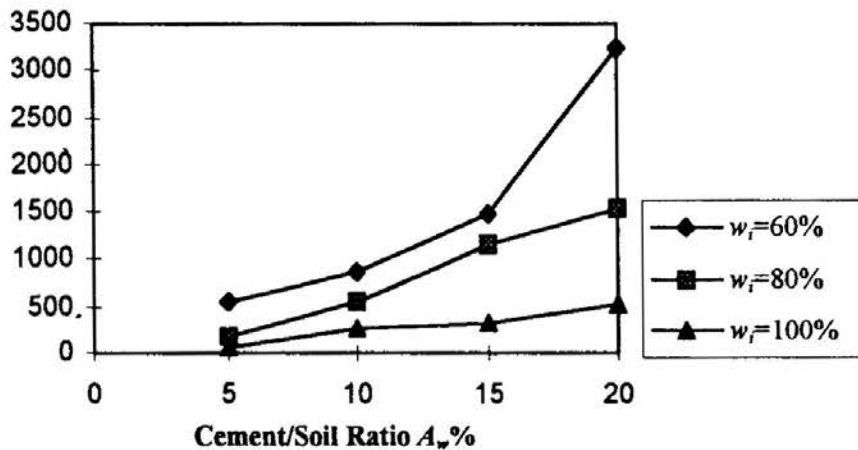


Fig. 9 Peak Deviator Stress q_{peak} vs. A_w and w_i at $\sigma_3 = 100$ kPa from CU Tests

STRENGTH AND STIFFNESS OF HONGKONG MARINE DEPOSITS

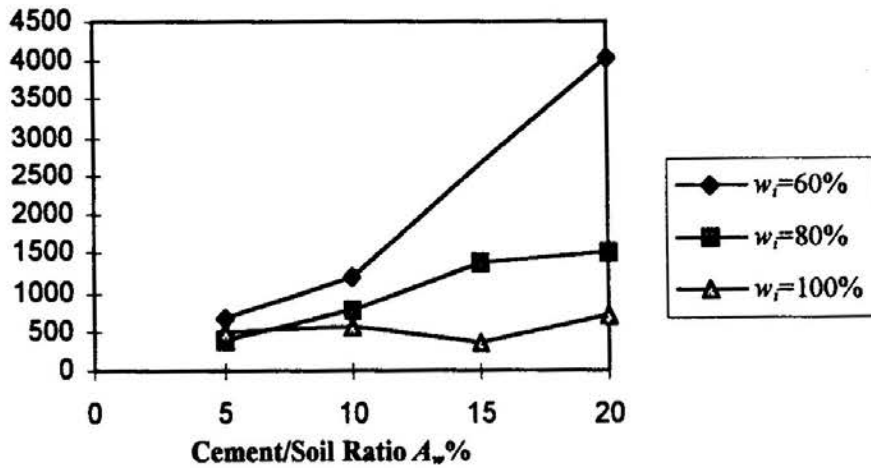


Fig. 10 Peak Deviator Stress q_{peak} vs. A_w and w_i at $\sigma_3 = 200$ kPa from CU Tests

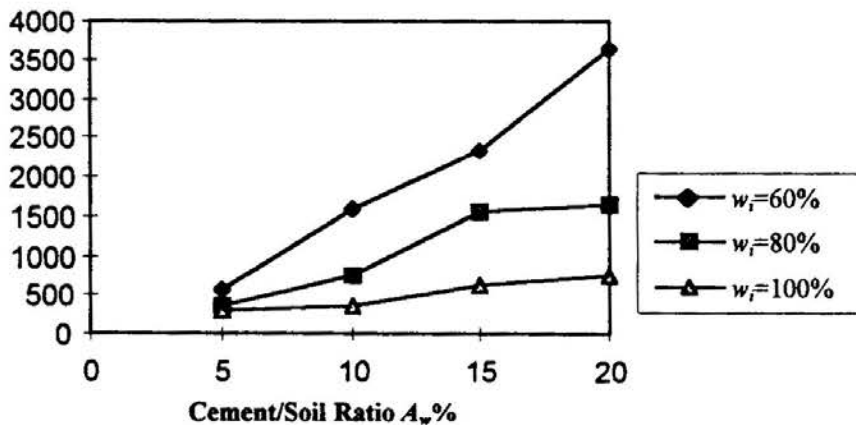


Fig. 11 Peak Deviator Stress q_{peak} vs. A_w and w_i at $\sigma_3 = 400$ kPa from CU Tests

As discussed in the preceding section, when the initial water content is low and the cement/soil ratio is high, the cement treated M.D. behaves like overconsolidated clay. For the cement treated M.D., like overconsolidated clay, the deviator stress (q) increases rapidly to a peak value at a strain of 0.7% to 2.5%, then gradually reduces to an almost unchanged constant value at large strain (>10%). This almost unchanged deviator stress at large strain is said here to be the residual deviator stress (q_{res}). The relationship between q_{res} and A_w and w_i are shown in Figs. 12, 13, and 14 for effective confining stress $\sigma_3 = 100$ kPa, 200 kPa, and 400 kPa. Similar to q_{peak} , q_{res} increases with the increase in A_w and the decrease in w_i .

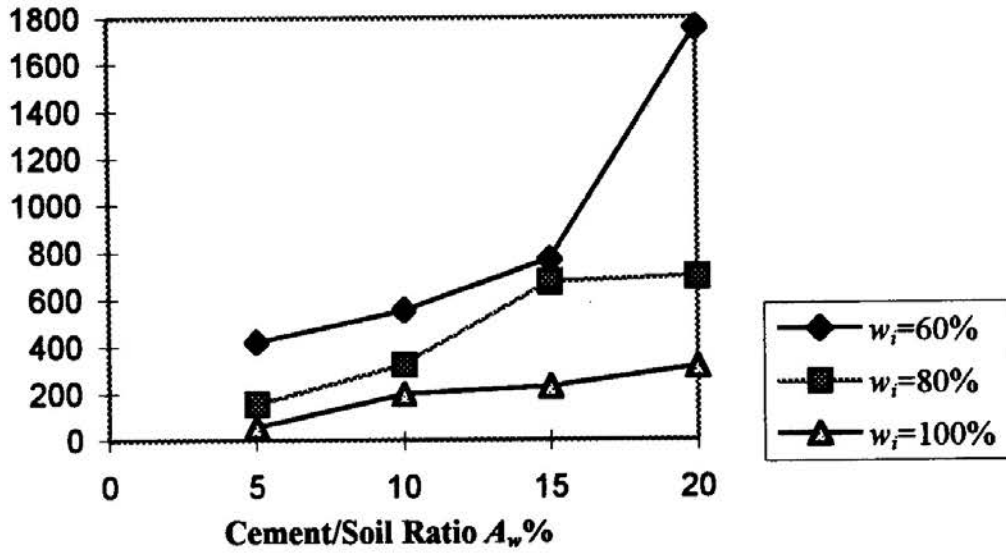


Fig. 12 Residual Deviator Stress q_{res} vs. A_w and w_i at $\sigma_3 = 100$ kPa from CU Tests

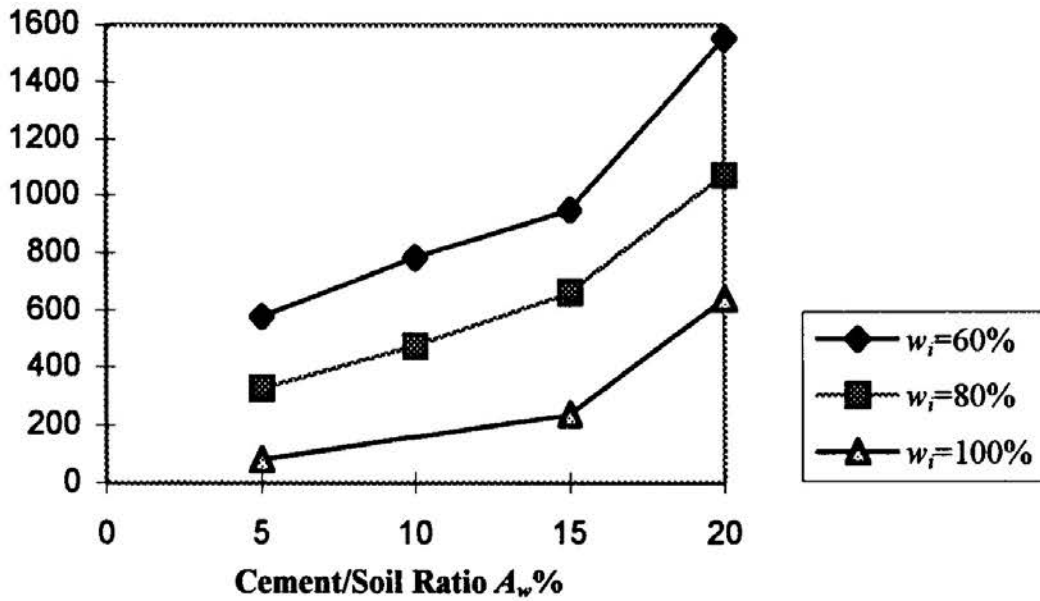


Fig. 13 Residual Deviator Stress q_{res} vs. A_w and w_i at $\sigma_3 = 200$ kPa from CU Tests

STRENGTH AND STIFFNESS OF HONGKONG MARINE DEPOSITS

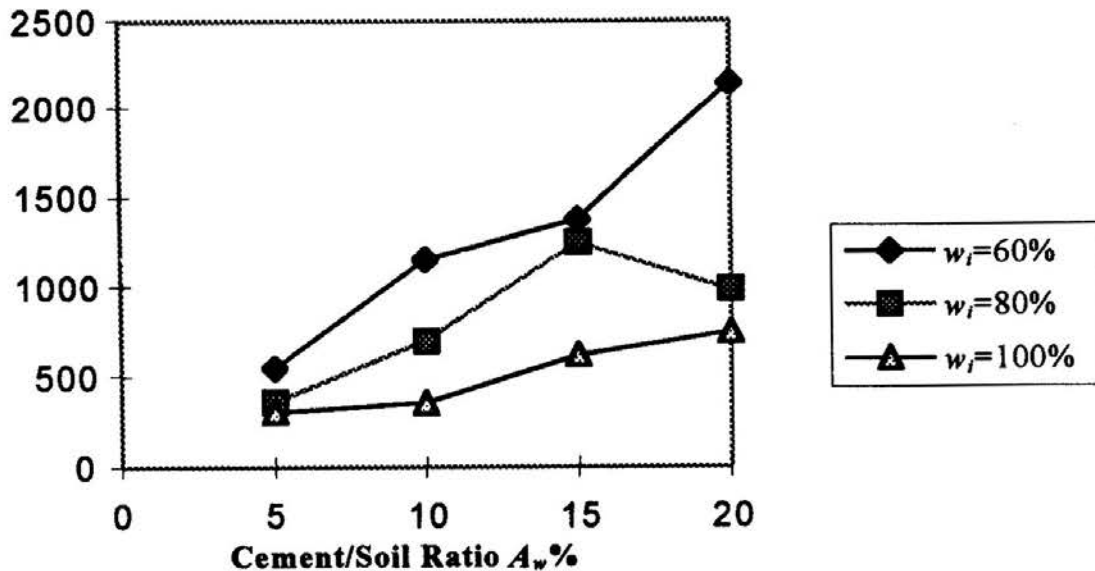


Fig. 14 Residual Deviator Stress q_{res} vs. A_w and w_i at $\sigma_3 = 400$ kPa from CU Tests

The relationships of (a) cohesion c' vs. A_w and w_i and (b) friction angle ϕ' vs. A_w and w_i are shown in Fig. 15 and Fig. 16. The cohesion c' increases with increase in A_w and decrease in w_i . The friction angle ϕ' decreases with increase in A_w and decrease in w_i . As cement content (or A_w ratio) increases, the cement treated soil shifts from a Mohr-Coulomb type of frictional materials towards a Von-Mises character with increase in c' and decrease in ϕ' .

The stress-strain relationship of the cement treated M.D. is non-linear. A simple way to describe the stiffness of the cement treated M.D. is to calculate the average Young's modulus E_{50} . E_{50} is defined as the ratio of q_{50}/ϵ_{50} where q_{50} is half of the peak deviator stress (q_{peak}) and ϵ_{50} is the axial strain corresponding to q_{50} , measured from the measured deviator stress-axial strain curve. The calculated E_{50} -values as related to A_w and w_i are shown in Figs. 17, 18 and 19 for confining pressure $\sigma_3 = 100$ kPa, 200 kPa and 400 kPa respectively. It is seen from these figures that Young's modulus E_{50} increases with increase in cement/soil ratio (A_w) and decrease in initial water content (w_i), similar to the peak deviator stress q_{peak} .

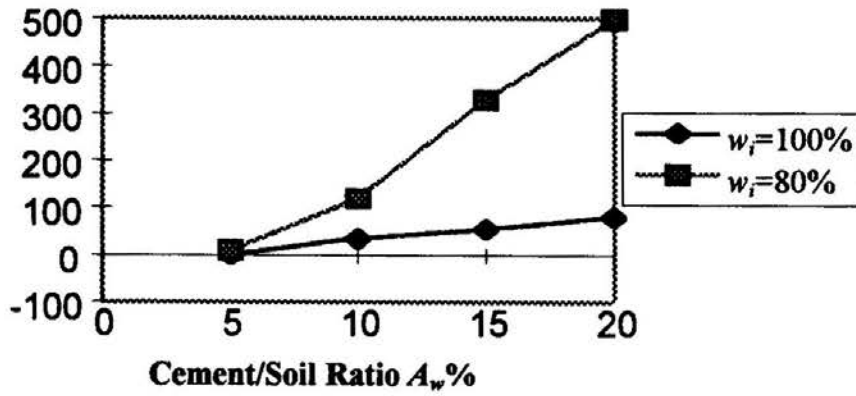


Fig. 15 Cohesion c' vs. A_w and w_i from CU Tests

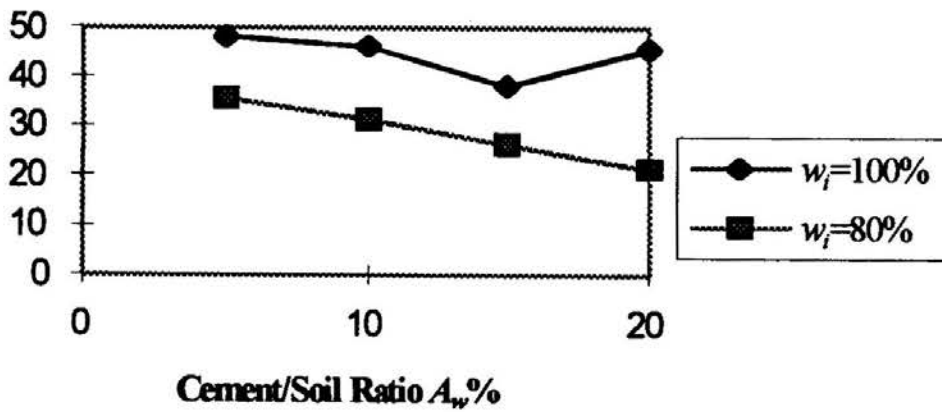


Fig. 16 Friction Angle ϕ' vs. A_w and w_i from CU Tests

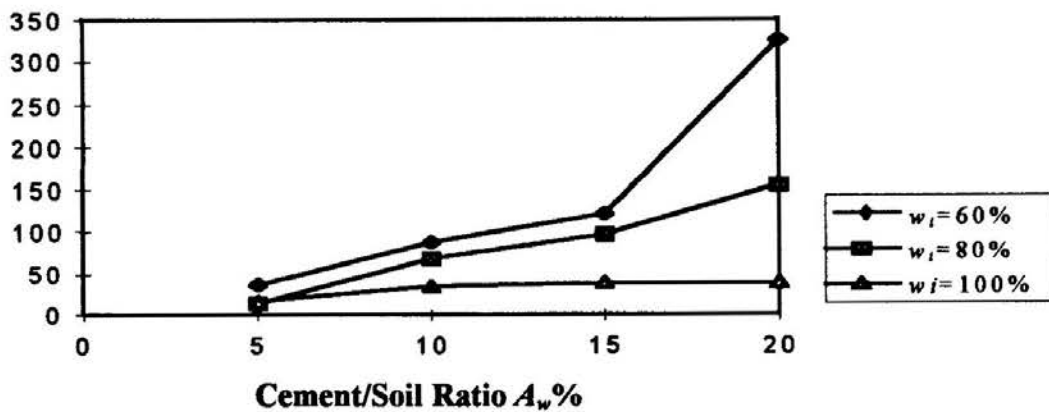


Fig. 17 Young's Modulus E_{50} vs. A_w and w_i at $\sigma_3=100\text{kPa}$ from CU Tests

STRENGTH AND STIFFNESS OF HONGKONG MARINE DEPOSITS

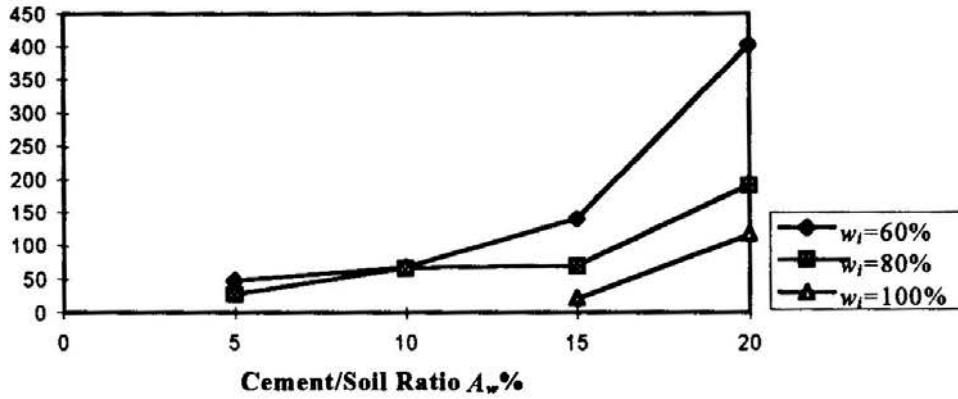


Fig. 18 Young's Modulus E_{50} vs. A_w and w_i at $\sigma_3 = 200$ kPa from CU Tests

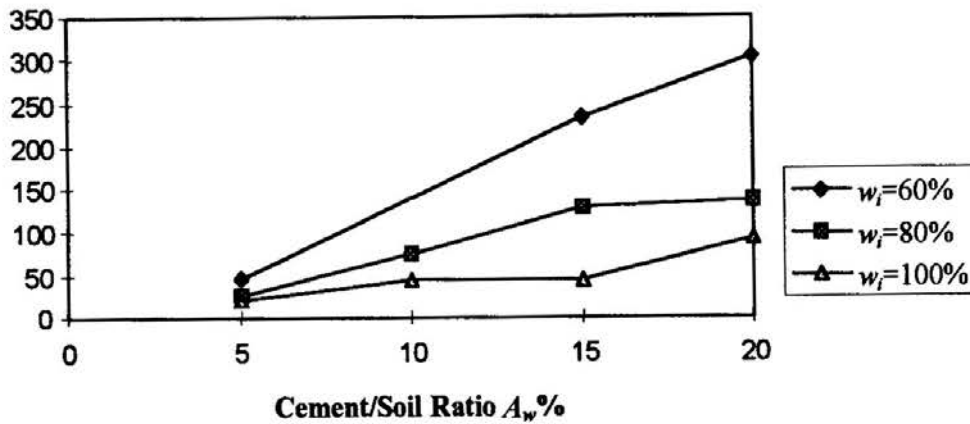


Fig. 19 Young's Modulus E_{50} vs. A_w and w_i at $\sigma_3 = 400$ kPa from CU Tests

It is seen from Figs.17, 18, 19 that the average Young's modulus E_{50} varied (a) from 10 MPa to 320 MPa for confining stress $\sigma_3 = 100$ kPa, (b) from 15 MPa to 410 MPa for $\sigma_3 = 200$ kPa, and (c) from 20 MPa to 300 MPa for $\sigma_3 = 400$ kPa. When the confining stress is too high, the cemented structure may be partially or fully destroyed and the resulting stiffness may be smaller than that of the M.D. with the same A_w and w_i but at a lower confining pressure. As mentioned in preceding section, E_{50} for untreated MD was 1.92 MPa, 13.0 MPa, 21.7 MPa for confining stress $\sigma_3 = 100$ kPa, 200 kPa and 400 kPa, respectively. Compared to the untreated M.D., the stiffness of cement treated M.D. was increased at various degree depending on A_w and w_i .

The correlation between E_{50} and q_{peak} is shown in Fig. 20. The relationship between E_{50} and q_{peak} can be expressed by

$$E_{50} = (35 \sim 180) q_{peak} \quad (1)$$

The mean value obtained by regression is

$$E_{50} = 89 q_{peak} \quad (2)$$

The correlation coefficient R^2 for the mean value in Fig. 20 is 0.91 indicating a good correlation. In Eq. (1), the ratio of E_{50}/q_{peak} is in the range from 35 to 180. A smaller ratio corresponds to lower A_w and higher w_i . While, a larger ratio corresponds to higher A_w and lower w_i . The correlation may be used to estimate Young's modulus of cemented treated soils if the consolidated undrained peak shear strength S_u is known since $S_u = q_{peak}/2$.

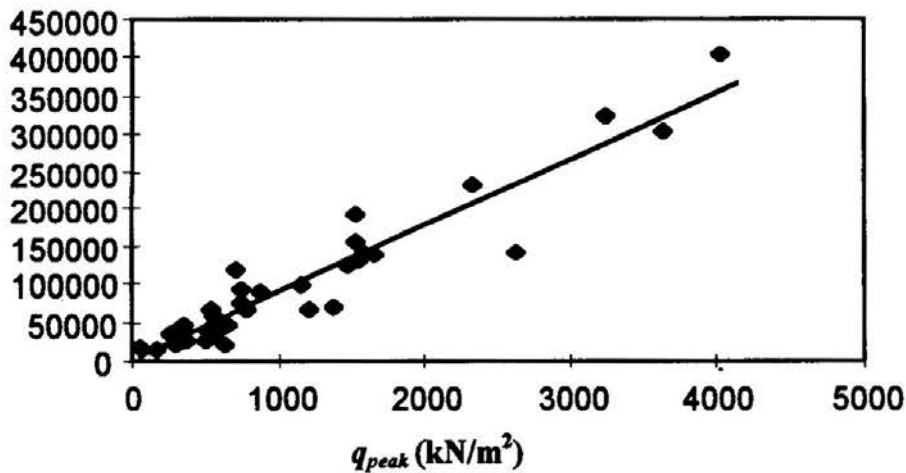


Fig. 20 Correlation between E_{50} and q_{peak}

REMARKS AND CONCLUSIONS

The preceding sections present (a) typical stress-strain curves, (b) shear strength and Young's modulus as related to the cement/soil ratio (A_w) and the initial water content (w_i) of a soft Hong Kong marine deposits mixed with cement and (c) correlation. From the test results, the following conclusions can be drawn on the general characteristics of the stress-strain-strength behavior of cement treated soils.

STRENGTH AND STIFFNESS OF HONGKONG MARINE DEPOSITS

1. Cement hardening/solidification in a soft soil changes the behavior of the soft soil from normally consolidated ductile behavior to overconsolidated behavior of relatively brittle and stiff.
2. The strength in terms of peak or residual deviator stresses (q_{peak} and q_{res}) and the stiffness in terms of average Young's modulus (E_{50}) from UC and CU tests increase with the increase in cement/soil ratio (A_w) and the decrease in initial water content (w_i) as well as the confining stress (σ_3) in CU tests.
3. The cohesion c' increases with the increase in A_w and the decrease in w_i . But the friction angle ϕ' decreases with the increase in A_w and the decrease in w_i . Adding more cement into the soil makes the cement treated soil to shift from a Mohr-Coulomb type of frictional materials to a Von-Mises character.
4. The Young's modulus (E_{50}) increases with the peak deviator stress q_{peak} or consolidated undrained shear strength S_u .

The following conclusions are considered specific for the soft Hong Kong marine deposits studied in this paper.

1. No significant improvement of the M.D. was obtained if using a cement/soil ratio $A_w = 5\%$ or less. The suggested A_w should be larger than 10%. However, too high a ratio may not be cost-effective.
2. The average Young's modulus E_{50} is correlated to q_{peak} by $E_{50} = 89q_{peak}$ for cemented treated Hong Kong marine deposits.

The quantitative relationships between the q_{peak} , q_{res} , E_{50} , c' and ϕ' and the A_w and w_i shown in the figures in this paper are specific for the M.D. tested under given test conditions. Those relationships may be used for similar soils and loading conditions. Caution must be exercised when applied or extended for other soils and in other test conditions. The shear strength q_{peak} and q_{res} and the stiffness modulus E_{50} normally increase with time but at a decrease rate. The time-dependent gain of the strength and stiffness is not studied in this paper. The improvement of the M.D. using cement in the field may not be the same as that measured in laboratory. However, results from laboratory tests provide a good understanding on the general stress-strain-strength characteristics and the effectiveness of the cement treatment. For field application, proper in-situ tests and quality assurance tests are recommended. Samples may be taken from in-situ cement treated soils for laboratory testing and evaluation.

YIN AND LAI

ACKNOWLEDGEMENT

The authors wish to thank Mr. Y.P. Leung, Mr. R. Leung, and Mr. G. Zhu for their assistance in laboratory testing program. Financial support from Research Grants Council of UGC of Hong Kong SAR Government of China and the Hong Kong Polytechnic University is gratefully acknowledged.

REFERENCES

- AAS, P.M. and ENGEN, A. (1993). Hong Kong seawall design study, *GEO Report No.30*, Geotechnical Engineering Office, Hong Kong.
- FENG, T.W. (1997). Postsolidification strength of a fine-grained soil. *Proceedings of the Second International Symposium on Structures and Foundations in Civil Engineering*, 7-10 January 1997, Hong Kong.
- KAMALUDDIN, M. and BALASUBRAMANIAM, A. S. (1995). Overconsolidated behavior of cement treated soft clay. *Proceedings of Tenth Asian Regional Conference on Soil Mechanics and Foundation Engineering*, pp. 407 - 412.
- KAWASAKI, T., NIINA, A., SAITOH, S., SUZUKI, Y., and HONJYO, Y. (1981). Deep mixing method using cement hardening agent. *Proceedings of the Tenth International Conference on Soil Mechanics and Foundation Engineering*, Vol. 1, pp. 721-724.

HYPERBOLIC MODEL PARAMETERS FOR MECHANICAL BEHAVIOR OF RECLAMATION SOILS

L.K. Chien¹ and Y.N. Oh²

ABSTRACT

In this study, based on a series of undrained triaxial tests, the fines content and relative density of sand were related to the hyperbolic model parameters to evaluate the influence of fines content on the mechanical behavior of reclaimed soil. The stress-strain curve obtained from the specimens prepared by moist tamping method and hydraulic sand fills method was used to obtain the relationships. From the analysis results a model was established to evaluate the mechanical behavior of reclaimed sandfill. From the results of the above-mentioned models, the stability of hydraulic filled land in Taiwan; and the influences of fines content and relative density on the mechanical behavior of the reclaimed soil can be evaluated. The results in this study may be a useful reference for geotechnical engineering stability analysis in coastal engineering designs and constructions, and for research purposes.

INTRODUCTION

Hydraulic sand fills is one of the most important reclamation method for coastal life space utilization. The arrangement of soil fabric and fines content would influenced the reclaimed soil behavior. In this study, the specimen soil was obtained from in-situ material in nearshore reclamation area of Yun-Lin Industrial Estate (Fig. 1). In the phenomena of soil masses and soil particles, the stress-strain relationship has been an important index in describing the soil behavior. In the past, before the rapid development of computers and numerical method, it was not feasible to perform analyses of stresses in soil particles for other than assumed linear elastic soil behavior. However, now with the availability of high speed computers and powerful numerical analytical techniques, it is possible to perform nonlinear, nonelastic stress analyses of soils. Thus, the stress-strain behavior of soil can be described in more details.

Numerical analysis methods have been widely applied in the geotechnical field. To describe the non-linear stress-strain relationship curve of soil in a satisfactory model, the success of the simulation method should be studied. In this paper, based on a series of

1 Associate Professor, Department of Harbor and River Engineering, National Taiwan Ocean University, 2 Pei-Ning Road, Keelung, Taiwan R.O.C.

2 Former Graduate Student, Department of Harbor and River Engineering, National Taiwan Ocean University, 2 Pei-Ning Road, Keelung, Taiwan R.O.C.

Note: Discussion is open until 1 September 1998. This paper is part of the *Geotechnical Engineering Journal*, Vol. 29, No. 1, June 1998. Published by the Southeast Asian Geotechnical Society, ISSN 0046-5828.

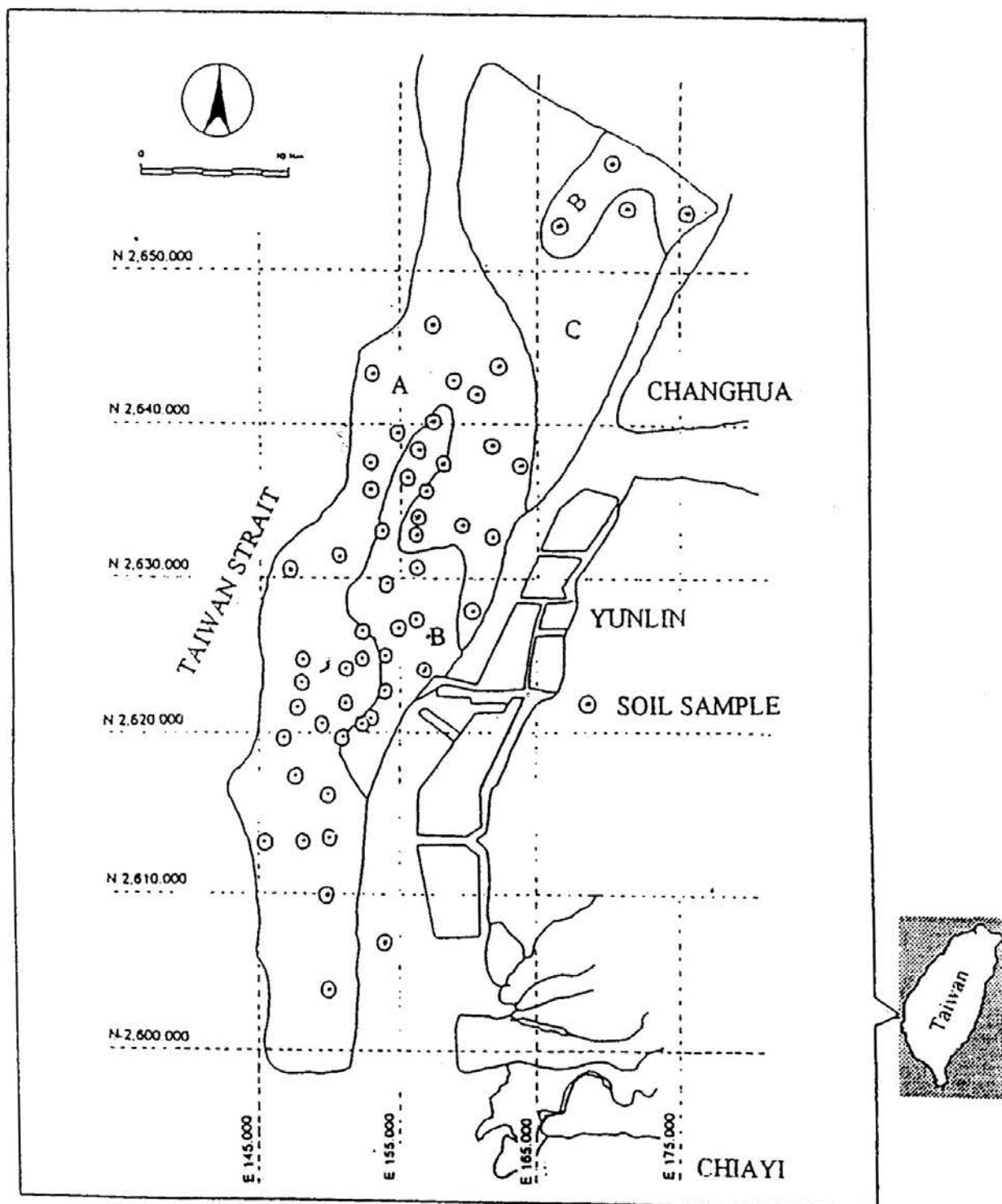


Fig. 1 Sketch of Soil Sampling in Yunlin Offshore Area of Taiwan (Sinotech, 1990)

HYPERBOLIC MODEL PARAMETERS

consolidated undrained triaxial test results, a hyperbolic model for non-linear analysis is developed, to perform the nonlinear stress-strain analysis for reclaimed soil. The influences of fines content on the mechanical behavior of reclaimed soil is discussed.

NONLINEAR HYPERBOLIC MODEL

In recent studies, Kondner (1970), Duncan, et al. (1970), Desai (1971) and Hansen (1963) have shown that the undrained stress-strain behavior of soil, can be described by a hyperbolic model. In this study, using the test results obtained from triaxial test, based on the deviator stress and axial strain, a nonlinear hyperbolic model is developed, to predict the deviator stress-strain relationship of triaxial test with different confining pressure, for the reclaimed sands.

The earliest concept on nonlinear hyperbolic model was introduced by Kondner in 1963. Kondner (1963) have shown that the nonlinear stress-strain of soil can be approximated by hyperbolae with a high degree of accuracy. Duncan and Chang (1970) later combined the hyperbolae with the finite element method. As shown in Fig. 2, a hyperbolic stress-strain curve is illustrated, and can be represented by the following equations:

$$(\sigma_1 - \sigma_3) = \varepsilon / (a + b\varepsilon) \quad (1)$$

where, σ_1 is the major principal stress, σ_3 is the minor principal stress; ε is the axial strain; a and b are the constants which can be determined by experiments.

The stress-strain curve can be written as:

$$\varepsilon / (\sigma_1 - \sigma_3) = 1 / E_i + \varepsilon / (\sigma_1 - \sigma_3)_{ult} = a + b\varepsilon \quad (2)$$

The stress-strain relationship in Eq. (2) can be expressed by Fig. 3. Theoretically, the stress-strain curve can be transformed and can be plotted in a straight line. But the linear relationship is not satisfactory. Therefore, Duncan and Chang (1970) proposed a two-point fitting method, and a stress level S is given.

In 1963, experimental studies conducted by Janbu (1963) have shown that the relationship between initial tangent modulus and confining pressure can be expressed as:

$$E_i = k P_a (\sigma_3 / P_a)^n \quad (3)$$

where, P_a is the atmospheric pressure (atm), E_i is tangent modulus, k is a modulus number and n is the exponent determining the rate of variation of E_i with σ_3 .

It is commonly found that the value of compressive strength $(\sigma_1 - \sigma_3)_f$ is smaller than the hyperbolic value or stress differences $(\sigma_1 - \sigma_3)_{ult}$. Therefore, a failure ratio R_f is shown as

CHIEN and OH

$$R_f = (\sigma_1 - \sigma_3)_f / (\sigma_1 - \sigma_3)_{ult} \quad (4)$$

In terms of Mohr-Coulumb Failure Criteria, the relationship between compressive strength and confining pressure, can be expressed as:

$$(\sigma_1 - \sigma_3)_f = (2c \cos \phi + 2 \sigma_3 \sin \phi) / (1 - \sin \phi) \quad (5)$$

where, c and ϕ is the Mohr-Coulomb strength parameters.

If the value of minor principal stress is constant, the tangent modulus can be expressed as:

$$E_t = \partial (\sigma_1 - \sigma_3) / \partial \epsilon \quad (6)$$

Substituting Eq. (3) and Eq. (5) into Eq. (6), the tangent modulus may be expressed as:

$$E_t = [1 - \{R_f (1 - \sin \phi) (\sigma_1 - \sigma_3) / (2c \cos \phi + 2 \sigma_3 \sin \phi)\}]^2 k P_a (\sigma_3 / P_a)^n \quad (7)$$

thus the tangent modulus is expressed as a function $E_t = f(R_f, c, \phi, k, n, \sigma_1, \sigma_3)$. The tangent modulus at any stress conditions can be determined by evaluating all the required parameters in Eq. (7). Using the tangent modulus, the deviator stress at any point can be determined, with the corresponding axial strain. Thus, the stress-strain relation of soil can be simulated.

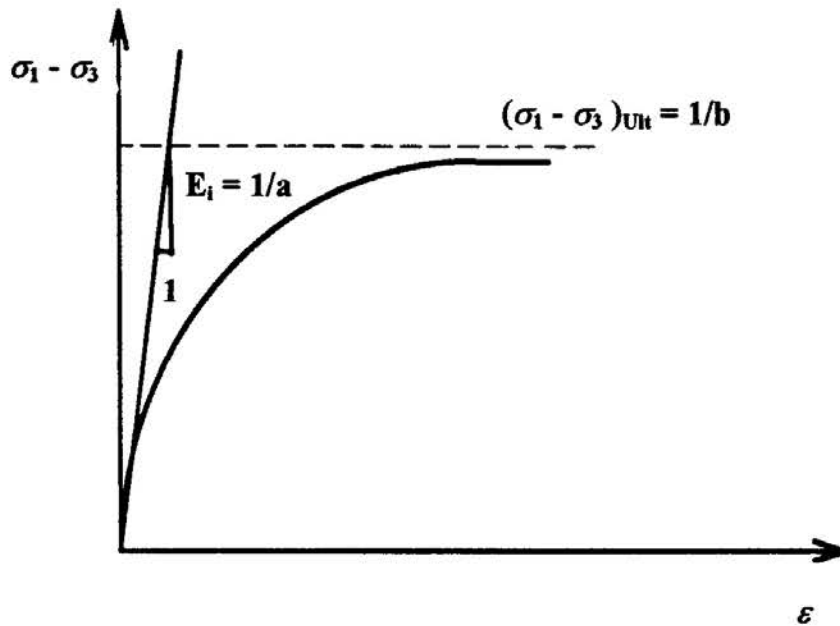


Fig. 2 Hyperbolic Stress-Strain Curve

HYPERBOLIC MODEL PARAMETERS

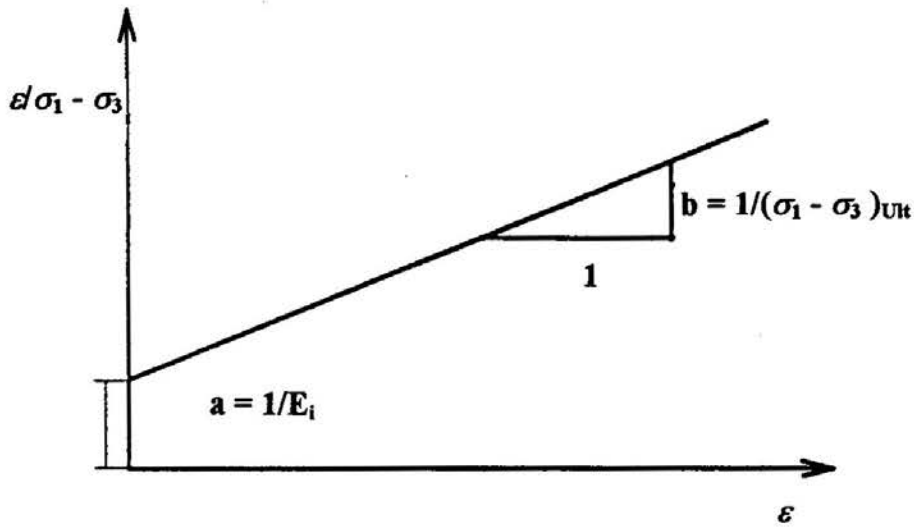


Fig. 3 Transformed Hyperbolic Stress-Strain Curve

INFLUENCE OF FINES CONTENT ON STRESS-STRAIN BEHAVIOR OF RECLAIMED SOIL

As mentioned above, the nonlinear hyperbolic model analysis is based on experimental data and results. Using the required mathematical formulas, the hyperbolic stress-strain model is developed to predict the stress-strain relation curve under different confining pressures. In this study, the soil samples were obtained from Yun-Ling offshore area in west coast Taiwan. The index properties and grain size distribution of the sand used are shown in Table 1. A series of consolidated-undrained triaxial test were conducted by Tsai (1994) and the authors. The experimental results showed that the stress-strain relationships have a good agreement with the hyperbolic relations. It was found that, under different fines content, there are differences in the stress-strain relation as shown in Fig. 4. Therefore, this showed that the fines content is an important factor influencing the mechanical behavior of reclaimed soil.

Table 1 Index Properties of Test Sample

Properties	Values			
Fines content (<i>F.C.</i>)(Grain Size < 0.075mm)	0 %	10 %	20%	30%
Specific gravity, <i>G_s</i>	2.691	2.696	2.698	2.701
Maximum dry density (g/cm ³)	1.590	1.680	1.760	1.790
Minimum dry density (g/cm ³)	1.199	1.205	1.214	1.197
<i>D₅₀</i> (mm)	0.164	0.155	0.146	0.137
<i>D₆₀</i> (mm)	0.169	0.165	0.157	0.155
<i>D₃₀</i> (mm)	0.138	0.129	0.109	0.074
<i>D₁₀</i> (mm)	0.100	0.074	0.046	0.025
Coefficient of uniformity, <i>C_u</i> = <i>D₆₀</i> / <i>D₁₀</i>	1.688	2.232	3.393	6.306
Coefficient of curvature, <i>C_c</i> = <i>D₃₀</i> ² / <i>D₆₀</i> <i>D₁₀</i>	1.347	1.353	1.630	1.477

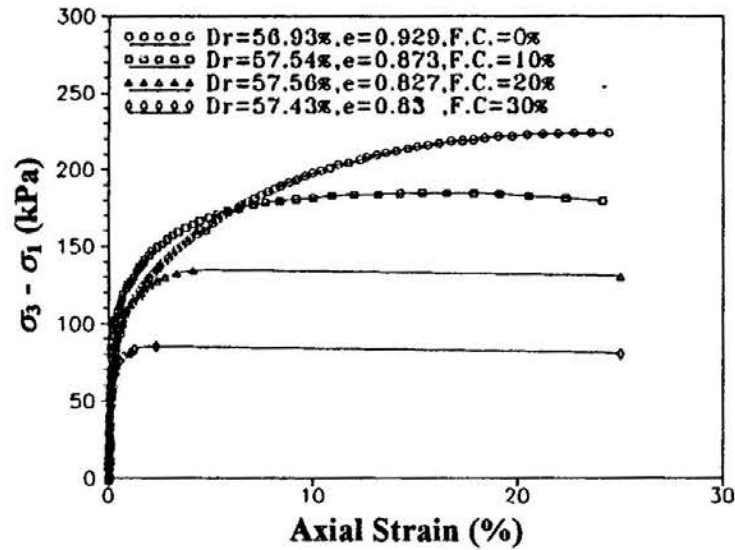


Fig. 4 Stress-Strain Relationship of Consolidated Undrained Triaxial Test (Moist Tamping Method)

Hyperbolic Model of Stress-Strain Relationship for Reclaimed Soil

The test specimen is prepared by moist tamping method with different relative density (35%, 55%, 70%), different confining pressure and different fines content (0%, 10%, 20%, 30%). Weight of the specimen and weight of fines are provided as a component to control the fines content. After the specimen is prepared, a vacuum of 19.6 kPa was applied on the top drain lead of the cell. The molds were then taken apart. Carbon dioxide was allowed to pass through the specimen for about 2 hours. In order for the carbon dioxide to be fully dissolved, water was allowed to pass through the specimen for about 3 hours. In order to obtain a 95% saturation, a back water pressure of 196 kPa was applied. After the consolidation process, a series of consolidated undrained triaxial tests was performed.

The stress-strain relation curve adopted from the consolidated undrained triaxial test for reclaimed soil were transformed, and re-expressed in linear relation. Based on the two point method proposed by Duncan and Chang (1970) and, Daniel and Olson (1974), the parameters such as *a* and *b* were determined. The parameters required for nonlinear hyperbolic model such as *k*, *n*, *φ* and *R_f* were determined (Table 2). Here, the reclaimed soil is mostly classified as silts and sand, and the fines are cohesionless. According to the experimental results conducted by Tsai (1994), the shear strength parameters of reclaimed soil is determined to be *c* = 0 kg/cm² and *φ* = 34.1°. Therefore, in this study, the strength parameter is defined as *c* = 0. Thus, Eq. (7) can be rewritten as

$$E_t = [1 - \{ R_f (1 - \sin \phi) (\sigma_1 - \sigma_3) / (2 \sigma_3 \sin \phi) \}]^2 k P_a (\sigma_3 / P_a)^n \quad (8)$$

HYPERBOLIC MODEL PARAMETERS

Taking the thickness of the reclaimed soil (10m~20m) into consideration, the confining pressure is assumed to be 98 kPa (1kg/cm²) to represent field confining pressure at mid-depth.

Table 2 The Calculated Results of Related Parameters for Hyperbolic Model Based on Two Points Method (70%, 95%) (Moist Tamping Method)

Initial Relative density <i>Dr</i> (%)	Fines content F.C.(%)	The related parameters for the hyperbolic model			
		<i>k</i>	<i>n</i>	ϕ	<i>R_f</i>
35	0.000	0.108	7.055	18.120	0.881
	10.000	-0.310	14.539	17.664	0.946
	20.000	-0.880	11.885	17.296	0.893
	30.000	-1.834	17.497	16.577	0.967
55	0.000	2.144	1.057	32.202	0.895
	10.000	0.805	3.395	29.020	0.969
	20.000	1.252	4.595	23.993	0.927
	30.000	0.283	9.893	17.655	0.999
70	0.000	1.999	0.595	39.859	0.668
	10.000	1.082	1.789	36.777	0.909
	20.000	0.983	3.378	32.613	0.896
	30.000	0.540	4.208	28.504	0.997

Relative Density in Hyperbolic Model

Under different relative density, the mechanical behavior of sand would have different results. In this study, the influence of relative density and fines content is considered in the hyperbolic model. Under different fines content (the relative density is set to be 55% as an index), the parameters for the model are determined. The results are shown in Figs. 5 – 8, and the relationships can be expressed by the following equations.

Under different fines content, the relationship between the parameter *k* and relative density (*Dr*) are expressed in Table 3. The relationship between the parameter *n* and relative density (*Dr*) with different fines content are shown in Table 4. The relationship between the parameter *f* and relative density (*Dr*) with different fines content are expressed in Table 5. For different fines content, the relationship between the parameter *R_f* and relative density (*Dr*) are illustrated in Table 6. Substituting the above parameters in to Eq. (8), with the changes in relative density, the stress-strain behavior of reclaimed soil under different density can be estimated.

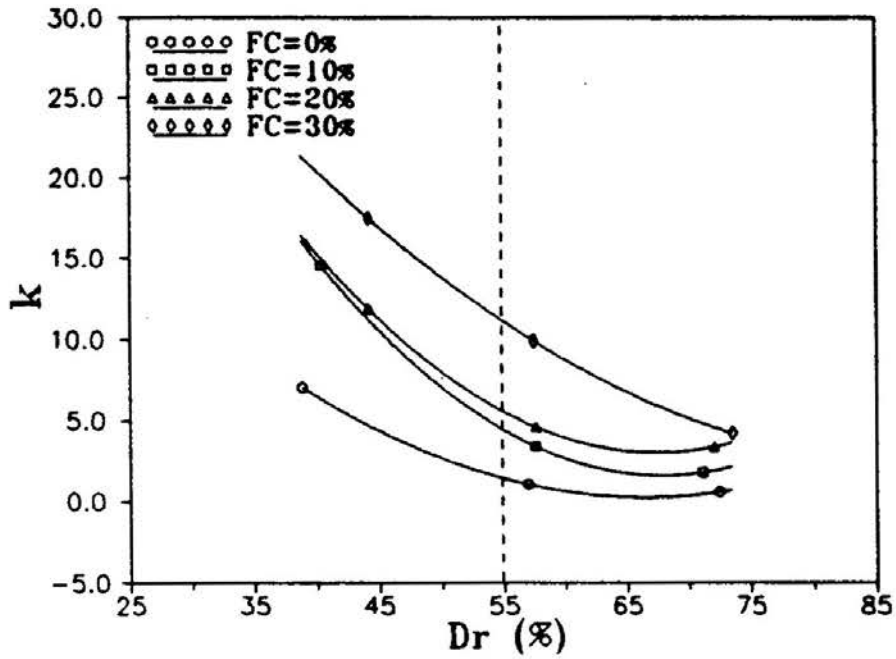


Fig. 5 Relationship Between Parameter k with Relative Density Under Different Fines Content

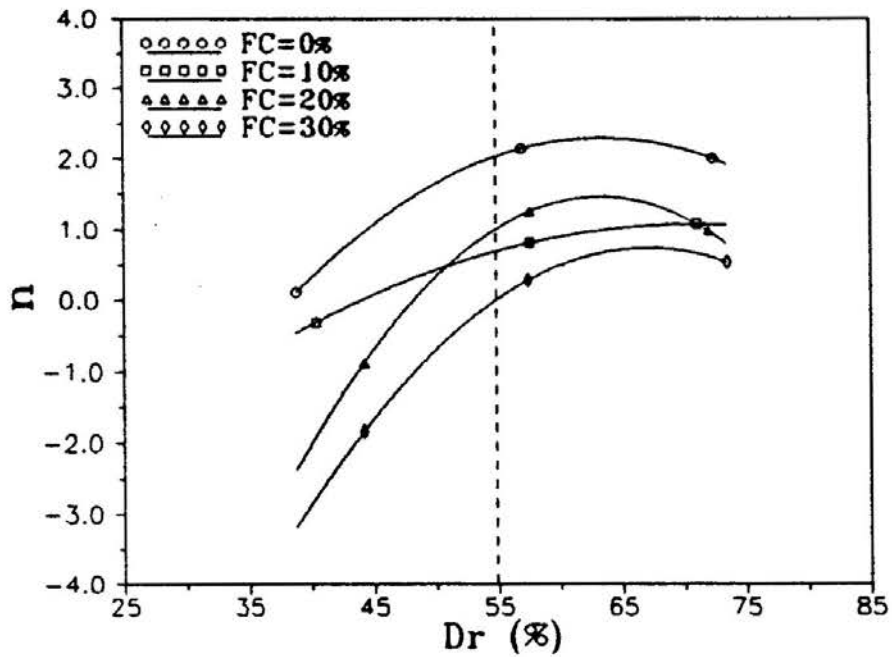


Fig. 6 Relationship Between Parameter n with Relative Density Under Different Fines Content

HYPERBOLIC MODEL PARAMETERS

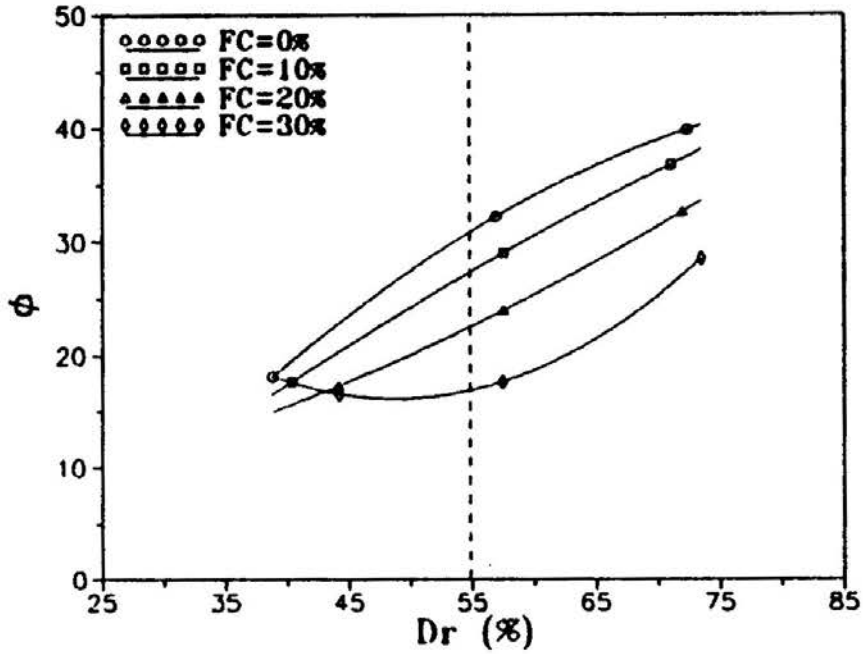


Fig. 7 Relationship Between Parameter ϕ with Relative Density Under Different Fines Content

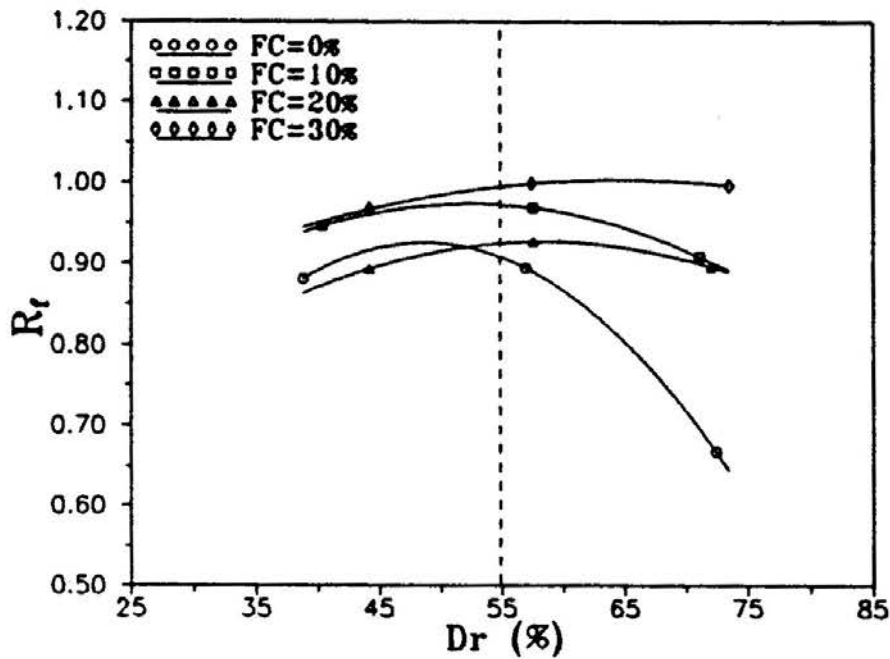


Fig. 8 Relationship Between Parameter R_f with Relative Density Under Different Fines Content

Table 3 The Relationship Between the Parameter k and Different Fines Content (FC) with Relative Density (Dr)

F.C.(%)	k
0	$1.419-0.204(Dr-55)+0.00897(Dr-55)^2$
10	$4.407-0.44(Dr-55)+0.0173(Dr-55)^2$
20	$5.534-0.407(Dr-55)+0.0165(Dr-55)^2$
30	$11.092-0.338(Dr-55)+0.00519(Dr-55)^2$

Table 4 The Relationship Between the Parameter n and Different Fines Content (FC) with Relative Density (Dr)

F.C.(%)	n
0	$2.036+0.0606(Dr-55)-0.00361(Dr-55)^2$
10	$0.699+0.0474(Dr-55)-0.00148(Dr-55)^2$
20	$1.02+0.106(Dr-55)-0.00639(Dr-55)^2$
30	$0.0239+0.009(Dr-55)-0.0049(Dr-55)^2$

Table 5 The Relationship Between the Parameter f and Different Fines Content (FC) with relative density (Dr)

FC(%)	ϕ
0	$30.964+0.652(Dr-55)-0.0084(Dr-55)^2$
10	$27.445+0.627(Dr-55)-0.00287(Dr-55)^2$
20	$22.616+0.529(Dr-55)-0.00354(Dr-55)^2$
30	$16.924+0.251(Dr-55)-0.0203(Dr-55)^2$

HYPERBOLIC MODEL PARAMETERS

Table 6 The Relationship Between the Parameter R_f and Different Fines Content (FC) with relative density (D_r)

FC(%)	R_f
0	$0.908-0.00581(D_r-55)-0.00046(D_r-55)^2$
10	$0.973-0.000941(D_r-55)-0.000188(D_r-55)^2$
20	$0.925+0.00114(D_r-55)-0.000168(D_r-55)^2$
30	$0.995+0.00169(D_r-55)-0.000087(D_r-55)^2$

Fines Content in Hyperbolic Model

Under different fines content, the equations showing the relationship between the required parameters and relative density for hyperbolic model can be rewritten, to discuss the influence of fines content on reclaimed soil.

$$k = A_1 + A_2(D_r - 55) + A_3(D_r - 55)^2 \quad (9)$$

$$n = B_1 + B_2(D_r - 55) + B_3(D_r - 55)^2 \quad (10)$$

$$\phi = C_1 + C_2(D_r - 55) + C_3(D_r - 55)^2 \quad (11)$$

$$R_f = D_1 + D_2(D_r - 55) + D_3(D_r - 55)^2 \quad (12)$$

where, $A_1, A_2, A_3, B_1, B_2, B_3, C_1, C_2, C_3, D_1, D_2, D_3$ is the related constants in Table 3 to Table 6.

Combining the above constants ($A_1 \sim D_3$) with Table 3 to Table 6, for different fines content, the results are shown in Fig. 9 to Fig. 20. The relations between fines content and the related constants are illustrated in Table 7.

Based on the above equations, the appropriate $A_1 \sim D_3$ constants are selected with different fines content. The related parameters for hyperbolic model can be determined by substituting the constants into the related equations with parameters k, n, ϕ and R_f (Eq. (9) ~ Eq. (12)). Considering the influences of fines content and relative density on the mechanical behavior of reclaimed soil, the stress-strain relation curve for reclaimed soil under different experimental conditions can be predicted.

In this study, the influence of confining pressure, relative density and fines content are considered, or the development of the hyperbolic model. Therefore, a

function $E_t = f(R_f, \phi, k, n, \sigma_1, \sigma_3, D_r, F.C.)$ is defined. Using the proposed model, calculations were done in the computers. Comparisons between model analysis results and test results are made as shown in Fig. 21 ~ Fig. 23. As shown in the figures, the simulated stress-strain relationships curves for reclaimed soil have reasonable good agreement with the test results.

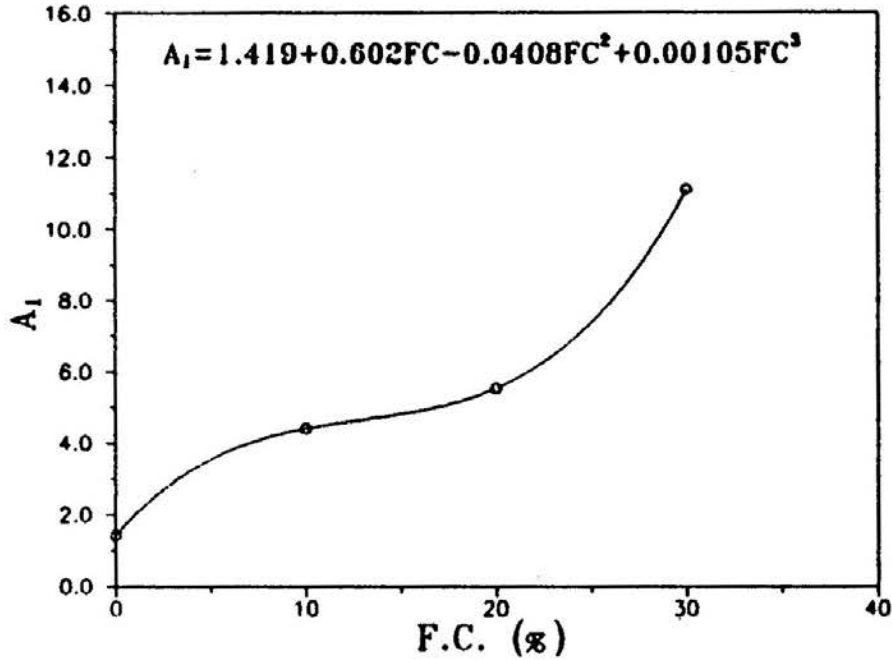


Fig. 9 Relationship Between the Constant A_1 with Fines Content

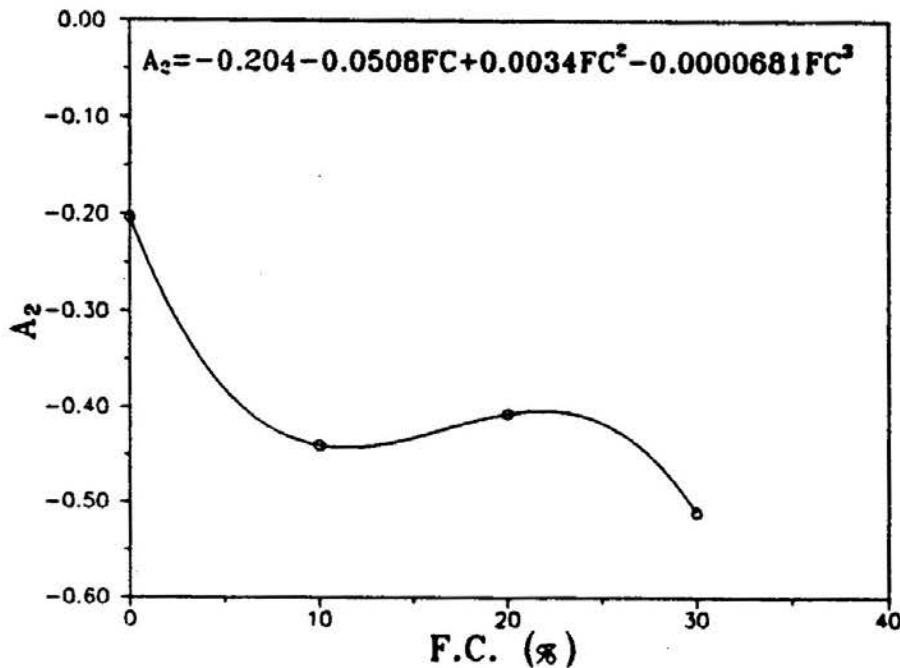


Fig. 10 Relationship Between the Constant A_2 with Fines Content

HYPERBOLIC MODEL PARAMETERS

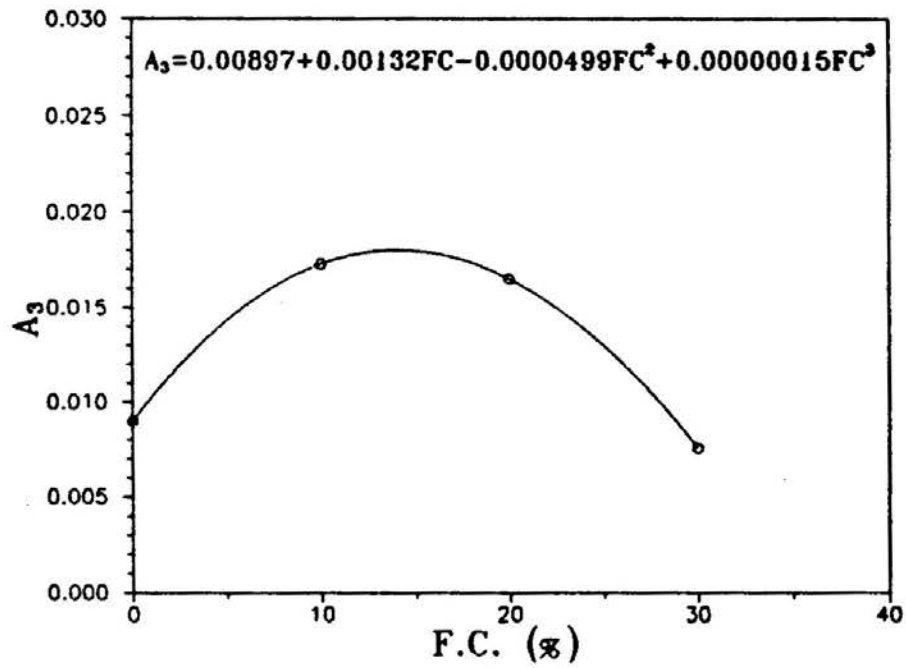


Fig. 11 Relationship Between the Constant A_3 with Fines Content

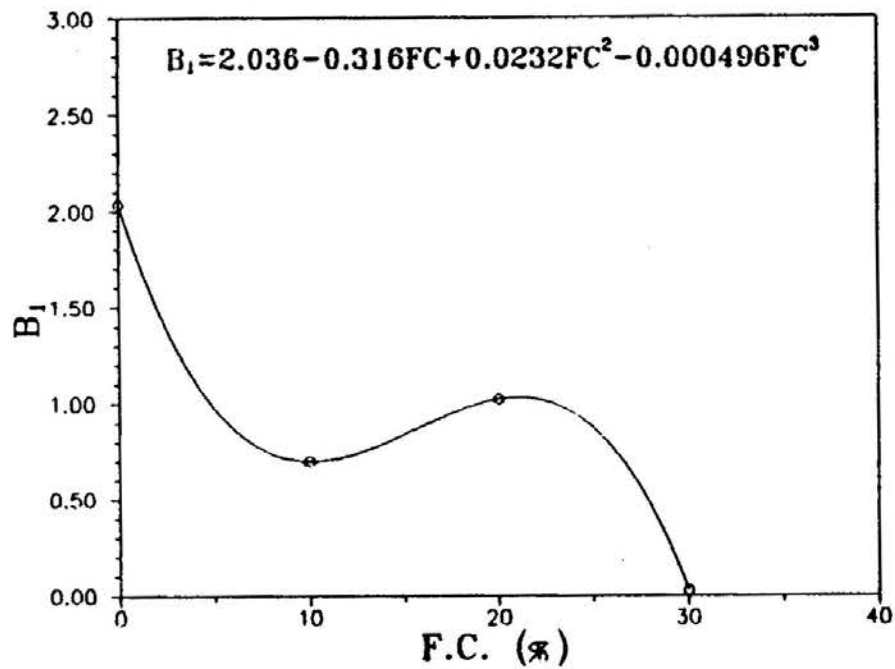


Fig. 12 Relationship Between the Constant B_1 with Fines Content

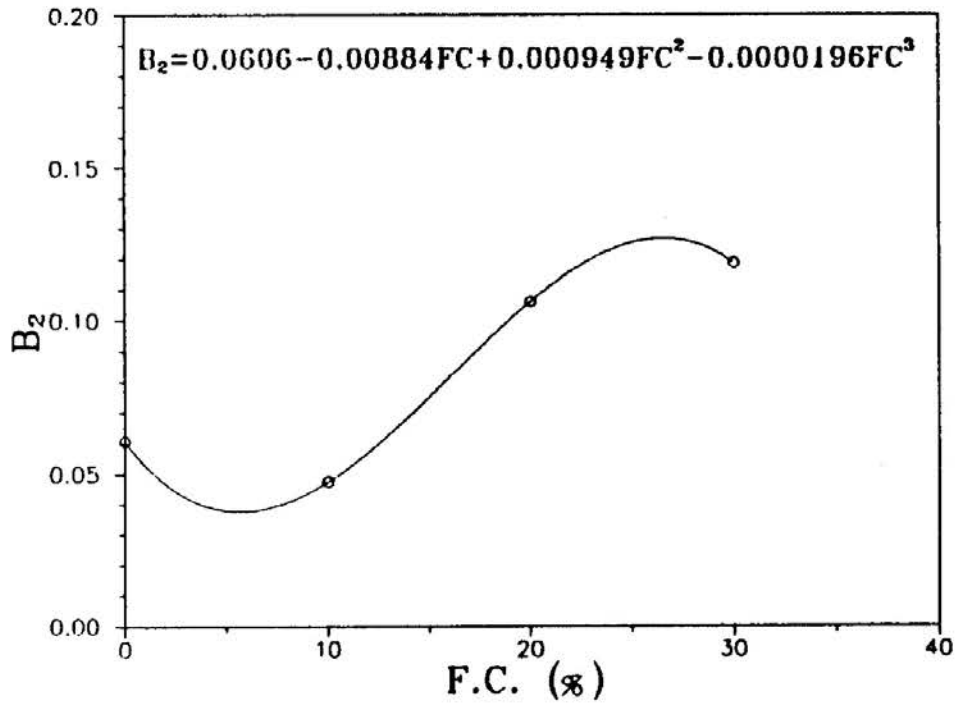


Fig. 13 Relationship Between the Constant B_2 with Fines Content

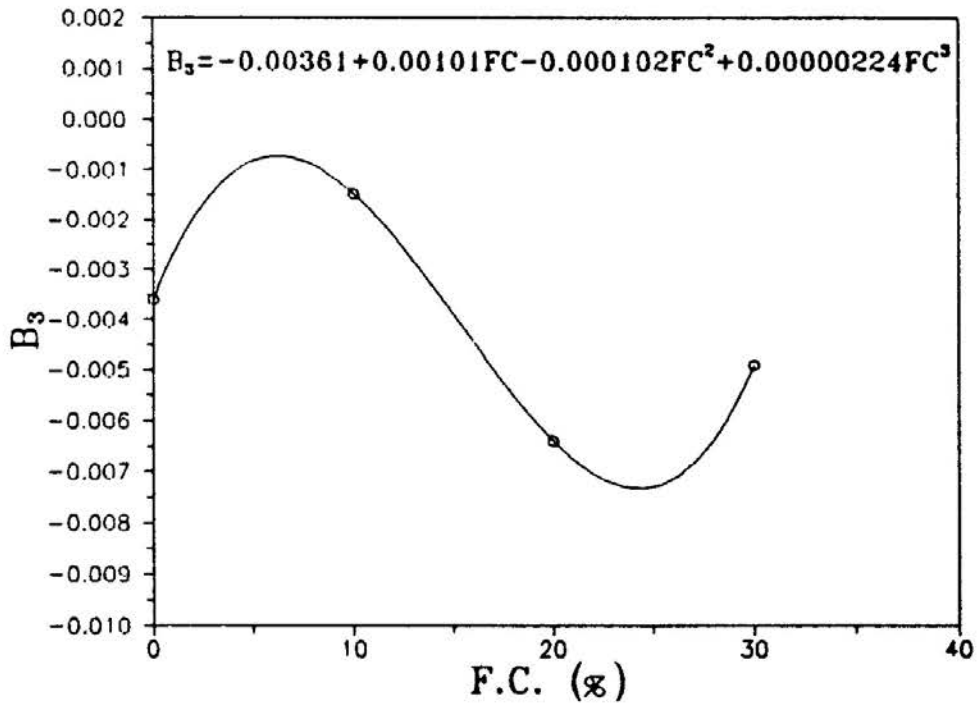


Fig. 14 Relationship Between the Constant B_3 with Fines Content

HYPERBOLIC MODEL PARAMETERS

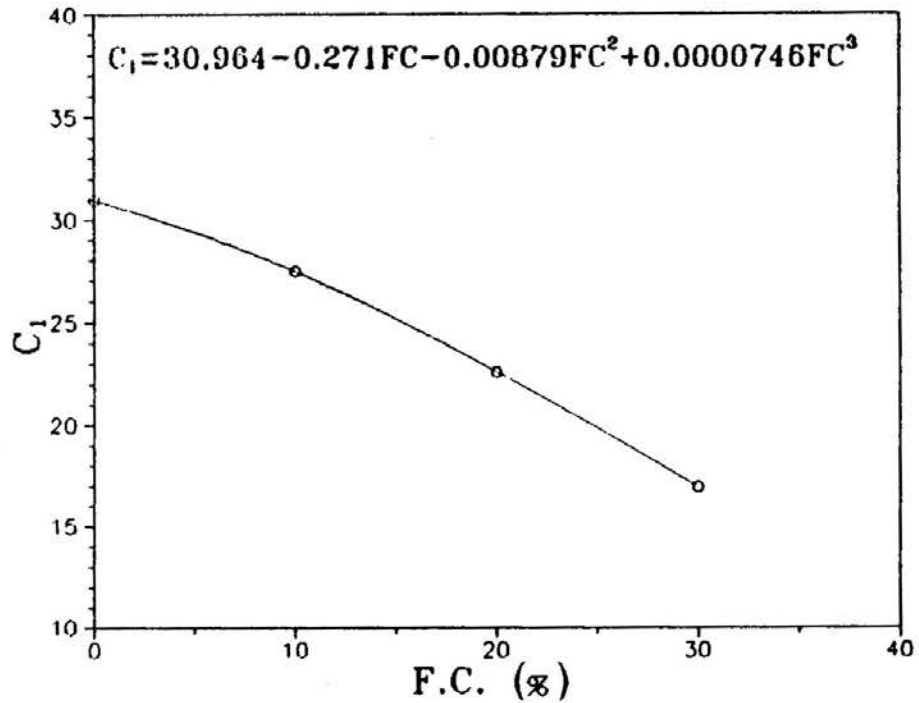


Fig. 15 Relationship Between the Constant C_1 with Fines Content

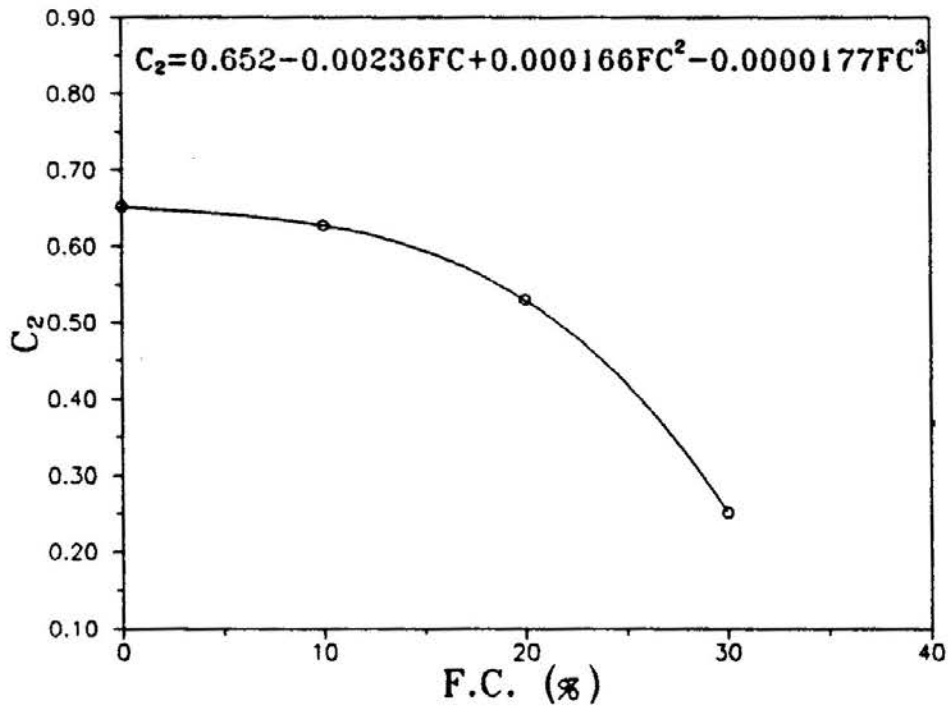


Fig. 16 Relationship Between the Constant C_2 with Fines Content

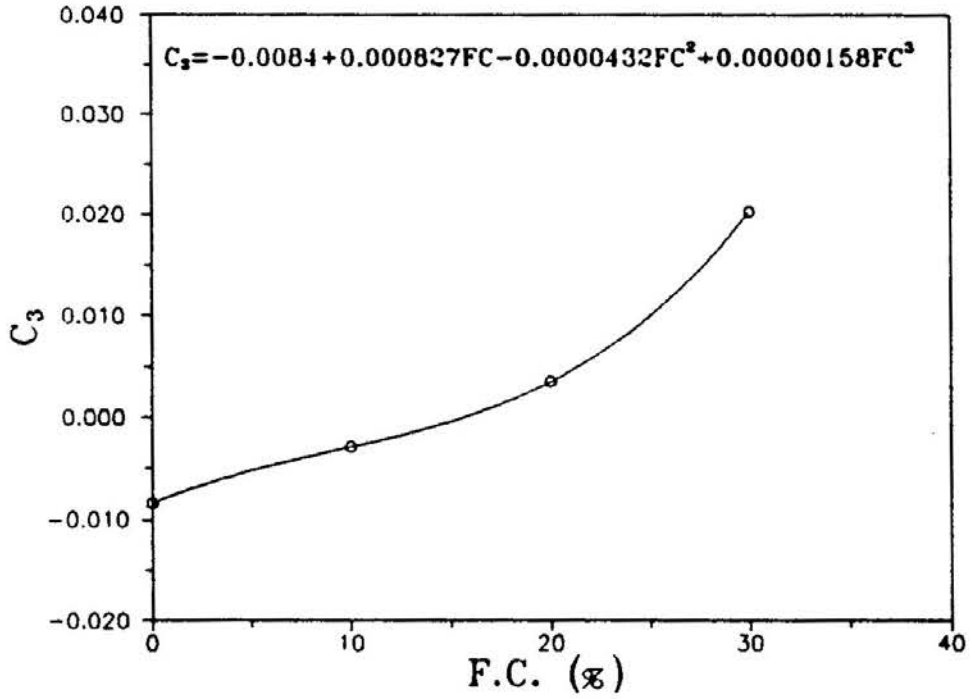


Fig. 17 Relationship Between the Constant C_3 with Fines Content

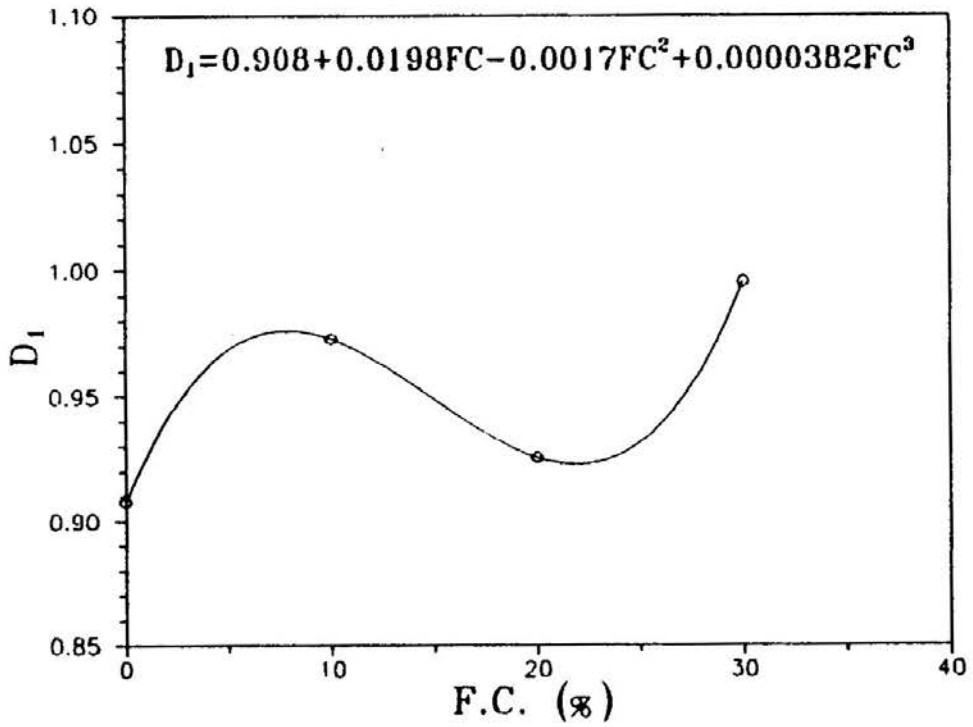


Fig. 18 Relationship Between the Constant D_1 with Fines Content

HYPERBOLIC MODEL PARAMETERS

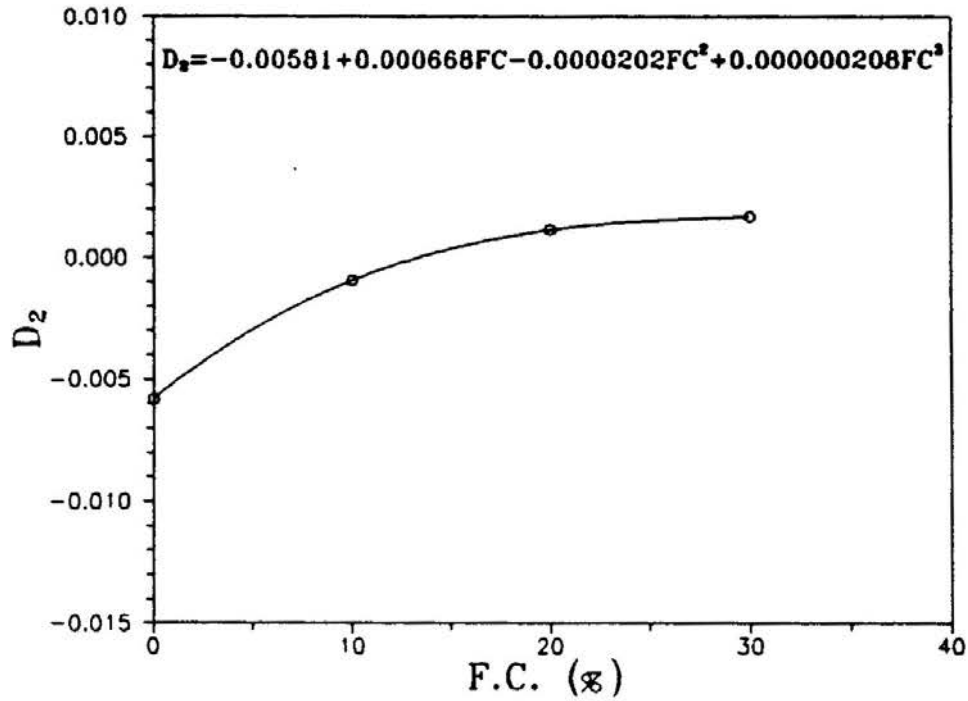


Fig. 19 Relationship Between the Constant D_2 with Fines Content

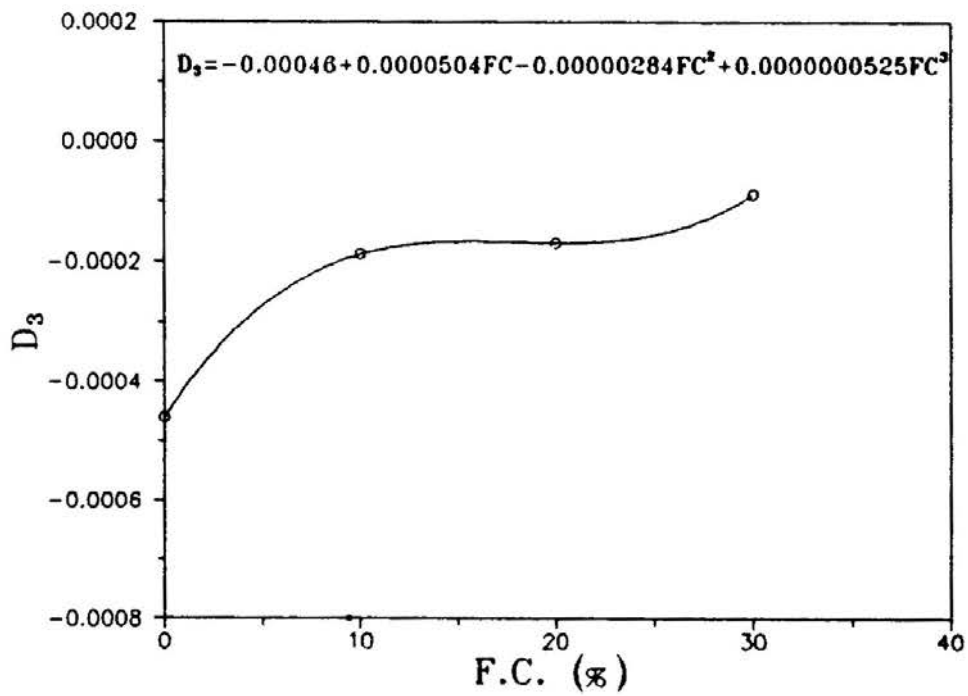


Fig. 20 Relationship Between the Constant D_3 with Fines Content

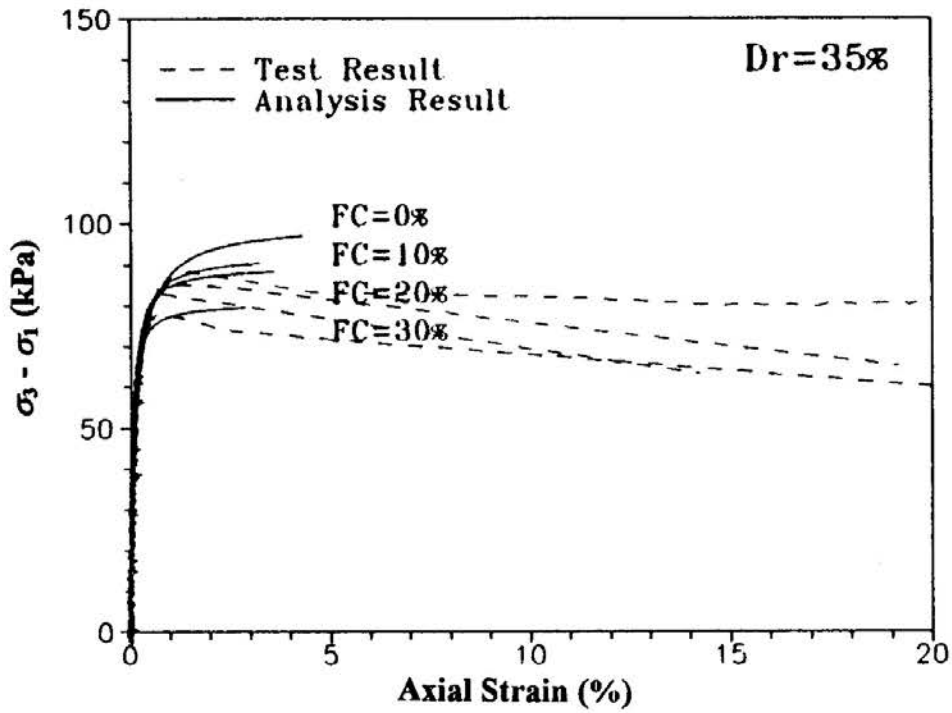


Fig. 21 Comparison Between the Test Results and Analysis Results (Relative Density = 35%)

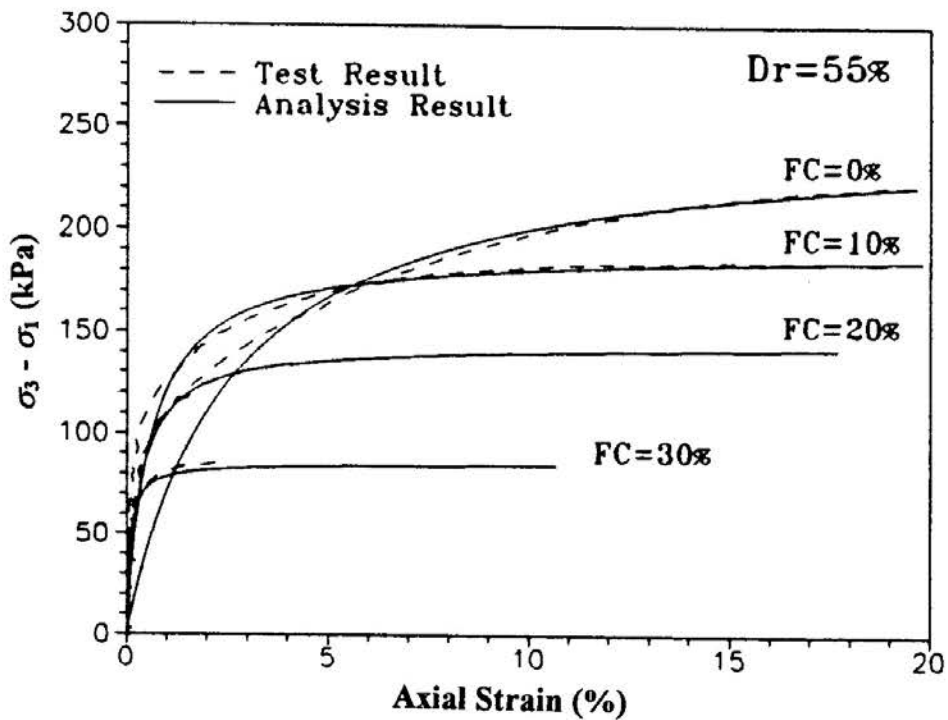
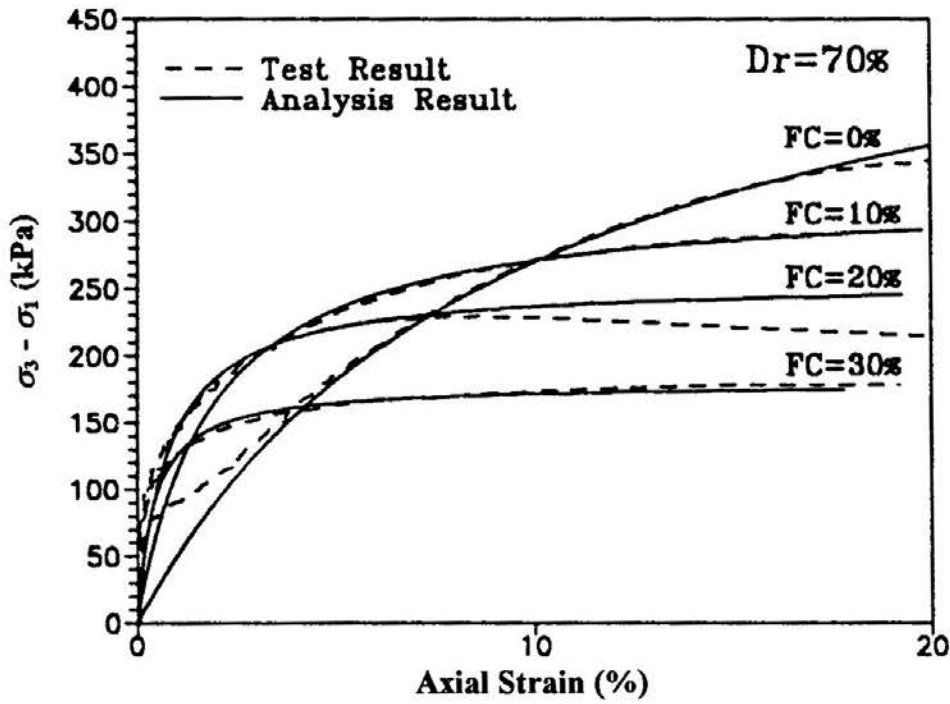


Fig. 22 Comparison Between the Test Results and Analysis Results (Relative density = 55%)

HYPERBOLIC MODEL PARAMETERS



**Fig. 23 Comparison Between the Test Results and Analysis Results
(Relative Density = 70%)**

Table 7 The Relations Between Fines Content and the Related Constants (A_1 - D_3)

Related constants	Fines Content, FC(%)
A_1	$1.419+0.602FC-0.0408FC^2+0.00105FC^3$
A_2	$-0.204-0.0508FC+0.0034FC^2-0.0000681FC^3$
A_3	$0.00897+0.00132FC-0.0000499FC^2+0.00000015FC^3$
B_1	$2.036-0.316FC+0.0232FC^2-0.000496FC^3$
B_2	$0.0606-0.00884FC+0.000949FC^2-0.0000196FC^3$
B_3	$-0.00361+0.00101FC-0.000102FC^2+0.00000224FC^3$
C_1	$30.964-0.271FC-0.00879FC^2+0.0000746FC^3$
C_2	$0.652-0.00236FC+0.000166FC^2-0.0000177FC^3$
C_3	$-0.0084+0.000827FC-0.0000432FC^2+0.00000158FC^3$
D_1	$0.908+0.0198FC-0.0017FC^2+0.0000382FC^3$
D_2	$-0.00581+0.000668FC-0.0000202FC^2+0.000000208FC^3$
D_3	$-0.00046+0.0000504FC-0.00000284FC^2+0.0000000525FC^3$

THE MECHANICAL BEHAVIOR OF RECLAIMED SOIL

The main purpose of this study, is to evaluate the mechanical behavior of the reclaimed soil by using the nonlinear hyperbolic model. To simulate the packing properties of the hydraulic filled sand, consolidated undrained triaxial test were conducted under different confining pressure with the specimens prepared by hydraulic sand fill method (Fig. 24); and the hyperbolic model was used to simulate the stress-strain relationship of the hydraulic filled soil. As shown in Fig. 25, the stress-strain relationship between moist tamping method and hydraulic sand fill method showed different results. This showed that, the mechanical behavior is influenced by the packing in the sands. As shown in Fig. 24, the stress-strain relationship with specimen prepared by hydraulic sand fill method, the axial strain can be separated into two steps during 3% of axial strain. During the triaxial test process, the particles in the loose sand would ride over each other. This would cause a drop in the excess pore water pressure, and an increase in the effective stress. Thus, the soil would show a hardening process. Therefore, in this study, two hyperbolic curves were adopted in the analysis model, to simulate the stress-strain relationship of the specimen prepared by hydraulic sand fill method.

As shown in the test results, the relative density in the specimen prepared by hydraulic sand fill method ranges in 24% to 50%, while the fines content ranges from 0% to 3%. In this study, the stress-strain relationship for the specimen prepared by hydraulic sand fill method is simulated. As shown in Table 8, the related parameters are calculated by different steps. The hyperbolic curve simulation results are shown in Fig. 26.

Considering the influence of fines content and packing properties on the mechanical behavior analysis model of the reclaimed soil, the stress-strain relationship between the specimen prepared by moist tamping method and hydraulic sand fill method were compared and the interrelation were discussed. In this study, based on the available test data, taking the specimen prepared by hydraulic sand fill method with relative density of $D_r = 30.4\%$ (after consolidation), with the first step of failure deviator stress, and 0% of fines content; and comparing with the specimen prepared by hydraulic sand fill method with $D_r = 38.8\%$ (after consolidation) and a failure deviator stress, the following mechanical behavior relation is obtained.

$$(\sigma_1 - \sigma_3)_{fH} = \alpha (\sigma_1 - \sigma_3)_{fMT} \tag{13}$$

where, α is the related constant for the first failure deviator stress for specimen prepared by hydraulic sand fill method, and the failure deviator stress for specimen prepared by moist tamping method.

From the test results conducted by Tsai (1994), the constant is obtained to be 0.94. Thus, the failure deviator stress for specimen prepared by hydraulic sand fill

HYPERBOLIC MODEL PARAMETERS

Table 8 The Calculated Results of Related Parameters for Hyperbolic Model Based on Two Points Method (70%, 95%) (Hydraulic Sand Fill Method)

Test No.	Confining pressure (kpa)	The related parameters for the hyperbolic model							
		First Step				Second Step			
		k_1	n_1	φ_1	R_n	k_2	n_2	φ_2	R_n
H2401U	98.000	12.647	0.816	16.209	1.023	0.040	0.435	13.396	0.129
H13402U	196.000	12.647	0.816	14.985	1.013	0.040	0.435	9.501	0.142
H10403U	294.000	7.017	1.119	12.936	0.910	0.077	-0.393	6.595	0.224

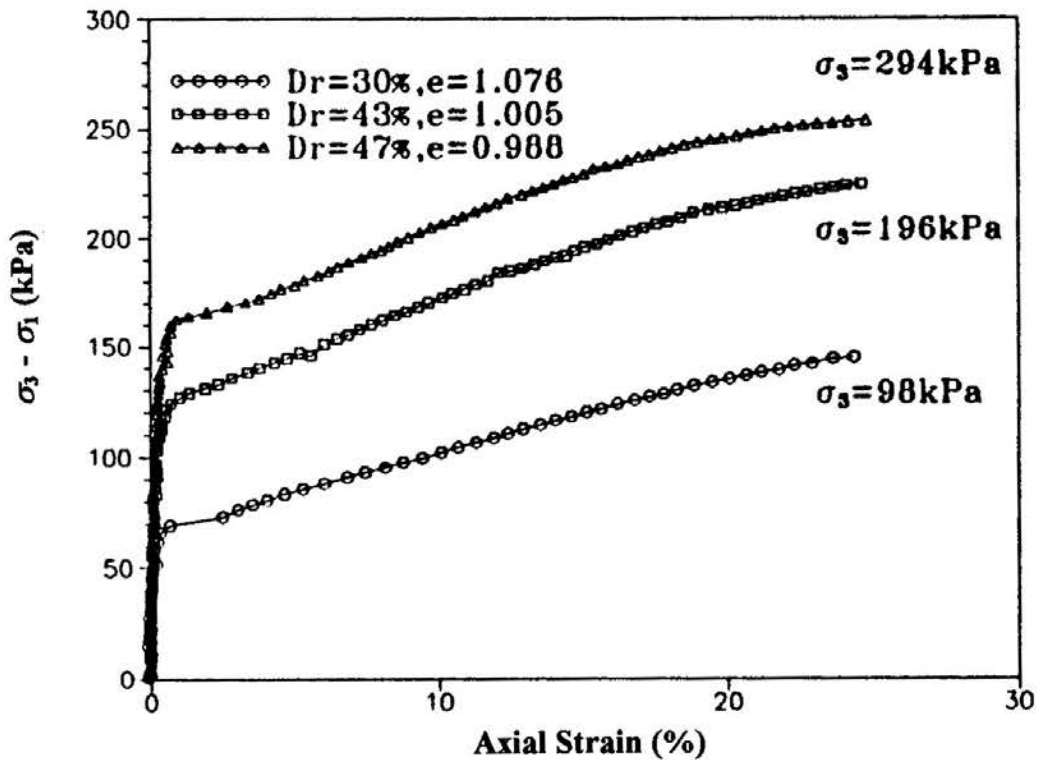


Fig. 24 Stress-Strain Relationship of Consolidated Undrained Triaxial Test (Hydraulic Sand Fill Method)

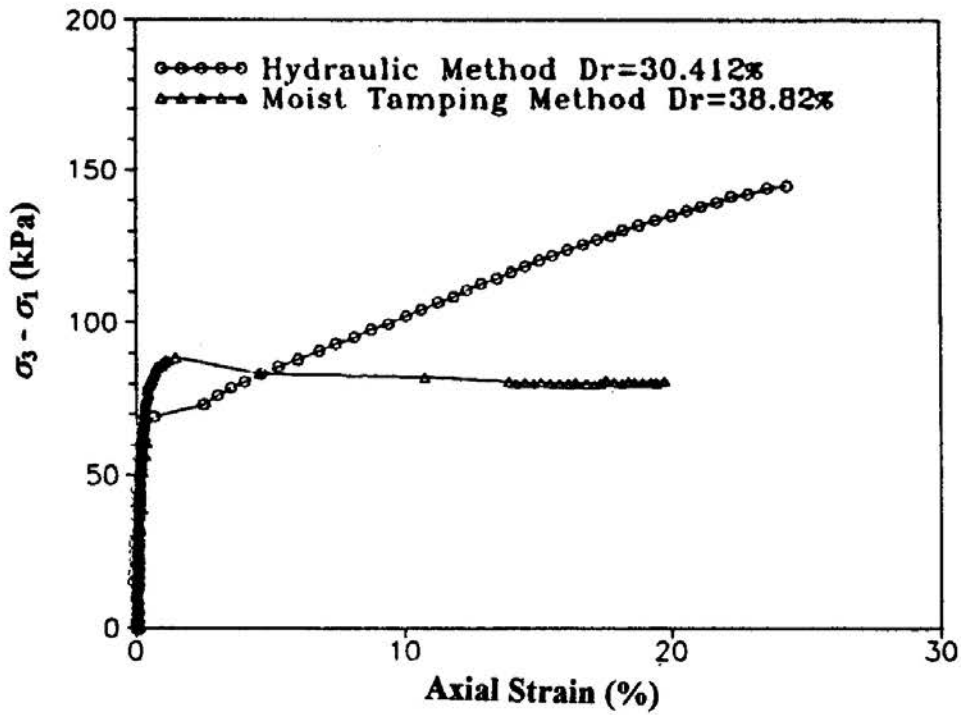


Fig. 25 Stress-Strain Relationship of Consolidated Undrained Triaxial Test with Different Specimen Preparation Method.

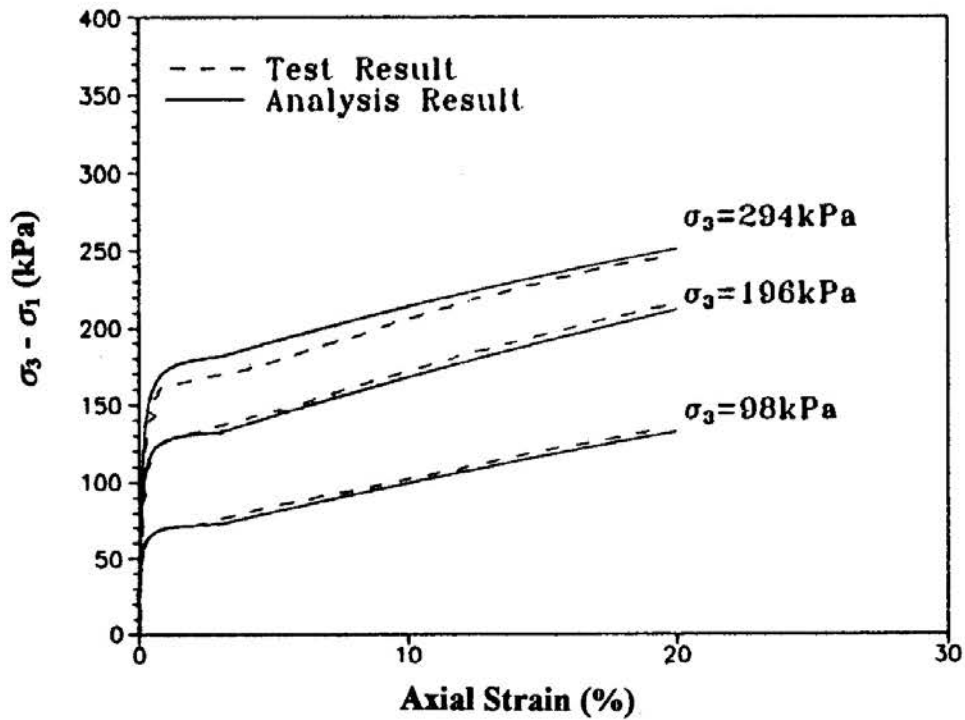


Fig. 26 Comparison Between Test Results and Analysis Results (Hydraulic Sand Fill Method)

HYPERBOLIC MODEL PARAMETERS

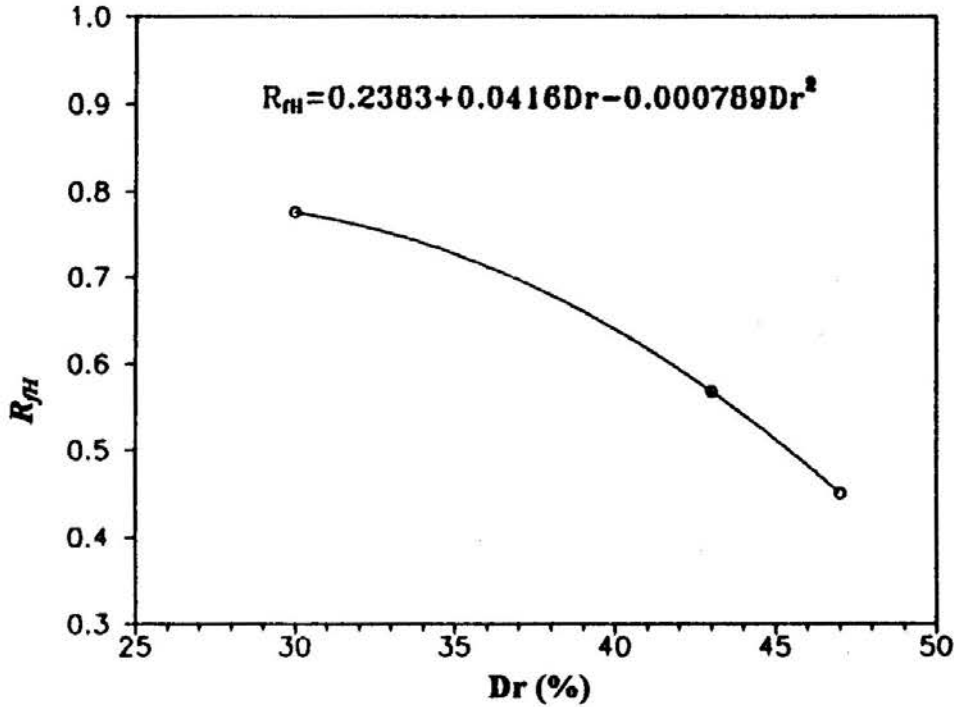


Fig. 27 Relationship Between Deviator Stress Ratio with Relative Density

method can be considered as the addition of first failure deviator stress and second failure deviator stress; and can be expressed as

$$(\sigma_1 - \sigma_3)_{fH} = (\sigma_1 - \sigma_3)_{fH1} + \Delta(\sigma_1 - \sigma_3)_{fH2} \quad (14)$$

In this study, the deviator ratio R_{fH} in the hyperbolic model is defined as the ratio between first failure deviator stress and the increment in the second deviator stress; and can be expressed as

$$R_{fH} = \Delta(\sigma_1 - \sigma_3)_{fH2} / (\sigma_1 - \sigma_3)_{fH1} \quad (15)$$

As shown in Fig. 24, under three different steps of confining pressure, it is found in the stress-strain relationship; that there is a good relationship between R_{fH} and the relative density after consolidation. As shown in Fig. 27, the analysis can be expressed as

$$R_{fH} = 0.2383 + 0.0416D_r - 0.000789D_r^2 \quad (16)$$

Thus, Eq. (16) can be rewritten as

$$(\sigma_1 - \sigma_3)_{fH} = (\sigma_1 - \sigma_3)_{fH1} + R_{fH} (\sigma_1 - \sigma_3)_{fH1} \quad (17)$$

Substituting Eq. (15) into Eq. (17), the equation can be rewritten as

$$(\sigma_1 - \sigma_3)_{FH} = \alpha (\sigma_1 - \sigma_3)_{MT} + R_{FH} \alpha (\sigma_1 - \sigma_3)_{MT} \quad (18)$$

Based on the above mentioned procedure and equations, using the known parameters such as relative density and fines content; and using the nonlinear hyperbolic analysis model for specimen prepared by moist tamping method; the mechanical behavior for hydraulic reclaimed soil can be predicted by using Eq. (18).

CONCLUSION

1. In this study, an evaluation method for the mechanical behavior of reclaimed soil is proposed based on consolidated undrained triaxial test results. Influence factors such as fines content and relative densities are added in the nonlinear hyperbolic model for reclaimed soil.
2. Fines content has significant influence on the mechanical behavior for reclaimed soil. In this study, based on the stress-strain relationship adopted from consolidated undrained triaxial test, the related parameters such as k , n , ϕ , and R_f can be obtained. The relations between the parameters with relative density and fines content were discussed.
3. The triaxial test was conducted with the specimen prepared by moist tamping method. As shown in the stress-strain relationship, the results are very different compared to the specimen prepared by hydraulic sand fill method. In this study, this relationship is discussed and Eq. (28) may be used to obtain deviator stress of hydraulic fill specimens from the results of moist tamping specimen.
4. To evaluate the mechanical behavior of the reclaimed soil, Eq. (28) was used. The influence of relative density and fines content were considered; and two-step methods were used to simulate the stress-strain relationship for the hydraulic reclaimed soil.
5. In this study, due to complicated influence factors, the specimen prepared by hydraulic sand fill method cannot be controlled precisely. Thus, the trend of the effects of relative density and fines content on the parameters cannot be determined. Therefore, based on the test results adopted from the specimen prepared by moist tamping method, an empirical transform method was developed. In the future, more experiments will be conducted to improve the model.

HYPERBOLIC MODEL PARAMETERS

ACKNOWLEDGMENT

This research was supported by Sinotech Engineering Consultants, Inc. (Taiwan) under Grant No. 7704, and was greatly appreciated.

REFERENCES

- CHEN, S.C. (1986). Nonlinear Stress-Strain Analysis for Saturated Clay. Master Thesis, National Central University, Chung-Li, Taiwan, R.O.C.
- CHIEN, L. K. (1993). *A Study on the Mechanical Behavior of Reclaimed Soil in Nearshore Taiwan*, Research Report, National Science Council of the Republic of China, Grant No. NSC-82-0209-E-019-510. Taipei: National Science Council of the Republic of China.
- DESAI, C.S. (1971). Nonlinear analysis using spline functions. *Journal of the Soil Mechanics and Foundations Division, ASCE*, Vol. 97, No. SM10, pp. 1461-1480.
- DUNCAN, J.M. and CHANG, C.Y. (1970). Nonlinear analysis of stress and strain in soil. *Journal of the Soil Mechanics and Foundations Division, ASCE*, Vol. 96, No. SM5, pp. 1629-1653.
- HANSEN, J.B. (1963). Hyperbolic stress-strain response: Cohesive soils. *Journal of the Soil Mechanics and Foundations Division, ASCE*, Vol. 89, No. SM4, Proc. Paper 3578, pp. 241-242.
- KONDNER, R.L. (1963). Hyperbolic stress-strain response: Cohesive soils. *Journal of the Soil Mechanics and Foundations Division, ASCE*, Vol. 89, No. SM1, pp. 115-143.
- SINOTECH ENGINEERING CONSULTANTS, INC. (1990). *Yunlin Offshore Development Project. Morphological Baseline Studies, Taipei, Taiwan.* (in Chinese). Taipei: Sinotech Engineering Consultants, Inc.
- TSAI, Y.M. (1994). *A Study on the Steady State Parameter and Engineering Properties of Reclaimed Soil in West Coast Taiwan* (in Chinese). Master Thesis, National Taiwan Ocean University, Keelung, Taiwan, R.O.C.

A SIMPLE ANALYSIS OF PILED RAFT FOUNDATIONS

C. Anagnostopoulos¹ and M. Georgiadis²

ABSTRACT

This paper presents a simple method for analysing piled rafts, which provides the axial loads carried by the various piles, the vertical loads transferred directly to the ground by the various segments of the raft, the foundation settlements and the bending moments and shear forces developing in the raft. The raft is divided into a number of disks of equivalent area, whose interaction with each other and with the piles is considered in the analysis. Pile to pile, pile to raft disk, raft disk to pile and raft disk to raft disk effects are taken into account. The raft can be analysed with any ordinary structural finite element program having plate elements and modelling the piles as vertical springs. The interaction between the various foundation elements and the non-linear pile response are taken into account through an iterative procedure. In an attempt to investigate the effect of raft rigidity on foundation settlements and raft bending moments and the effect of the assumption that the piles support the entire building load on piled raft response, the analysis was applied to a typical 3x3 piled raft.

INTRODUCTION

Piled rafts are usually employed to reduce total and differential settlements of buildings founded in cohesive soils. The raft is often on its own able to provide adequate bearing capacity and only few widely spaced piles are added to the foundation to keep settlements below a certain limit. Part of the building loads is transferred to the ground by the piles and the remaining part by the raft. There is a large number of approaches which have been proposed for the analysis of piled rafts. The most conservative of them, which due to its simplicity is often adopted in the design of such foundation systems, considers that the entire building and foundation load is carried by the piles, resulting in very expensive solutions. A less conservative approach considers that the raft carries its own weight and the piles carry all the building loads. Eurocode 2 (1995) recommends that the raft carries a portion of the total load which produces acceptable settlements, while the remaining load is supported by the piles.

1 Assistant Professor, Department of Civil Engineering, Aristotle University of Thessaloniki, GR-54006, Greece.

2 Associate Professor, Department of Civil Engineering, Aristotle University of Thessaloniki, GR-54006, Greece.

Note: Discussion is open until 1 September 1998. This paper is part of the *Geotechnical Engineering Journal*, Vol. 29, No. 1, June 1998. Published by the Southeast Asian Geotechnical Society, ISSN 0046-5828.

A rigorous analysis of a piled raft system presents a very complex problem involving several interaction effects among the various foundation elements. It can be fully confronted with the use of three-dimensional finite elements, which however, due to their requirements in large computational resources, are rather impractical for use in conventional design problems. Early numerical analyses of piled rafts, based on the boundary element method and the integration of Mindlin's equation (Butterfield and Banerjee, 1971; Davis and Poulos, 1972), were limited in predicting the response of only rigid rafts. Similarly, a simplified method presented by Randolph (1983), which combines the individual stiffnesses of the pile group and the raft, provides the settlement and the proportion of the load supported by the raft and the piles for only rigid rafts. Several other numerical methods of analysis of various degrees of complexity take into account the bending deformation of the raft and the interaction between all raft and pile elements (Hain and Lee, 1978; Clancy and Randolph, 1993; Poulos, 1994; Yamashita, et al., 1994).

The approach described in the present paper considers four types of interaction factors among the various foundation elements, which are determined from simple analytical expressions. Its main advantage is that it does not require any special software and can be easily applied to practical design problems. The only requirement is the use of an ordinary structural analysis finite element code with plate elements, such as SAP90 (1992), for the analysis of the raft.

FOUNDATION MODEL

The piled raft is modelled as a slab supported by a series of vertical springs which represent the axial pile stiffnesses. The analysis is conducted with the widely used finite element computer code SAP90, using bending plate elements. A typical piled raft foundation and its numerical model are shown in Fig. 1. Part of the building load is supported by the pile springs, while the remaining part is directly applied to the ground through several uniformly loaded disks. The number of these disks and their diameter are independent of the number and the position of the foundation piles. They are selected to represent most appropriately the entire raft layout. Similarly, the load intensity which acts on these disks can vary and depends on the distribution of the building loads.

The distribution of the total load among the various foundation elements (piles and raft sections) is achieved through an iterative procedure. Based on an initial relatively arbitrary distribution, pile settlements and stiffnesses are determined taking into account the interaction effects among the various foundation elements. Subsequently, the raft on vertical springs behavior is analysed and new settlements and load distributions are determined. The iterations continue until the final load distribution, settlements and raft bending moments and shear forces are obtained.

A SIMPLE ANALYSIS OF PILED RAFT FOUNDATIONS

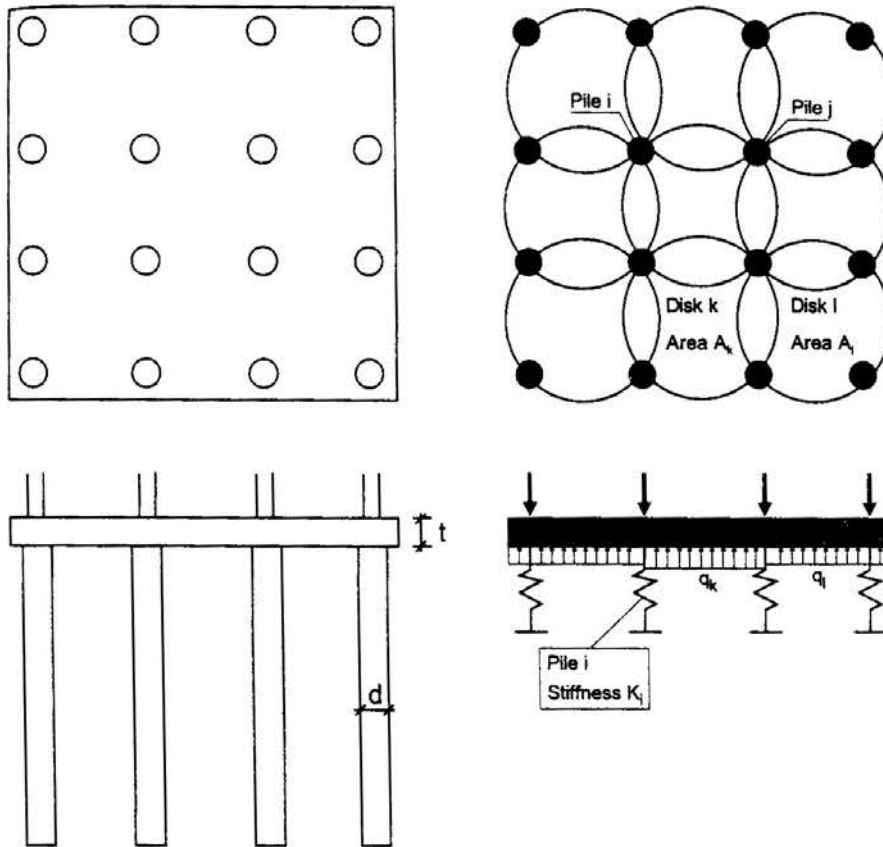


Fig. 1 Typical Piled Raft and its Numerical Modelling

INTERACTION FACTORS

As shown in Fig. 2, four types of interaction effects are taken into account in the analysis : pile to pile, pile to raft disk, raft disk to pile and raft disk to raft disk. Their magnitude is determined considering linear elastic soil behavior.

Pile to Pile Interaction

The interaction factor α_{ij} among piles i and j (Fig. 2a) is defined as the ratio:

$$\alpha_{ij} = \rho'_{i,j} / \rho'_{i,i} \quad (1)$$

where $\rho'_{i,j}$ is the elastic settlement of pile i caused by a unit load on pile j , and $\rho'_{i,i}$ is the elastic settlement of pile i caused by its own unit load.

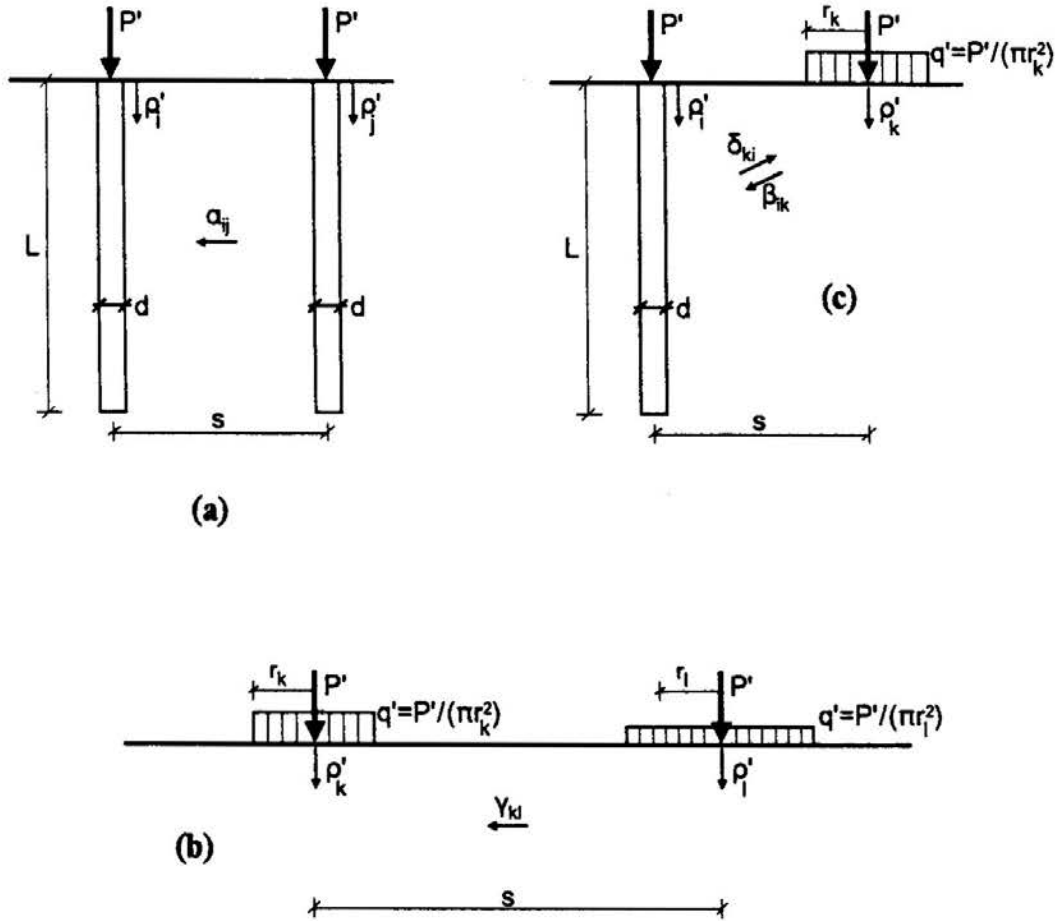


Fig. 2 Interaction Effects: (a) Pile to Pile, (b) Raft Disk to Raft Disk, (c) Pile to Raft Disk and Raft Disk to Pile

Values of α_{ij} can be obtained from graphs provided by Poulos and Davis (1980) as a function of pile spacing to pile diameter ratio (s/d), pile length to pile diameter ratio (L/d) and pile elastic modulus to soil elastic modulus ratio ($K=E_p/E_s$).

Raft Disk to Raft Disk Interaction

The interaction factor γ_{kl} which describes the effect of disk l on the settlement of disk k (Fig. 2b) is defined as:

$$\gamma_{kl} = \rho'_{k,l} / \rho'_{k,k} \tag{2}$$

where $\rho'_{k,l}$ is the settlement of disk k caused by a unit load P' on disk l , and $\rho'_{k,k}$ is the settlement of disk k caused by its own unit load P' .

A SIMPLE ANALYSIS OF PILED RAFT FOUNDATIONS

The settlements $\rho'_{k,l}$ and $\rho'_{k,k}$ are determined using elasticity theory through Eq. (3) and Eq. (4), respectively (Poulos and Davis, 1974; Timoshenko and Goodier, 1970):

$$\rho'_{k,l} = [P' (1 - \nu_s^2) H_l] / [\pi E_s r_l] \quad (3)$$

$$\rho'_{k,k} = P' (1 - \nu_s^2) / [2 E_s r_k] \quad (4)$$

where r_k is the radius of disk k , ν_s is the Poisson's ratio of the soil and H_l is a non-dimensional factor depending on the disk spacing s and the radius r_l of the disk l (Table 1).

Table 1 H_l Versus s/r_l Relationship

s/r_l	1	1.5	2	3	4	6	8	10
H_l	1.27	0.71	0.52	0.34	0.25	0.17	0.13	0.10

Combination of Eqs. (2), (3), and (4) provides the interaction factor γ_{kl} of disk l to disk k :

$$\gamma_{k,l} = [2 H_l r_k] / [\pi r_l] \quad (5)$$

Pile to Raft Disk Interaction

The interaction factor δ_{ki} which describes the effect of pile i on the settlement of disk k (Fig. 2c) is defined as:

$$\delta_{ki} = \rho'_{k,i} / \rho'_{k,k} \quad (6)$$

where $\rho'_{k,i}$ is the settlement of disk k caused by a unit load P' on pile i . This settlement can be determined from the following equation :

$$\rho'_{k,k} = P' I_p / L E_s \quad (7)$$

where I_p is a non-dimensional factor which can be derived from graphs presented by Poulos and Davis (1980), as a function of L/d , s/L and ν_s .

Combination of Eqs. (4), (6) and (7) yields the interaction factor δ_{ki} :

$$\delta_{ki} = 2 r_k I_p / L (1 - \nu_s^2) \quad (8)$$

Raft Disk to Pile Interaction

The interaction factor β_{ik} which describes the effect of disk k on the settlement of pile i (Fig. 2c) is defined as:

$$\beta_{ik} = \rho'_{i,k} / \rho'_{i,i} \quad (9)$$

where $\rho'_{i,k}$ is the settlement of pile i caused by a unit load P' on disk k , and $\rho'_{i,i}$ is the settlement of pile i due to its own unit.

According to Maxwell's theorem the settlement $\rho'_{i,k}$ is equal to the settlement $\rho'_{k,i}$ defined above. The single pile settlement $\rho'_{i,i}$ is:

$$\rho'_{k,i} = P' I I E_s d \quad (10)$$

where I is a non-dimensional factor which can be derived from graphs presented by Poulos and Davis (1980), as a function of L/d , $K=E_p/E_s$, ν_s and the thickness of the soil layer.

Combination of Eqs. (7), (9) and (10) yields the interaction factor β_{ik} :

$$\beta_{i,k} = I_p d / I L \quad (11)$$

ITERATIVE ANALYSIS

The proposed method of analysis comprises the following steps, leading to the determination of foundation settlements, pile loads, raft bending moments and shear forces.

1. The raft is divided into a number of disks and the interaction factors among these disks and the piles (α_{ij} , β_{ik} , γ_{kl} and δ_{ki}) are determined.
2. An initial distribution of the total vertical load P_g is made among the n piles of the raft (P_i , $i=1 \div n$) and the m surface disks (q_k , $k=1 \div m$), shown in Fig. 1. This can be done using the relationships proposed by Randolph (1983) for rigid piled rafts, which give the ratio λ of the load supported by the raft (P_r) to the total load (P_g):

$$\lambda = P_r / P_g \quad (12)$$

Alternatively, an initial arbitrary assumption can be made that the raft supports about a quarter of the total load.

A SIMPLE ANALYSIS OF PILED RAFT FOUNDATIONS

3. Using this load distribution, the settlements (ρ_i) and axial stiffnesses (K_i) of all piles can be determined through the following relationships which take into account the pile to pile and raft disk to pile interactions:

$$\rho_i = \rho_{is} + \rho' \sum_{\substack{j=1 \\ j \neq i}}^n (P_j \alpha_{ij}) + \rho' \sum_{k=1}^m (q_k A_k \beta_{ik}) \quad (13)$$

$$K_i = P_i / \rho_i \quad (14)$$

where ρ' is the elastic settlement of a single pile for unit load (Eq. 10), ρ_{is} the settlement of a single pile caused by an axial load equal to P_i and A_k is the area of raft element k . The settlement ρ_{is} can be determined through either a non-linear analysis such as a t-z analysis (Georgiadis, et al., 1989; Kraft, et al., 1981), or a linear analysis using the following equation:

$$\rho_{is} = \rho' P_i \quad (15)$$

4. Having determined the stiffnesses K_i of the vertical springs which represent the n piles and the distributed loads q_k supported by the m raft elements, an ordinary structural analysis finite element code, such as SAP90, can be used to analyse the raft on linear springs behaviour. This analysis provides a new distribution of the axial loads (P_i') among the n piles (where $\sum_{i=1}^n P_i' = \sum_{i=1}^n P_i$), the average settlements \bar{y}_k of the m raft elements and the raft bending moments and shear forces.
5. The average raft settlements are introduced into the following equations which take into account raft disk to raft disk and pile to raft disk interactions, to determine new distributed raft loads (q_k^l , $k = 1 \div m$).

$$\bar{y}_k = y_k' q_k^l A_k + y_k' \sum_{\substack{l=1 \\ l \neq k}}^m (q_l^l A_l \gamma_{kl}) + y_k' \sum_{i=1}^n (P_i' \delta_{ki}) \quad (16)$$

where y_k' is the settlement of raft disk k caused by a unit load (Eq. 4) and A_k , A_l are the areas of raft elements k and l .

6. These raft loads are used to establish the new proportion λ^l of the total load P_g , supported by the raft:

$$\lambda^l = \frac{\sum_{k=1}^m (q_k^l A_k)}{P_g} \quad (17)$$

ANAGNOSTOPOULOS AND GEORGIADIS

The difference among the new and previous raft loads (ΔP) is distributed to the piles whose new axial loads become :

$$P_i' = P_i \left(1 + \frac{\Delta P}{\sum P_i'} \right) \quad (18)$$

where

$$\Delta P = (\lambda - \lambda') P_g \quad (19)$$

$$\sum P_i' = (1 - \lambda) P_g \quad (20)$$

- Steps 3 to 6 are repeated using the new pile and raft loads until convergence is achieved and the final load distribution, foundation settlements and raft bending moments and shear forces are determined.

APPLICATION

The method described in the previous section was applied to analyse a piled raft foundation consisting of a 3x3 group of 25 m long concrete piles and a 21 m x 21 m raft (Fig. 3). The piles were embedded into a uniform clay profile of $E_s=5\text{MPa}$ and $\nu_s=0.50$. The raft supported nine column loads of 1.50 MN each and a uniformly distributed load of 24 kPa. The analysis investigated the effect of the raft flexural rigidity (D) on bending moments and settlements and the results are shown in Figs. 4 and 5. These figures present the variation of bending moment and settlement, respectively, along the cross sections A , B , and C of the raft (Fig. 3) as a function of D , defined as :

$$D = \frac{Et^3}{12(1-\nu^2)} \quad (21)$$

where E and ν are the elastic modulus and Poisson's ratio of the raft, respectively ($E = 2.9 \times 10^7 \text{kPa}$ and $\nu = 0.20$), and t is the raft thickness. The analysis was performed for $D = 315, 1060, \text{ and } 2515 \text{ MN.m}$, corresponding to raft thicknesses of 0.50 m, 0.75 m and 1.0 m.

As expected, an increase in raft rigidity increases bending moments and reduces total and differential settlements. Comparing the behavior of the 0.50 m thick raft to that of the 1.0 m thick raft, it is noticed that the maximum bending moment is about half, the maximum settlement is about 15% larger and the differential settlement (difference between settlements at the center and the corner of the raft) is about 2.50 times greater.

A SIMPLE ANALYSIS OF PILED RAFT FOUNDATIONS

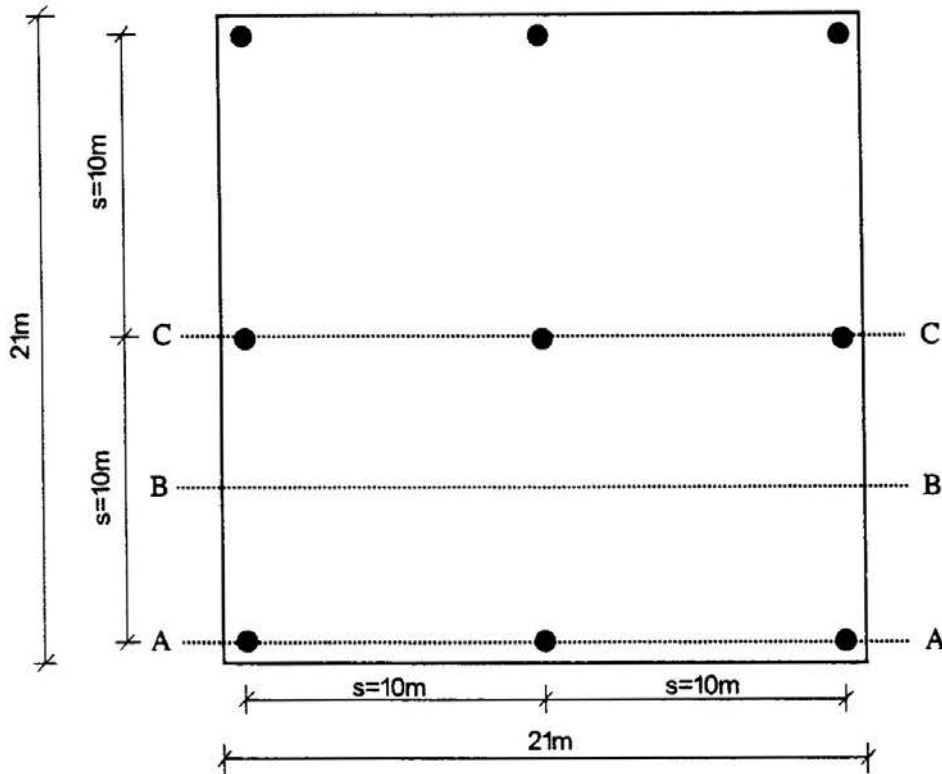


Fig. 3 Analyzed Piled Raft

For comparison, the settlement of a rigid piled raft of the same geometry and loading condition was computed according to the method described by Poulos and Davis (1980). This uniform raft settlement of 105 mm is in good agreement with the non uniform settlements of the flexible raft, which ranged between 95 mm and 130 mm. The proposed method of analysis revealed that about 80% of the total load is supported by the piles and the remaining 20% is transferred to the ground through the raft. Using the simplified approach proposed by Randolph (1983) for rigid piled rafts, it was derived that the piles support 70% of the total load and that the uniform foundation settlement is about 100 mm.

In order to investigate the effect of raft contribution in supporting part of the total load, an additional analysis of the 0.75 m thick piled raft was performed, in which the entire load was transferred to the ground through the piles. This consideration had a very significant effect on raft bending moments and differential settlements, while the effect on maximum foundation settlement was rather small. Ignoring raft contribution resulted in 50% higher bending moments, 25% higher differential settlement and 3% higher maximum foundation settlement.

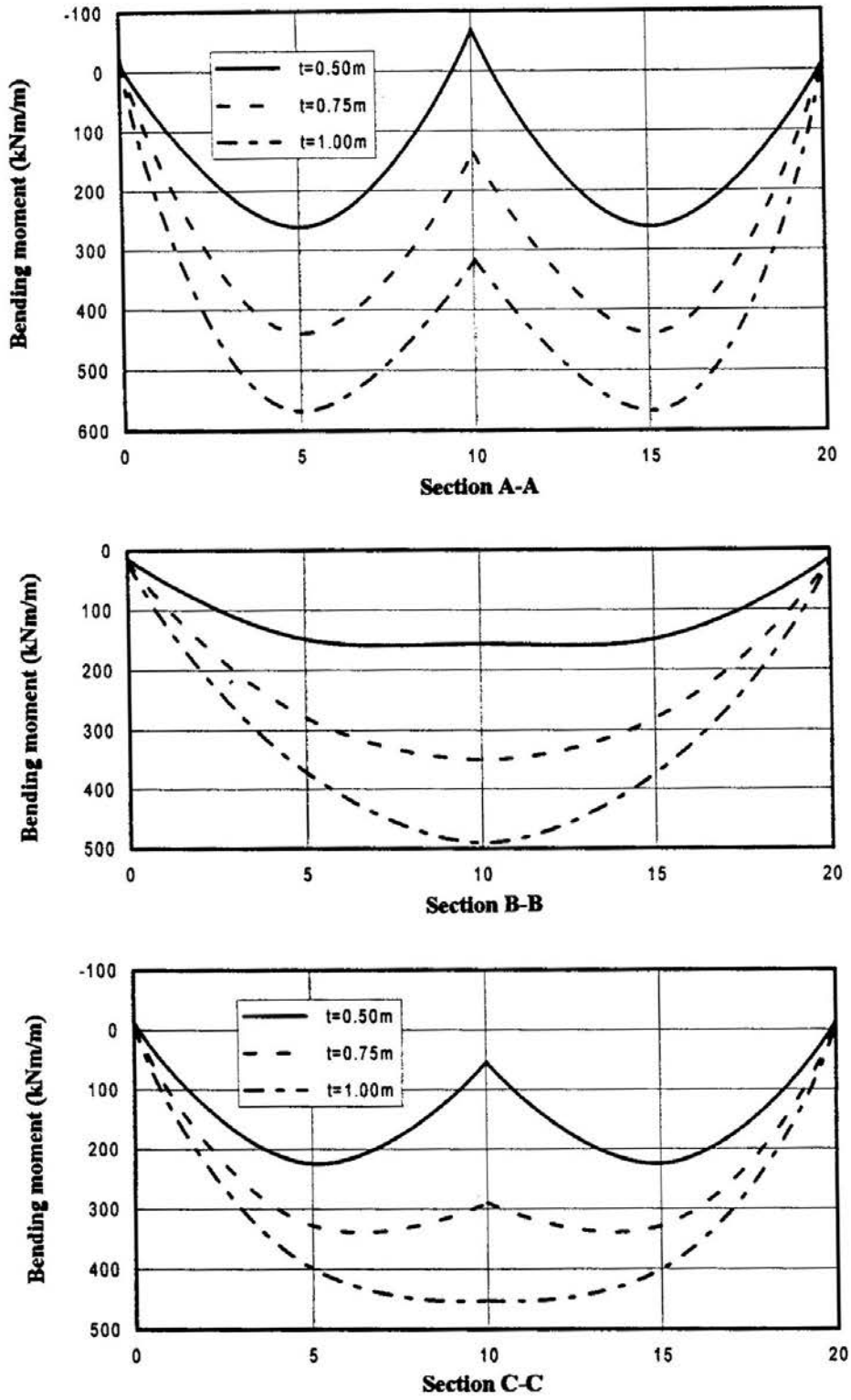


Fig. 4 Effect of Raft Rigidity on Bending Moments

A SIMPLE ANALYSIS OF PILED RAFT FOUNDATIONS

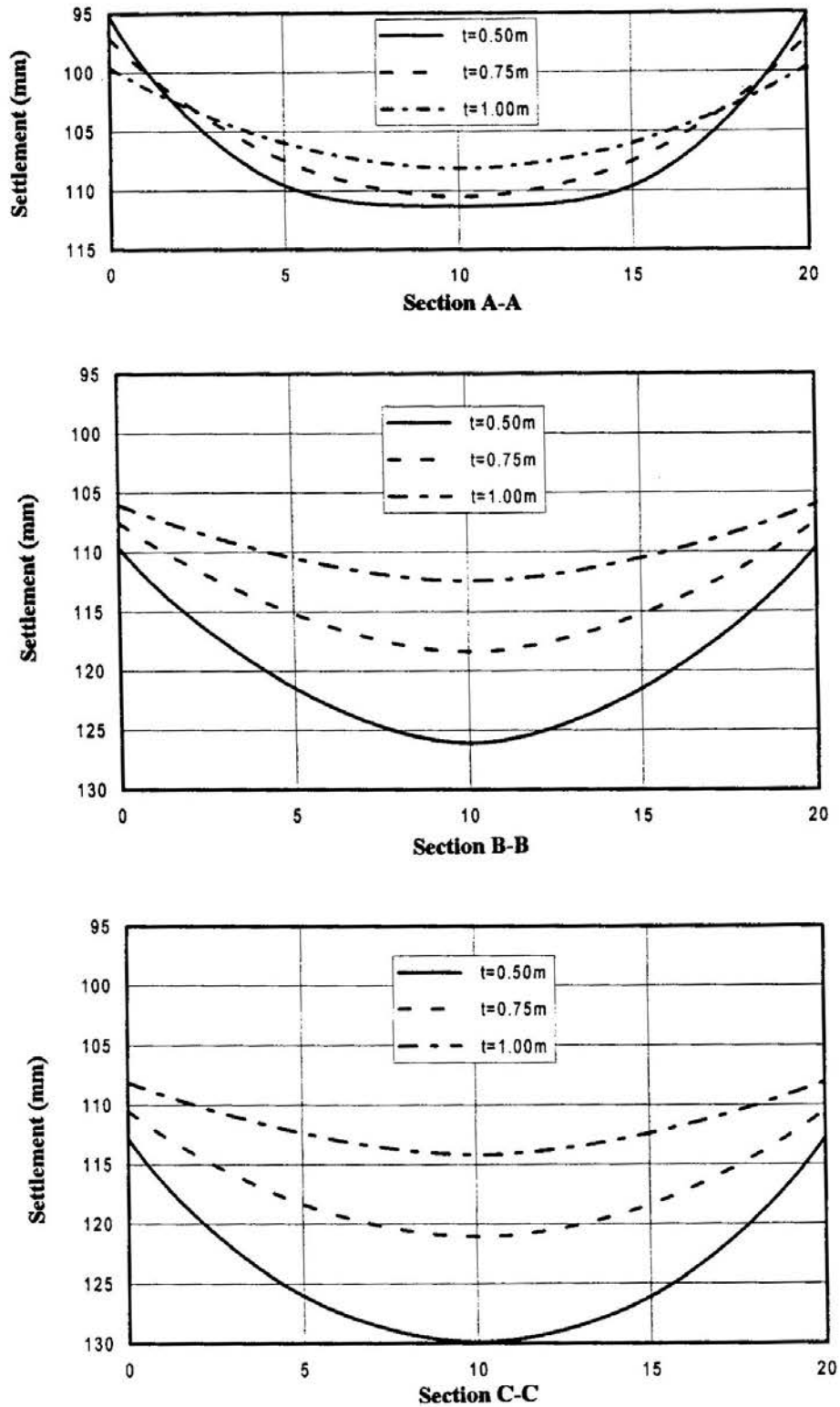


Fig. 5 Effect of Raft Rigidity on Foundation Settlement

ANAGNOSTOPOULOS AND GEORGIADIS

It is noted that the iterative computation process was very smooth, achieving convergence after about four iterations. The load supported by the raft decreased gradually from about 50% of the total load at the first iteration to 25% at the second, 21% at the third and stabilized to about 20% at the fourth iteration.

CONCLUSIONS

A simple method for analysing piled rafts of any flexural rigidity has been presented. The main advantage of the method is that although it does not require the use of any special software, it takes into account, in an approximate manner, the interaction among the several pile and raft elements and the non-linearity of the pile behavior. Interaction factors determined using elasticity theory are introduced together with a widely used structural analysis finite element computer program into an iterative procedure to calculate the loads supported by each pile and the raft, the total and differential settlements of the foundation and the bending moments of the raft.

The method was applied to a piled raft containing a 3x3 pile group. This application demonstrated that the rigidity of the raft affects significantly bending moments and differential settlements. It was also found that the consideration of a raft which is not in contact with the ground increases both bending moments and differential settlements.

REFERENCES

- BUTTERFIELD, R. and BANERJEE, P.K. (1971). The elastic analysis of compressible piles and pile groups. *Geotechnique*, Vol. 21, No. 1, pp. 43-60.
- CLANCY, P. and RANDOLPH, M.F.P.K. (1993). An approximate analysis procedure for piled raft foundations. *International Journal for Numerical and Analytical Methods in Geomechanics*, Vol. 17, pp. 848-869.
- DAVIS, E.H. and POULOS, H.G. (1972). The analysis of pile raft systems. *Australian Geomechanics Journal*, Vol. G2, No. 1, pp. 21-27.
- EUROCODE 2 (1995). Design of concrete structures - Part 3: Concrete foundations. Prepared for the Commission of European Communities, Brussels.
- GEORGIADIS, M.; PITILAKIS, K.; TSOTSOS, S. and VALALAS, D. (1989). Settlement of a liquid storage tank founded on piles. *Proceedings of the Twelfth International Conference on Soil Mechanics and Foundation Engineering*, Rio de Janeiro, Vol. 2, pp.1057-1060.

A SIMPLE ANALYSIS OF PILED RAFT FOUNDATIONS

- HAIN, S. J. and LEE, I.K. (1978). The analysis of flexible pile-raft systems. *Geotechnique*, Vol. 28, No. 1, pp. 65-83.
- KRAFT, L.M., RAY, R.P. and KAGAWA, T. (1981). Theoretical t-z curves. *ASCE, Journal of Geotechnical Engineering Division*, Vol. 107, GT11, pp. 1543-1561.
- POULOS, H.G. (1994). An approximate numerical analysis of pile-raft interaction. *International Journal for Numerical and Analytical Methods in Geomechanics*, Vol. 18, pp. 73-92.
- POULOS, H.G. and DAVIS, E.H. (1974). *Elastic Solutions for Soil and Rock Mechanics*. New York: John Wiley and Sons.
- POULOS, H.G. and DAVIS, E.H. (1980). *Pile Foundations. Analysis and Design*. New York: John Wiley and Sons.
- RANDOLPH, M.F. (1983). Design of piled raft foundations. *Proceedings of the International Symposium on Recent Developments in Laboratory and Field Tests and Analysis of Geotechnical Problems*, Bangkok, pp. 525-537.
- SAP90 (1992). *Computer Program for the Finite Element Analysis of Structures*. Berkeley, USA: Computers and Structures, Inc.
- TIMOSHENKO, S.P. and GOODIER, J.N. (1970). *Theory of Elasticity* (Third Edition). New York: McGraw-Hill.
- YAMASHITA, K. KAKURAI, M. and YAMADA, T. (1994). Investigation of a piled raft foundation on stiff clay. *Proceedings of the Thirteenth International Conference on Soil Mechanics and Foundation Engineering*, New Delhi, Vol. 2, pp.543-546.

ROCK SLOPE STABILIZATION ALONG RAILROAD AT FUSHUN MINE

M.S. Wang¹, X.L. Wu² and M.C. Wang³

ABSTRACT

This paper presents a successful case history of stabilizing unstable rock slopes along the main railroad in Fushun mine which is located in northeastern China. The side slopes were intercepted with terraces which support roadways for mining operations. The unstable rock slopes were stabilized using ground anchors based on the principle that unstable rock blocks can be made stable against toppling by binding them together. In most cases, the ground anchors were installed in the direction normal, as much as possible, to the orientation of the discontinuities. Also installed were anchors dipping deep into the stable zone crossing the potential sliding surface. The anchor tendons were 36 mm diameter threaded steel rods and were grouted without pre-stressing along the entire length. Each exposed end of the anchor was protected using a reinforced concrete cap. For performance monitoring of the anchor systems, eight pairs of measuring points were established along existing cracks. Each pair consisted of two points which were fixed across the crack. The relative movement between the two fixed points was monitored. Only slight movement has been detected as of today indicating that the unstable rock slopes have been stabilized successfully.

INTRODUCTION

Fushun is an important industrial city in northeastern China. Fushun mine is a large surface mine of which the open pit is approximately 6.6 km long in the east-west direction, 2.2 km wide in the south-north direction, and 300 m deep. It is a coal mine having a top coal seam thickness ranging from about 20 m to 145 m with an average of approximately 55 m. The side slopes are multi-staged with intercepting terraces of various widths. In each stage, slope angle and height also vary. Each terrace supports a roadway for mining operations. Since the beginning of mining, there have been 54 occurrences of slope slides. From April through June of 1978, four slides occurred involving a total of approximately 20.8 million cubic meter of sliding mass. The slides, which were later stabilized and corrected using steel piles, destroyed the railroad and blocked the waterway, interrupting the mining operation for more than one-half year.

1 Professor Emeritus, Department of Civil and Transportation Engineering, Northeastern University, Shenyang, China 110006.

2 Graduate Student, Department of Civil and Environmental Engineering, The Pennsylvania State University, University Park, PA 16802, U.S.A.

3 Professor, Department of Civil and Environmental Engineering, The Pennsylvania State University, University Park, PA 16802, U.S.A.

Note: Discussion is open until 1 September 1998. This paper is part of the *Geotechnical Engineering Journal*, Vol. 29, No. 1, June 1998. Published by the Southeast Asian Geotechnical Society, ISSN 0046-5828.

In 1987, along the twelfth terrace (counting downward from the ground surface) between stations W200 and W800, within a stretch of about 600 m on the north border, slope slides took place resulting in 50 mm to 100 mm wide cracks at the top as well as 300 mm to 400 mm settlement at a nearby petroleum refinery. Since the twelfth terrace supported the main railroad for mining operation, the extreme urgency for maintaining the operation of the main transportation facility prompted the use of steel piles for slope stabilization. Unfortunately, installation of 361 steel *H*-piles, each 12.35 m long, at the bottom of the slope was unable to stop the slide. An investigation was, therefore, undertaken to develop an economical as well as effective technique to stabilize the slope. This paper presents the results of the investigation.

SITE GEOLOGY

The site is full of geological complexities. The rock formations are randomly folded. Two major faults cross the slopes and are interconnected by a network of discontinuities. The site is dominated by grayish to greenish shales interbedded with oil shales. The shales are with distinct cleavages and are weathered to various degrees. A river runs nearly parallel with the north boundary of the mine at approximately 1000 m away. Under the influence of this river, the wastewater discharged from a petroleum refinery near the north border seeps into the mine pit. Another river at approximately 150 m away from the west boundary also causes seepage into the open mine.

The ground is composed of a 5 m to 30 m thick sedimentary soil deposit at top which is a cohesive soil containing some fine to coarse gravels. It is underlain successively by a greenish to grayish shale stratum of about 120 m to 530 m in thickness, an 80 m to 157 m thick oil shale stratum, then the coal seam. The coal seam has varying thickness, as mentioned above, and dips from north to south.

STABILIZATION SCHEME

After a careful examination and consideration of the geological condition and the ineffectiveness of the steel *H*-piles, the technique of ground anchoring was adopted to formulate the needed stabilization scheme. In order to utilize the steel wire strands available at the site, the first attempt was made using these strands as tendons. To increase the anchorage capacity, the end of each strand was enlarged with an explosive. This was accomplished by first sheathing the bottom of the strand in a metal pipe having 1.0 m in length, 108 mm in diameter with 3.5 mm in wall thickness. At the bottom portion of the pipe, six longitudinal slots of 600 mm in length were made equally spaced along the periphery of the pipe. The end of the wire strand was untwined and was then pulled back into the unslotted portion of the pipe to make space for the explosive. The amount of explosive was adjusted to make an enlarged hole of about 400 mm to 700 mm in diameter. The Portland cement grout used had a 3:1 sand to cement ratio and a 0.4 ~ 0.35 water to cement ratio.

ROCK SLOPE STABILIZATION ALONG RAILROAD

The wire strand anchors were tested in the field. Test results showed that the anchorage capacity reached above 100 metric tons, but was below the wire strand capacity. Because of this relatively low anchorage capacity and the tedious installation process, the wire strand tendon was replaced by the threaded steel rod tendon. The steel rod had a diameter of 36 mm and was grouted along the entire length. Since field tests of the steel rod anchor system attained the desired capacity, it was adopted for stabilizing the unstable slopes.

ANCHOR LOAD ANALYSIS

To estimate the needed anchor load, thirteen vertical cross sections were taken at approximately 50 m apart through the unstable slopes. These cross sections show that the great majority of cleavages and/or joints tilt forward toward the slope (Figs. 1 and 2). The load in the anchor rods which cross these joints/cleavages can be estimated by taking into account the various possible modes of slope failure. Possible failure modes include toppling, plane sliding, wedge sliding, combination of toppling and sliding along joints or along potential failure planes, and others. The specific failure mode which will take place depends on the slope angle, shear strength characteristics of rock, nature of discontinuity, and other influencing factors (Goodman, 1980).

The most likely failure mode in the present case is toppling with or without sliding. The predominant forward tilting pattern of cleavages/joints at the site can be effectively utilized to make the slope more stable by binding the jointed blocks together. The effectiveness of this stabilization technique is explained below.

Assuming that the toppling mode of failure prevails, the load required to stabilize the blocks on an inclined plan against toppling varies with the number of blocks, block dimension, and inclination angle as shown in Fig. 3. In the figure T , W , B , H , e , and α denote the balanced load, block weight, width, height, moment arm of W about point 0, and inclination angle, respectively. The rock at this site has internal friction angles of $\phi_t = 16^\circ$ and $\phi_n = 34^\circ$, and cohesions of $c_t = 3 \text{ t/m}^2$ and $c_n = 30 \text{ t/m}^2$ for shearing in the directions tangential and normal to the joints, respectively. These values were estimated from a geological report of Fushun Coal Mine. For these rock properties, it can be shown, by taking moments about point 0, that for a block having $B = 10 \text{ cm}$, $H = 50 \text{ cm}$ with $\alpha = 30^\circ$, the balanced load varies with the number of blocks such that $T_1 = 0.326 W$ for one block, $T_2 = 0.307 W$ for two blocks, $T_3 = -0.60 W$ for three blocks, and so forth. These figures show that the force required to prevent the jointed blocks from toppling is greatest for one block then decreases with increasing block number. When three blocks are bound together, they become stable with respect to toppling without external supports. For the case that blocks slip along the inclination plane, the sliding resistance on the slip plane should be considered in the determination of balanced force. The sliding resistance equals the sum of frictional and adhesive forces.

Laboratory model tests were conducted to determine the load distribution along the anchor rod. The test specimens were concrete blocks having two different sizes –

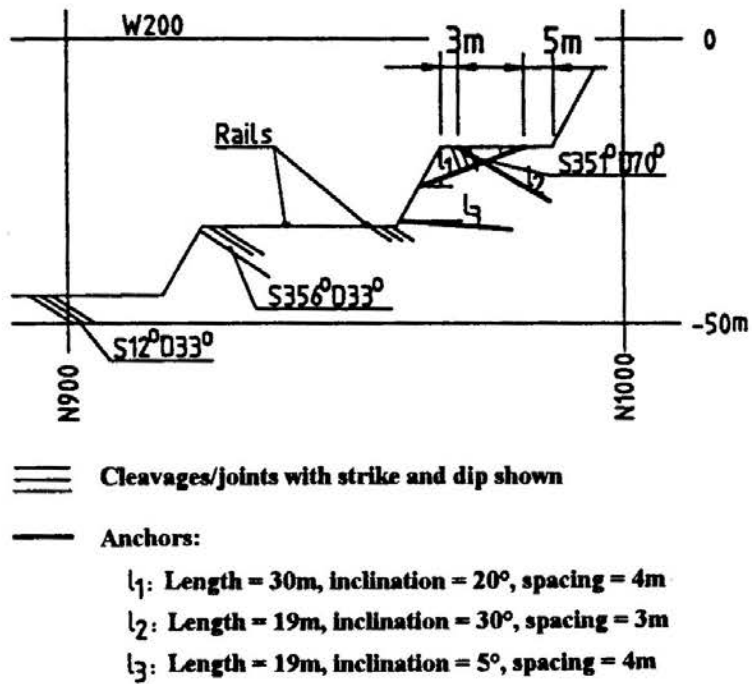


Fig. 1 Cross-Section and Anchor Layout for Slopes at Station W200

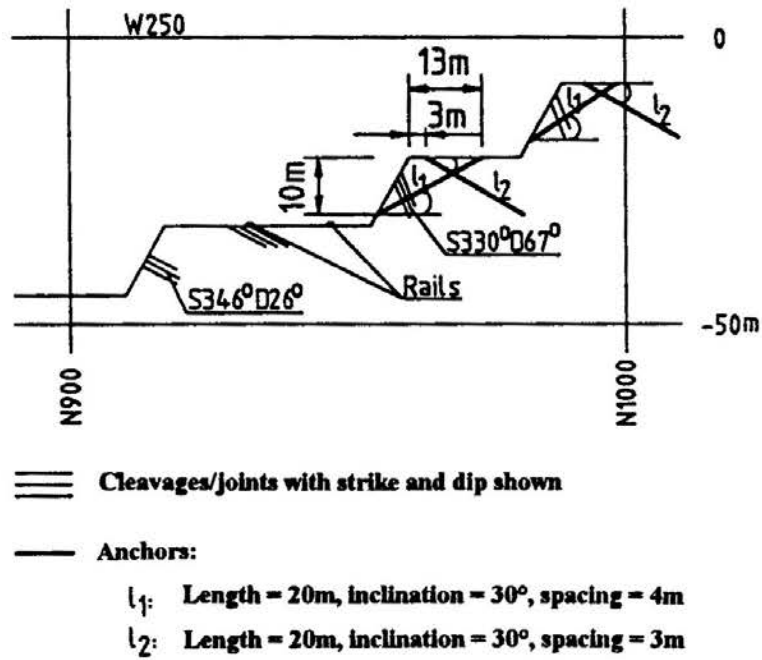


Fig. 2 Cross-Section and Anchor Layout for Slopes at Station W250

ROCK SLOPE STABILIZATION ALONG RAILROAD

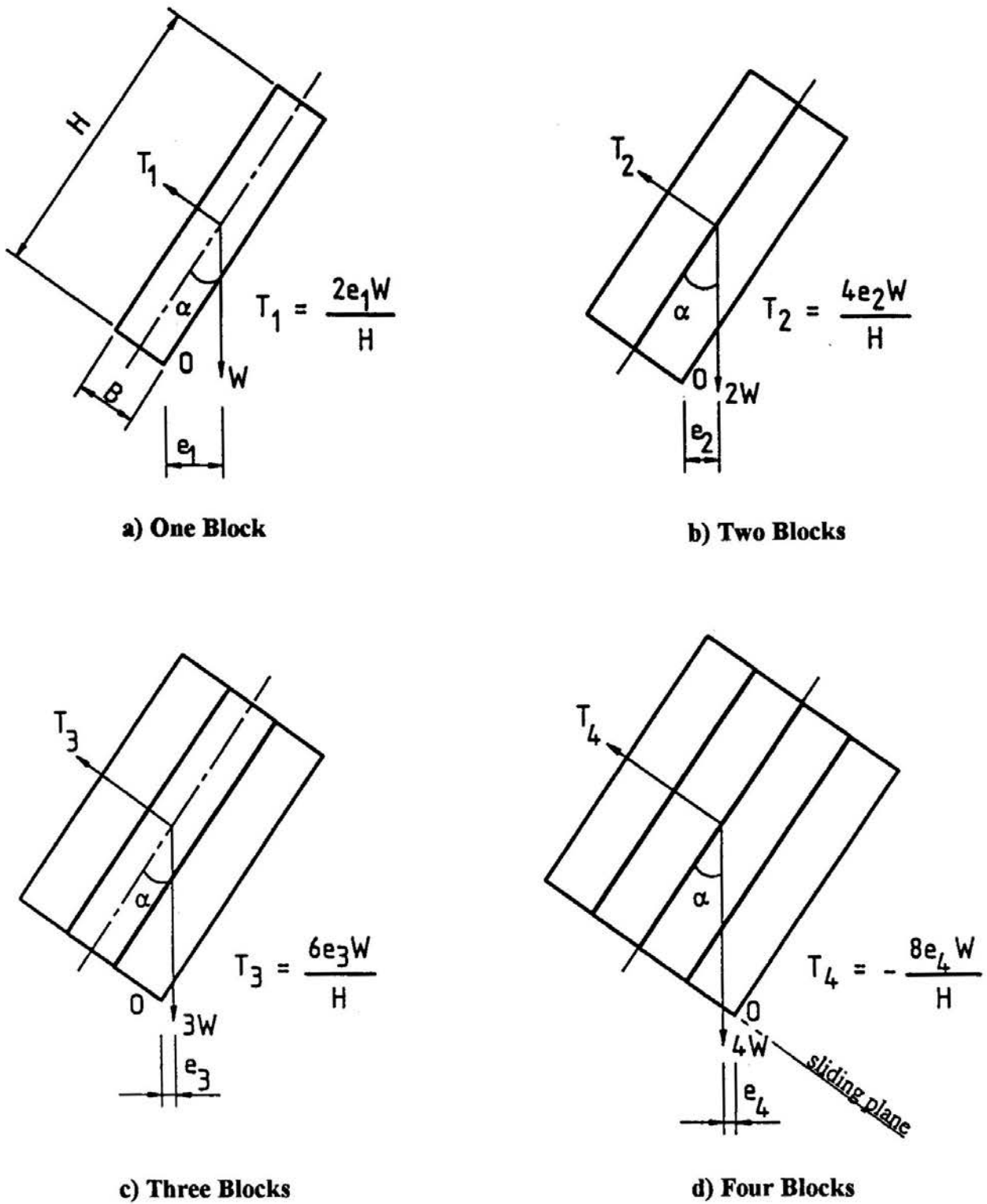


Fig. 3 Moment Equilibrium of Jointed Blocks on an Inclined Plane

100 mm wide by 100 mm long by 500 mm high with 12.2 kg mass, and 50 mm wide by 100 mm long by 500 mm high with 6.1 kg mass. A total of 11 blocks for the 100 mm wide specimens and 19 blocks for the 50 mm wide specimens were tested.

The test specimens were placed together upright touching one another face to face on a platform. One end of the platform could be lifted to any desired height. A groove was made at the midheight on each side of the block; and a continuous metal strip was attached in the groove using cement mortar to simulate the grouted anchor rod. At each block interface, strain gages were installed on the metal strip to monitor anchor load. A schematic view of the test set-up is shown in Fig. 4. The anchor loads were measured for five levels of inclination angle, i.e., 11.5°, 17.5°, 23.5°, 30.0°, and 37.0°. Results of the measurements showed that the anchor load decreased rapidly with the number of interface from a maximum at the first interface (bottommost) then became a negative value around the third to the seventh interface depending on block size, and the angle of inclination. Such a variation in anchor load resembles the results of the preceding analysis.

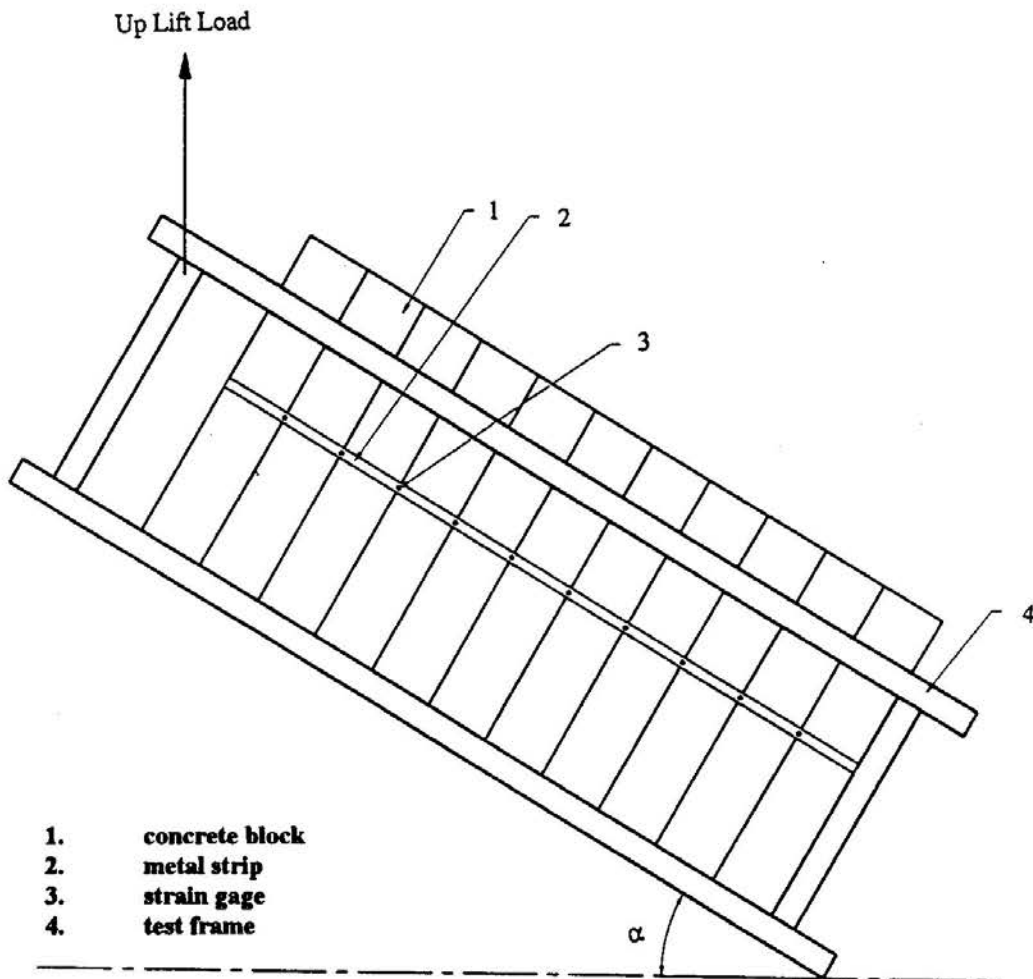


Fig. 4 Schematic View of Test Set-up

ROCK SLOPE STABILIZATION ALONG RAILROAD

As mentioned earlier, rock slope failure may involve more than just toppling. Also the critical failure surface is not necessarily planar. Moreover, the unstable rock blocks are irregular in shape with varying sizes. Thus, the conditions considered in the model testing and analysis were overly simplified. Even with this over-simplification, the anchor load distribution data demonstrated an important point that unstable blocks can be made stable with respect to toppling by binding them together. As a result, the anchor load as well as anchor length needed for stabilizing rock blocks from toppling failure will be considerably smaller when compared with the condition of unbound blocks. Tying the blocks together can be achieved by grouting the steel rod anchors along their entire length. This principle was applied to the unstable slopes of the coal mine.

ANCHOR DESIGN

Between stations W200 and W800, slopes which showed some sign of distress were investigated. Possible modes of failure including toppling, planar sliding, and rotational sliding were analyzed. For stations which require stabilization, the anchors were placed in the direction normal to the cleavages/joints direction as much as possible to increase stability against toppling. For sliding stability, the anchors were oriented counter-clockwise from the potential sliding surface by an amount which is as close as possible to the internal friction angle of the rock (ϕ).

In most cases, stabilization of the slope was made by installing fully grouted anchors without post-tensioning across cleavages/joints to stabilize rock blocks from toppling by binding the jointed rocks together (l_1 in Figs. 1 and 2). Another set of anchors which penetrated deep into the stable zone from either the bottom or the top of the slope (l_2 in Figs. 1 and 2) provided stability against sliding. These anchors extended beyond the potential failure surface for about 5 m to 7 m in length which was determined from the estimated anchor load and bond strength.

Each end of the anchor, except for that dipping into the ground, was attached and locked to a steel plate which was then covered with a reinforced concrete cap for protection against corrosion and other possible damaging effects. Figure 5 shows the details of the anchors and concrete caps. In the design of the reinforced concrete caps, both allowable bearing stress at the base of the cap and allowable bending stress at the anchor rod were analyzed. For a design anchor load of 100 tons, the cap has a square base, 1500 mm each side, with a thickness of 100 mm at edge and 150 mm at center.

Of the thirteen cross-sections taken between stations W200 and W800, two cross-sections (Sta W200 and W250) are shown in Figs. 1 and 2. Also included in the figures are the anchor layout. The stability of each stabilized slope was analyzed for plane, wedge, and rotational slides. For rotational slide, the method of slices based on the simplified Bishop method was used (Bishop, 1955). The values of safety factor obtained from the analysis are 1.60 (Sta W200) and 1.31 (Sta W250); these values are smaller than those obtained for plane and wedge sliding modes of failure.

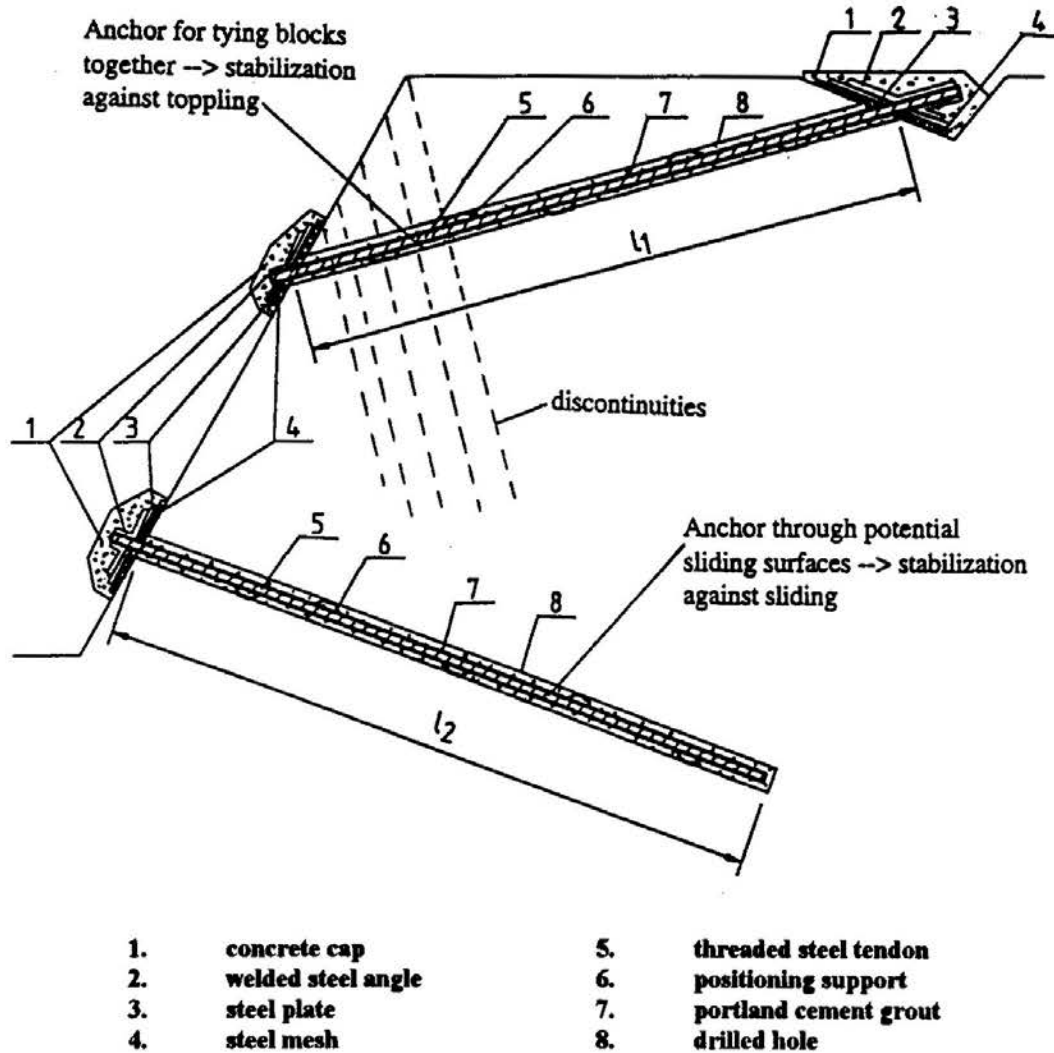


Fig. 5 Schematic of Anchor Details

PERFORMANCE

The entire stabilization work was completed in October 1988. In November 1989, a careful visual inspection did not find visible slope movement. Furthermore, in December 1989, eight pairs of measurement points were established along the existing cracks. Each pair consisting of two points were located across the crack with a spacing varying from 6.285 m to 11.467 m. The distance between the two points in a pair was measured once a month for seven consecutive months. Results of the measurement showed that the largest and smallest relative movements in a pair were 12 mm and 2 mm, respectively. Even eight years later today, no visible deterioration is seen, indicating that the slopes have been stabilized effectively.

ROCK SLOPE STABILIZATION ALONG RAILROAD

SUMMARY AND CONCLUSIONS

This case history presented an effective method of using ground anchors for rock slope stabilization along the main railroad of the surface coal mine at Fushun, an industrial city in northeastern China. The rock formations at the site were predominantly weathered shales which were randomly folded with distinct cleavages and joints. The ground anchors were installed based on the principle that unstable rock blocks can be made stable against toppling by binding them together.

The anchors were made of threaded steel rods and were grouted without prestressing along the entire length. They were installed normal to the cleavages/joints direction, when possible, to effectively bind the jointed blocks together to stabilize against toppling. Also installed were anchors dipping deep into the stable zone to provide stability against sliding. The ends of anchors on the ground surface were locked to steel plates which were then covered with reinforced concrete caps. A total of 441 fully grouted anchors were constructed throughout the unstable region. The anchors had a diameter of 36 mm with a length ranging from about 17 m to 41 m. As of today, there has been no visible sign of deterioration in the stabilized rock slopes, indicating that the anchoring system has successfully achieved the goal of stabilization.

Based on the results of this investigation, it can be concluded that using anchors to tie the unstable rock blocks together is an effective method for stabilizing unstable rock slopes. The anchors used in this project were not post-tensioned. Post-tensioning may increase the frictional resistance between jointed rock blocks. However, it may cause separation of the blocks from the underlying rock mass resulting in a decrease in sliding resistance. A salient feature of this method of stabilization is the utilization of unstable blocks to provide toppling resistance. The use of unstable blocks results in a saving of anchor materials. Therefore, this method of rock slope stabilization is effective and economical.

REFERENCES

- GOODMAN, R. E. (1980). *Introduction to Rock Mechanics*. New York: John Wiley and Sons.
- BISHOP, A. W. (1955). The use of the slip circle in the stability analysis of slopes. *Geotechnique* V, No. 1, pp. 7-17.

PVD IMPROVEMENT OF SOFT BANGKOK CLAY WITH COMBINED VACUUM AND REDUCED SAND EMBANKMENT PRELOADING

D.T. Bergado¹, J.C. Chai², N. Miura³ and A.S. Balasubramaniam⁴

ABSTRACT

The proposed site of the Second Bangkok International Airport (SBIA) comprising a total land area of 8.0 km by 4.0 km, is situated on a 16.0 m thick very soft to soft Bangkok clay. At the proposed site, a previous study has been successfully conducted involving the use of prefabricated vertical drain (PVD) with conventional preloading using sand embankment surcharge. Vacuum-assisted consolidation provides an alternative in reducing the length of preloading period. In this method, the soft clay foundation is preloaded by reducing the pore pressures through the application of vacuum pressure in combination with reduced amounts of sand surcharging. Two full scale and fully instrumented test embankments each with base area of 40 m by 40 m were constructed. In Embankment 1, hypernet drainage system combined with 15.0 m PVD length were used. For Embankment 2, perforated and corrugated pipes combined with nonwoven heat-bonded geotextiles were used as drainage system combined with 12.0 m PVD length. Among the foundation instrumentation, vibrating wire piezometers were installed in the foundation subsoil at varying depths to measure both negative and positive pore pressures. The undrained shear strength obtained after improvement was found to be 1.5 to 2.0 times higher than before improvement. Embankment 2 indicated higher drainage efficiency demonstrating 20% to 30% accelerated settlement rate compared to Embankment 1. After 45 days of vacuum pressure application, the test embankments were raised to a maximum height of 2.50 m. The surface settlements in Embankments 1 and 2 were 0.74 m and 0.96 m, respectively, after 140 days. Finite element methods (FEM) was utilized to investigate the influence factors. First, the vacuum preloading was simulated numerically by obtaining reasonable fit in the settlement values. Then, the effects of vacuum preloading was investigated by (a) simulating the field conditions, (b) maintaining higher vacuum pressures, and (c) no vacuum loading. The results of FEM analysis demonstrated the efficiency of combined vacuum preloading and reduced sand surcharging. Finally, the performance of

1 Professor of Geotechnical Engineering, School of Civil Engineering, Asian Institute of Technology Bangkok, Thailand.

2 Associate Professor, Department of Civil Engineering, Saga University, Saga 840, Japan.

3 Professor and Director of ILT, Department of Civil Engineering, Saga University, Saga 840, Japan.

4 Chair Professor of Geotechnical Engineering, School of Civil Engineering, Asian Institute of Technology, Bangkok, Thailand.

Note: Discussion is open until 1 September 1998. This paper is part of the *Geotechnical Engineering Journal*, Vol. 29, No. 1, June 1998. Published by the Southeast Asian Geotechnical Society, ISSN 0046-5828.

Embankment 2 as compared to the previous studies using conventional surcharging, demonstrated a 60% acceleration in the rate of settlement and 4 months reduction in the preloading time.

INTRODUCTION

At the site of the proposed Second Bangkok International Airport (SBIA), the presence of 16.0 m thick, weak, and compressible soft Bangkok clay pose a lot of foundation problems (AIT, 1995). For economic utilization of the proposed site, ground improvement techniques are necessary. In this regard, ground improvement with prefabricated vertical drain (PVD) has been studied successfully using conventional sand surcharge (Bergado, et al., 1997). Since sand materials are increasingly expensive being sourced from far distances, vacuum-assisted preloading can be viable alternative. In this method, instead of increasing the effective stresses in the soil mass by increasing the total stresses, vacuum preloading relies on increasing the effective stresses by decreasing the pore pressures. Thus, vacuum preloading combined with reduced sand surcharging can shorten the consolidation period considerably without endangering the stability of the test embankment.

In this study, two full scale embankments, namely: Embankment 1 and Embankment 2, were constructed at the SBIA site with PVD lengths of 15.0 m combined with hypernet drainage system and 12.0 m with corrugated pipe drainage system, respectively. The PVDs consisted of Mebra Drains and were installed at 1.0 m spacing in triangular pattern. The test embankments with base dimensions of 40 m by 40 m were constructed in stages up to a height of 2.50 m in order to provide surcharge and combined with a vacuum pressure of -60 kPa continuously for a period of 5 months.

PRINCIPLES OF VACUUM CONSOLIDATION TECHNIQUE

Vacuum consolidation was proposed in early 1950s by Kjellman (1952). Isolated studies of vacuum induced consolidation continued for the next two decades (Holtz, 1975). Vacuum-assisted consolidation provides an effective alternative to surcharging for preloading soils. Instead of increasing the effective stress in the soil mass by increasing the total stress by means of conventional mechanical surcharging, vacuum assisted consolidation preloads the soil by reducing the pore pressure while maintaining constant total stress. Figure 1 presents a typical layout of a vacuum-assisted consolidation with PVD. Figure 2 graphically portrays the initial total stress in the ground and pore pressure induced due to (a) conventional surcharge and (b) vacuum loading applied at the ground surface assuming 100% efficiency (vacuum pressure of -100 kPa). Vacuum-assisted consolidation with PVD was tested in China and was

PVD IMPROVEMENT OF SOFT BANGKOK CLAY

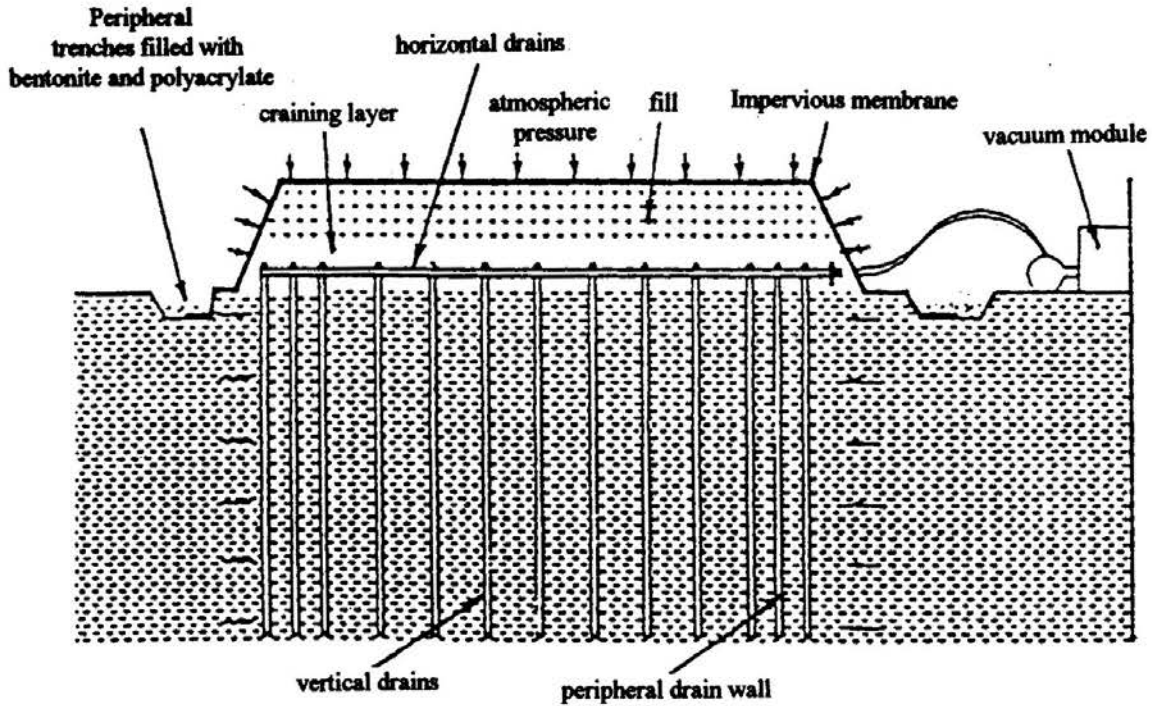


Fig. 1 Schematic Layout of Vacuum Consolidation (Cognon, et al., 1994)

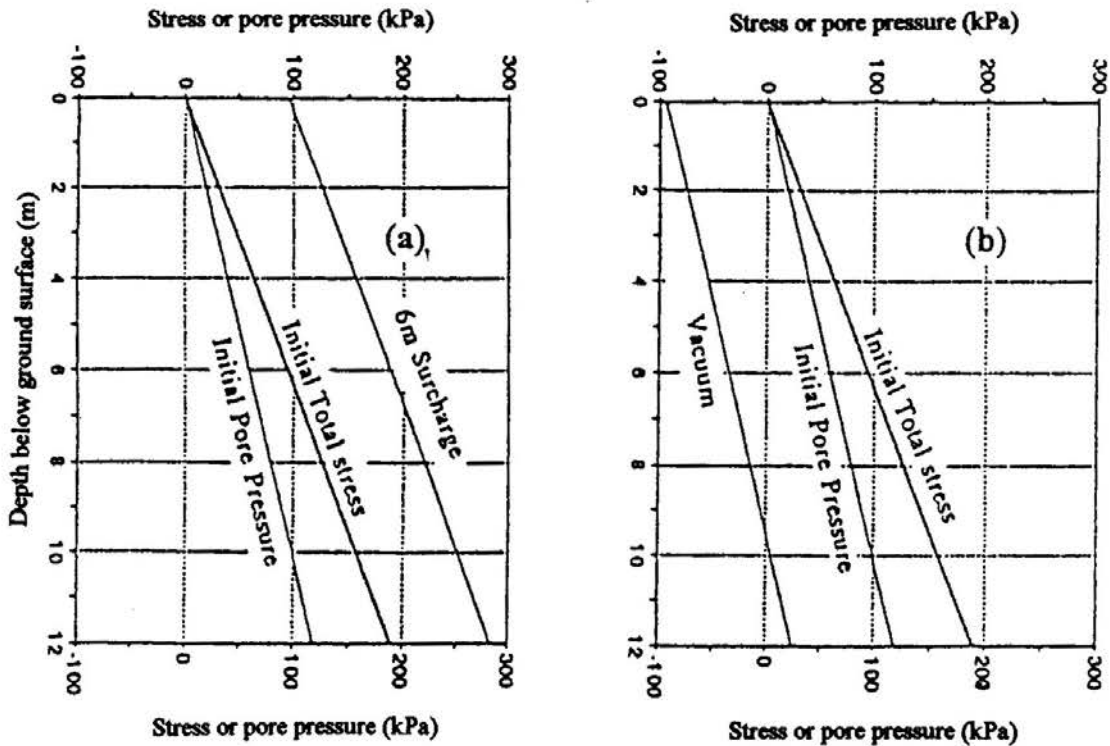


Fig. 2 Theoretical Pore Pressure and Vertical Stress Distribution during Surcharge and Vacuum Consolidation (Assuming 100% Efficiency) (Cognon, et al., 1994)

presented by Choa (1989) with approximately 70% to 80% efficiency. Jacob, et al. (1994) reported an average vacuum efficiency of 40% to 50% compared to a target value of 70% for a test section with PVD on a hydraulic landfill area.

SITE DESCRIPTION AND SOIL PROFILE

The proposed site of the Second Bangkok International Airport (SBIA) is located at Nong Ngu Hao in the Central Plain of Thailand. Figure 3 shows the project area of about 8 km by 4 km situated about 25 km east of Bangkok Metropolis.

The soil profile at the site can be divided into 5 sublayers as shown in Fig. 4. It consists of a 1.0 m thick weathered clay layer overlying very soft to soft dark gray layer which extends from 1.0 m to 10.5 m depth. Underneath the soft clay layer, a 2.5 m thick medium clay layer can be found. The light-brown stiff clay layer can be encountered at 14.0 m to 21.0 m depth. The undrained shear strength of the very soft to soft clay layer increased from 13 kPa to 27 kPa with depth. The groundwater level was found at about 0.50 m depth. The initial piezometric level is lower than the theoretical hydrostatic pressure below 6.0 m depth due to the excessive withdrawal of groundwater causing ground subsidence (Fig. 10).

FULL SCALE TEST EMBANKMENT

Two full scale test embankments each with base area of 40 m by 40 m with different drainage systems were constructed on soft Bangkok clay with PVD. In Embankment 1 (TV 1), hypernet drainage system with 15 m PVD length were used. For Embankment 2 (TV 2), perforated and corrugated pipes combined with nonwoven geotextiles with 12 m length PVD were utilized. The plan of the test area is given in Fig. 5. Also shown in Fig. 5 are the locations of boreholes and field vane tests as well as the dummy area. The working platforms which also served as drainage blankets were constructed with thickness of 0.30 m for Embankment 1 and 0.80 m for Embankment 2.

The PVDs were installed from the working platforms to a depth of 15 m for TV1 and 12 m for TV2. As shown in Fig. 6, the PVDs were installed in triangular pattern with 1.0 m spacing. The parameters related to the behavior of PVD are listed in Table 1.

The cross-sections of TV1 and TV2 are shown in Figs. 7 and 8, respectively. The drainage layers of the test embankments are also shown in Figs. 7 and 8 consisting of, respectively, hypernet for TV1 and perforated and corrugated pipes covered with geotextiles for TV2. The geotextile consisted of 136 g/m² nonwoven spunbonded polypropylene with high modulus. The hypernet (or geonet) consists of a grid of HDPE

PVD IMPROVEMENT OF SOFT BANGKOK CLAY

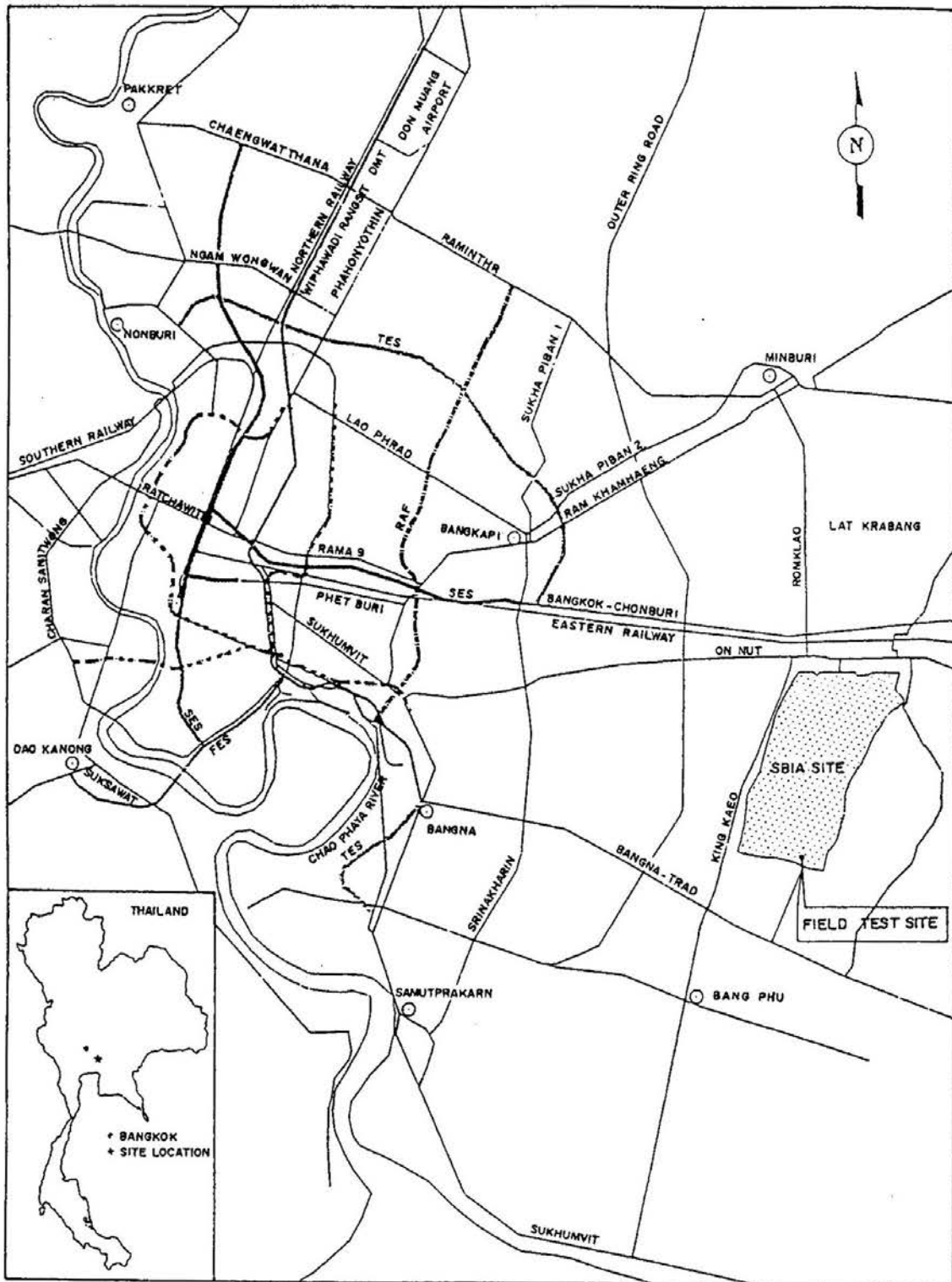


Fig. 3 Location of Nong Ngu Hao Site

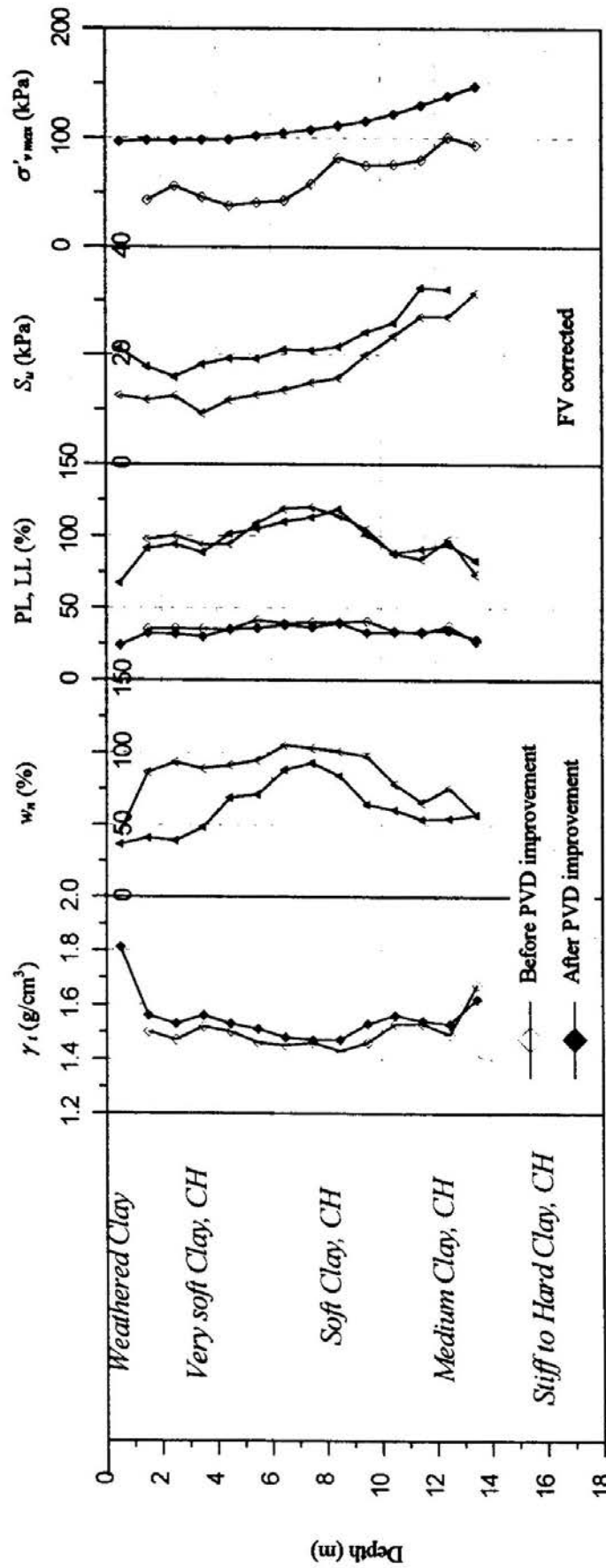


Fig. 4 Soil Profile and Soil Properties

PVD IMPROVEMENT OF SOFT BANGKOK CLAY

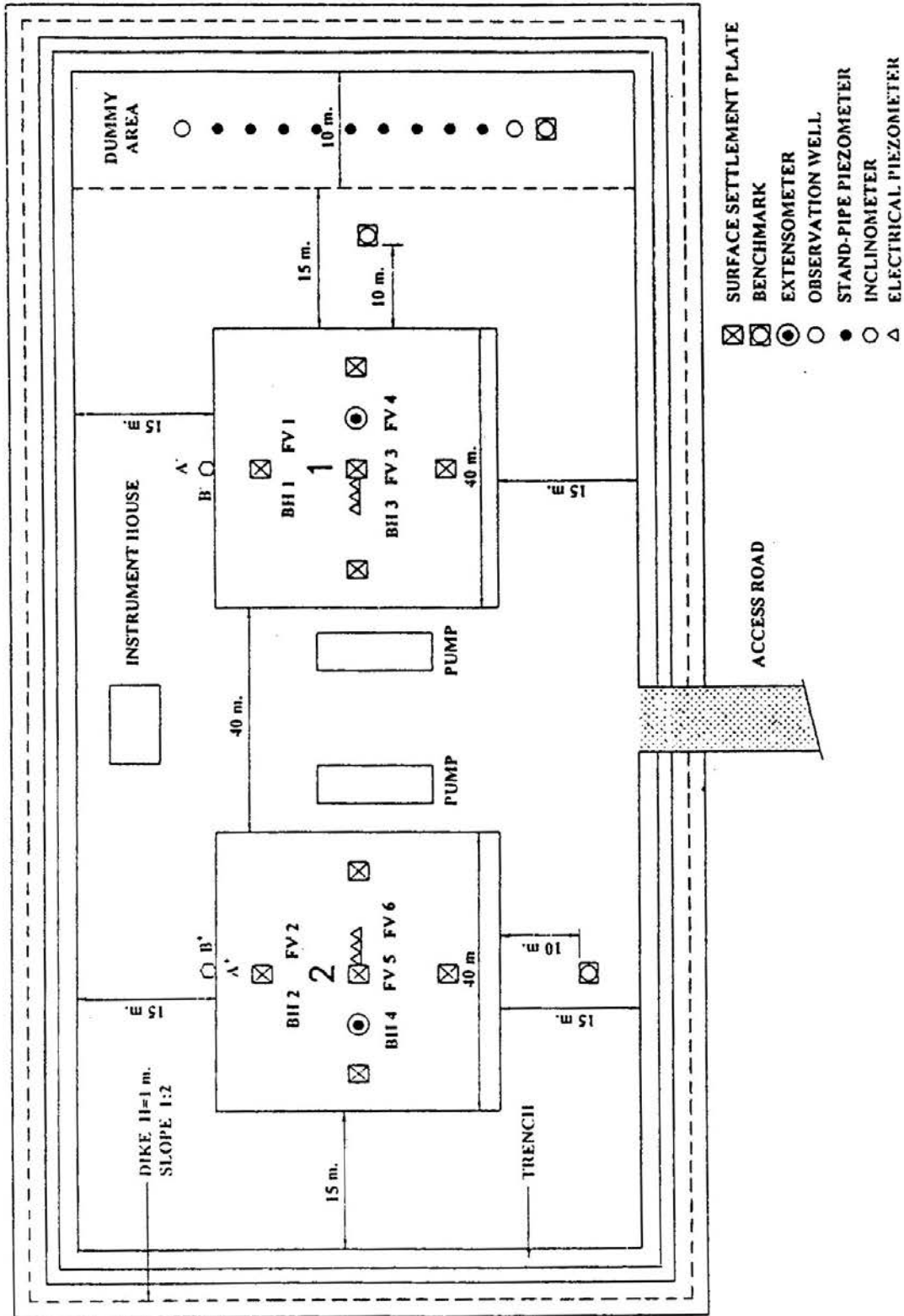


Fig. 5 Layout of Monitoring Instrumentations and Locations of Boreholes and Field Vane Tests

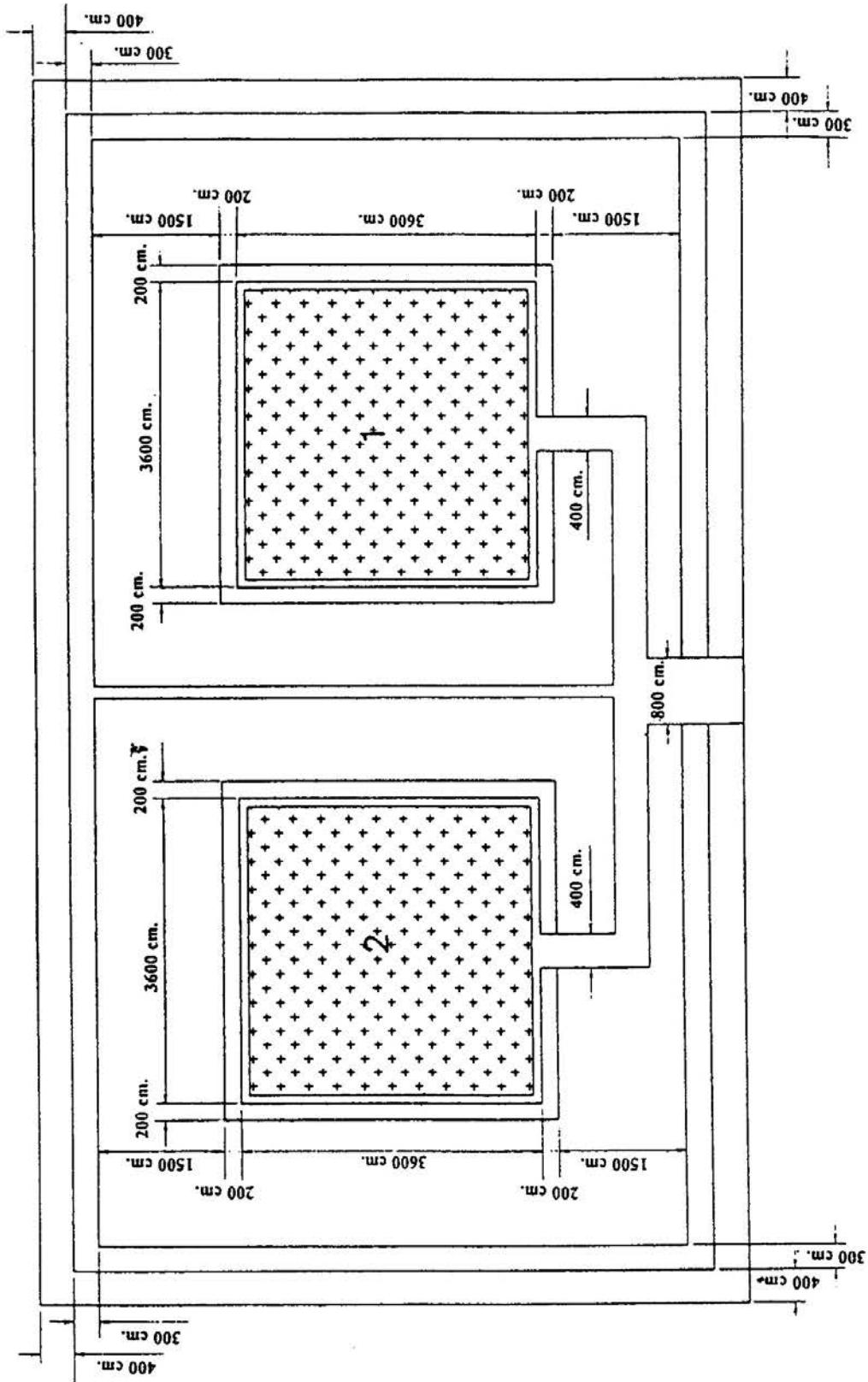


Fig. 6 Plan of the Vertical Drain

PVD IMPROVEMENT OF SOFT BANGKOK CLAY

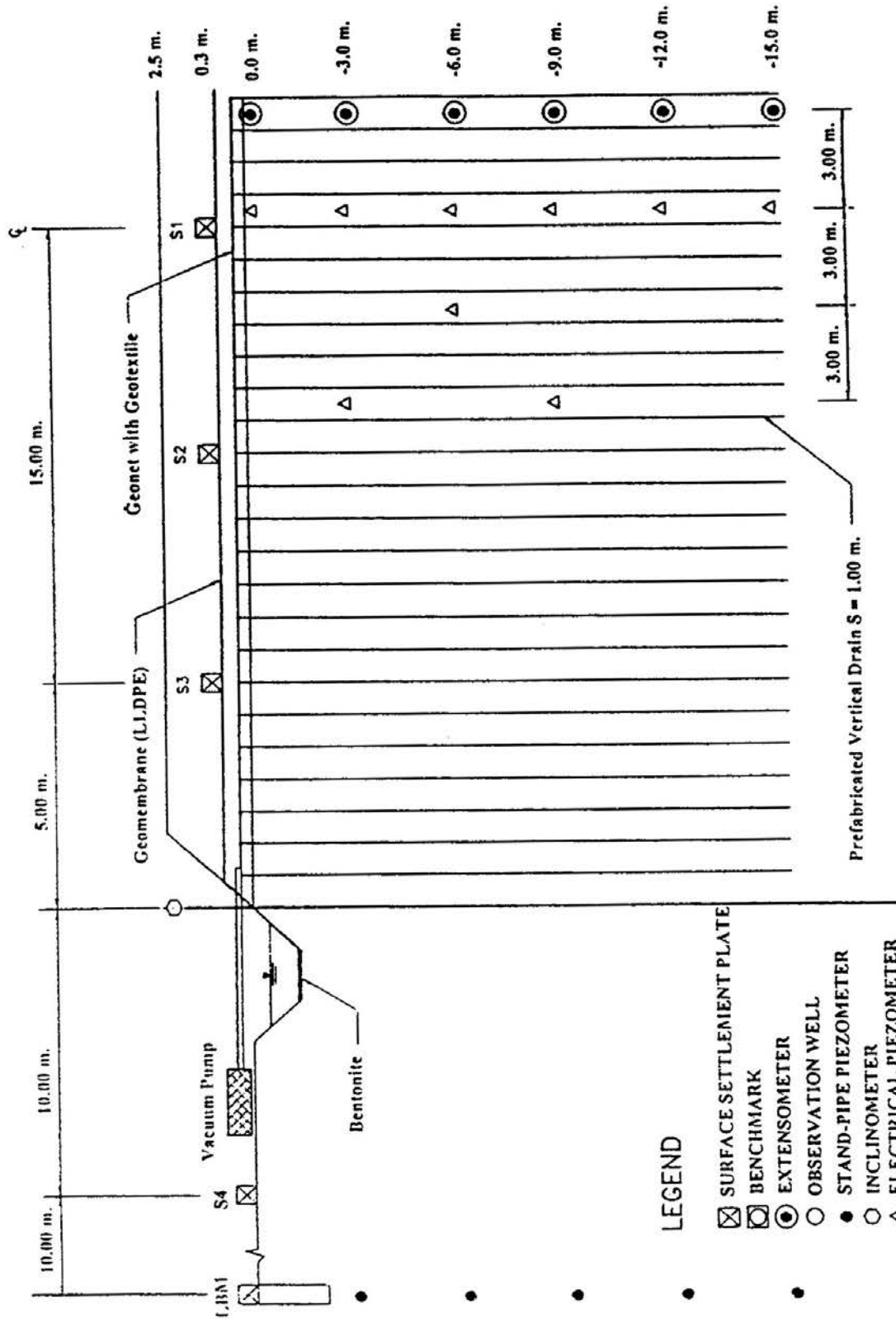


Fig. 7 Cross-Section of Embankment 1 with 15.0 m Long PVD and Locations of Monitoring Instrumentations

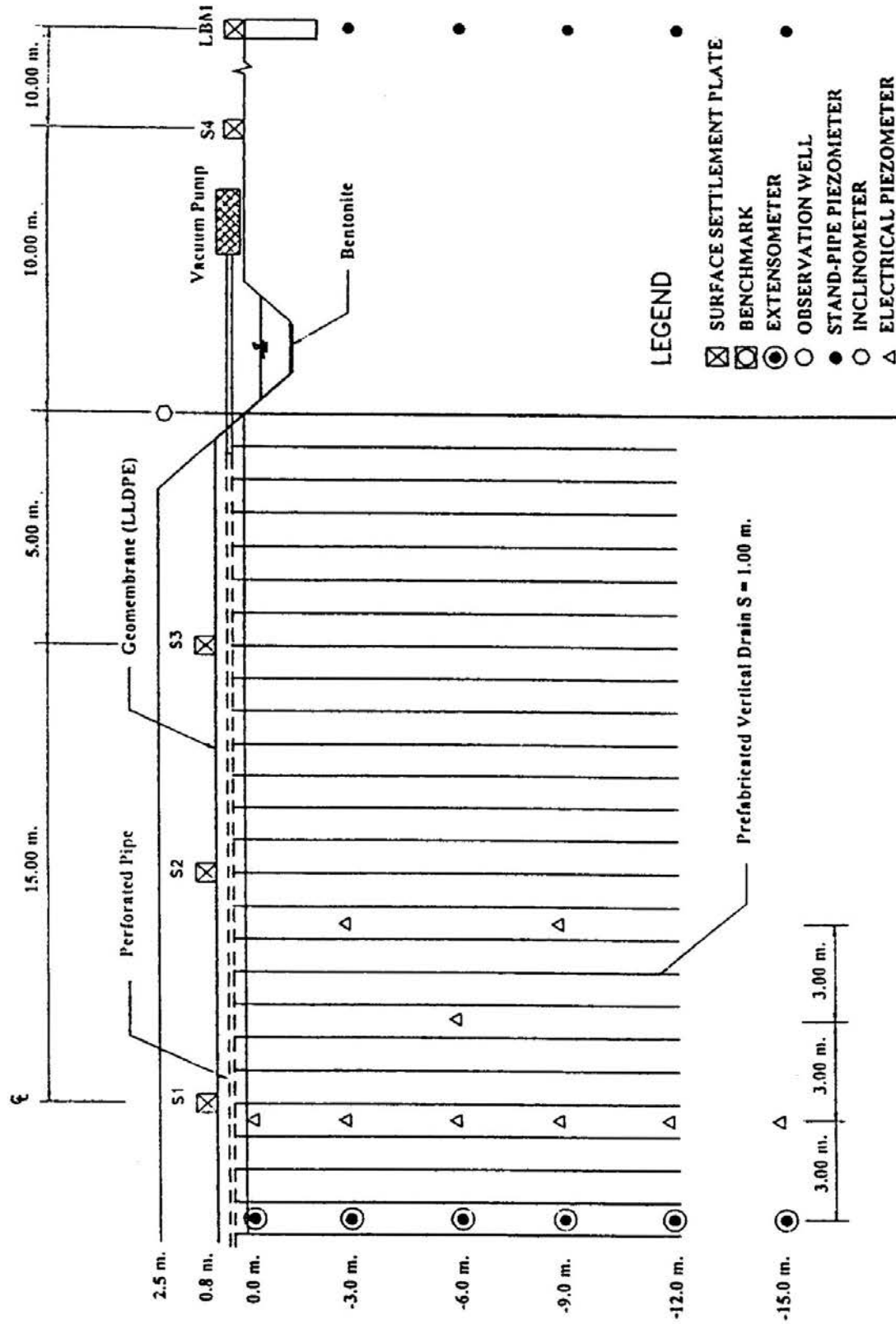


Fig. 8 Cross-Section of Embankment 2 with 12.0 m Long PVD and Location of Monitoring Instrumentations

PVD IMPROVEMENT OF SOFT BANGKOK CLAY

Table 1 Parameters of Vertical Drain

Spacing, S	1.0 m (triangular pattern)
Diameter of drain, d_w	50 mm
Diameter of smear zone, d_s	300 mm
Ratio of K_v/K_s	10
Drainage length, l	15 m for TV1 and 12 m for TV2
Discharge capacity, q_w (per drain)	50 m ³ /year

threads which are melted together at their intersections. The hypernet has discharge capacity of 8×10^{-3} m³/s per meter width. One layer of hypernet was placed over the whole area. The perforated and corrugated pipes consists of 5 pieces of Mebra tubes with 80 mm diameter and 297 g/m weight. On top of the drainage system, a water and air tight LLDPE geomembrane liner was placed. The geomembrane liner was sealed by placing the edges at the bottom of the perimeter trench and covered with 300 mm layer of sand-bentonite and submerged underwater.

COMBINED VACUUM PRESSURE AND SURCHARGE PRELOADING

In each embankment, the water collection system was connected to vacuum pump capable of supplying -70 kPa vacuum pressure continuously. A back-up pump was also provided. After applying the vacuum pressure for 45 days, the embankments were raised in stages up to a height of 2.50 m. Embankment 1 and, similarly, Embankment 2 were raised from 0.30 m and 0.80 m height, respectively. The stage loading diagrams with time are shown in Fig. 11 for both Embankments 1 and 2.

FIELD INSTRUMENTATIONS

The field instrumentations for monitoring of embankment behavior include surface settlement plates, subsurface multipoint extensometers, vibrating wire electrical piezometers, and inclinometers. In the dummy area, the instrumentations include standpipe piezometers, surface settlement plates (or benchmarks), and observation wells. Figures 5, 7 and 8 show the typical layout of instrumentations for the test embankments. The vibrating wire piezometers were installed under the test embankments at 3.0 m depth intervals together with the sensors for the multipoint extensometers. The surface settlement plates were placed directly on top of the geomembrane liner. The inclinometers were placed at the edges of each test embankment. At the dummy area, observation wells, standpipe piezometers and a benchmark were also installed.

FEM ANALYSES OF VACUUM CONSOLIDATION

Considering that most finite element codes used in practice do not include special drainage element, a simple approximate method for modeling the effect of PVD has been proposed by Chai and Miura (1997). From the macro point of view, PVD increases the mass permeability in the vertical direction. Consequently, it is possible to establish a value of the vertical permeability which approximately represents the combined vertical permeability of the natural subsoil and the radial permeability towards the PVD. This equivalent vertical permeability (K_{ve}) is derived based on equal average degree of consolidation together with the following assumptions:

1. The deformation mode of PVD improved subsoil is close to one-dimensional. Thus, one-dimensional consolidation theory can be used to represent the consolidation in the vertical direction and the unit cell theory of Hansbo (1979) for radial consolidation is applicable.
2. The total degree of consolidation is the combination of vertical and radial consolidation by using the relationship proposed by Scott (1963).

In order to obtain a one-dimensional expression for the equivalent vertical permeability, an approximate equation for consolidation in vertical direction is proposed as follows:

$$U_v = 1 - \exp(-3.54) T_v \quad (1)$$

where U_v is the vertical degree of consolidation and T_v is the dimensionless time factor. The equivalent vertical permeability, K_{ve} , can be expressed as:

$$K_{ve} = \left(1 + \frac{2.26L^2 K_h}{FD_e^2 K_v} \right) K_v \quad (2)$$

where:

$$F = \ln\left(\frac{D_e}{d_w}\right) + \left(\frac{K_h}{K_s} - 1\right) \ln\left(\frac{d_s}{d_w}\right) - \frac{3}{4} + \frac{\pi 2L^2 K_h}{3q_w} \quad (3)$$

where D_e is the equivalent diameter of a unit PVD influence zone, d_s is the equivalent diameter of the disturbed zone, d_w is the equivalent diameter of PVD, K_h and K_s are the undisturbed and disturbed horizontal permeability of the surrounding soil, respectively, L is the PVD length for one-way drainage, and q_w is the discharge capacity of PVD. The effects of smear and well-resistance have been incorporated in the derivation of the equivalent vertical permeability.

PVD IMPROVEMENT OF SOFT BANGKOK CLAY

For numerical modeling, the ground was divided into 5 sublayers and represented by modified Cam clay model (Roscoe and Burland, 1968). The adopted model parameters are listed in Table 2. Part of the values in Table 2 were evaluated based on laboratory consolidation test results and part of them were determined empirically. The values of permeability were determined by referring to the back-calculated data of previous test embankments in the adjacent area (Chai, et al., 1996). The estimated initial stresses water pressure and the size of yield locus are given in Table 3. The factor of hydraulic pressure drawdown due to excessive pumping of groundwater was considered for evaluating the initial stresses.

With the soil parameters in Table 2, and the compression modulus corresponding to the yielding stress (size of yielding locus in Table 3), for a point 5.0 m below ground surface (middle of very soft to soft clay layer), a coefficient of consolidation of about $7 \text{ m}^2/\text{yr}$ can be obtained. This value is comparable with the field value obtained from dissipation tests using the piezocone apparatus in Fig. 13 (Hanh et al, 1998). This indicates that the piezocone dissipation test is useful for determining the field coefficient of consolidation.

SIMULATION OF VACUUM CONSOLIDATION

The analyses were conducted under plane strain condition. The vacuum consolidation was simulated by fixing the excess pore pressure at ground surface of the test area. There are discrepancies between the measured vacuum pressure in the sand mat and at the ground surface. The adopted values are based on the measured values at ground surface with adjustment on the vacuum pressure at the early stage (<20 days). This is because the measurement yielded low vacuum pressures at the early stages but there were considerable settlements.

In this study, first the vacuum consolidation were simulated numerically. After obtaining a reasonable fitting of settlement magnitudes, the distribution as well as the variation of vacuum pressure in the ground was studied. Then, the effect of vacuum was studied using higher vacuum (-60 kPa) and no vacuum. Figures 9(a) and 9(b) show the adopted vacuum pressure-time curves for both test embankments. The higher vacuum cases are also shown in the figures. The measured total pore pressures at different depths with time are given in Fig. 10(a). The measured total and excess pore pressures in the subsoils at Embankment 2 are plotted with depth in Fig. 10(b). The loading histories of the test embankments (Fig. 11) according to the field record were also used in the simulations.

LATERAL DEFORMATIONS

The lateral displacements obtained from FEM analyses are compared to the measured values after 45 days of vacuum application in Figs. 15(a) and 15(b) for both embankments. For both embankments, especially Embankment 1, the simulated data are comparable to the measured data below 2.0 m depth. However, for both embankments, the measured data do not agree with the simulations near the ground surface. An explanation for these discrepancies is the possible disturbances of the

CONSOLIDATION SETTLEMENTS

Figure 9 illustrates the construction stages of both test embankments together with the settlement-time curves at varying depths. In Embankment 1, the maximum settlement after 144 days at the ground surface, 3 m, 6 m, 9 m and 12 m depths were 0.74 m, 0.48 m, 0.26 m and 0.09 m, respectively. The corresponding values in Embankment 2 were 0.97 m, 0.70 m, 0.35 m and 0.11 m, respectively.

Using FEM analysis, the calculated settlements are compared with the observed values in Figs. 12(a) and 12(b). Although there are slight discrepancies, it is considered that FEM analysis simulated the measured data reasonably well.

BENEFICIAL EFFECTS OF VACUUM CONSOLIDATION

To quantify the beneficial effects of vacuum consolidation, Figs. 14(a) and 14(b) compare the surface settlements at the center of the test embankment obtained from the FEM analyses with the corresponding measured data assuming no vacuum pressure, with vacuum pressure that simulates the field conditions, and at higher vacuum pressure. For Embankment 1 in Fig. 14(a), at about 140 days and no vacuum case, a settlement of 0.43 m can be obtained. With vacuum pressure as indicated by solid line in Fig. 9(a), the settlement was 0.73 m. If the high vacuum pressure of -60 kPa (dashed line in Fig. 9a) was maintained, the settlement would be 1.30 m. The beneficial effects of vacuum consolidation have been demonstrated.

Figure 14(b) compares the numerical results of no vacuum, with vacuum, and higher vacuum cases with the measured settlement data for Embankment 2. The trends are similar to Embankment 1. For no vacuum, the slight difference in loading history of Embankments 1 and 2 does not have significant effects on foundation settlements. The vacuum consolidation is effective if the vacuum preloading can be maintained for longer periods and if leaks are prevented. The results have indicated that even with PVD installation, high vacuum pressure need to be maintained for 4 to 5 months to achieve higher degree of consolidation.

PVD IMPROVEMENT OF SOFT BANGKOK CLAY

inclinometer casings near the ground surface. When applying vacuum pressure at the ground surface, the effective stress increment in the top soil layer will be approximately the same for both horizontal and vertical directions. Therefore, based on the principles of soil mechanics, the vacuum pressure application would induce an inward lateral deformation, if the effect of the embankment fill surcharge is neglected.

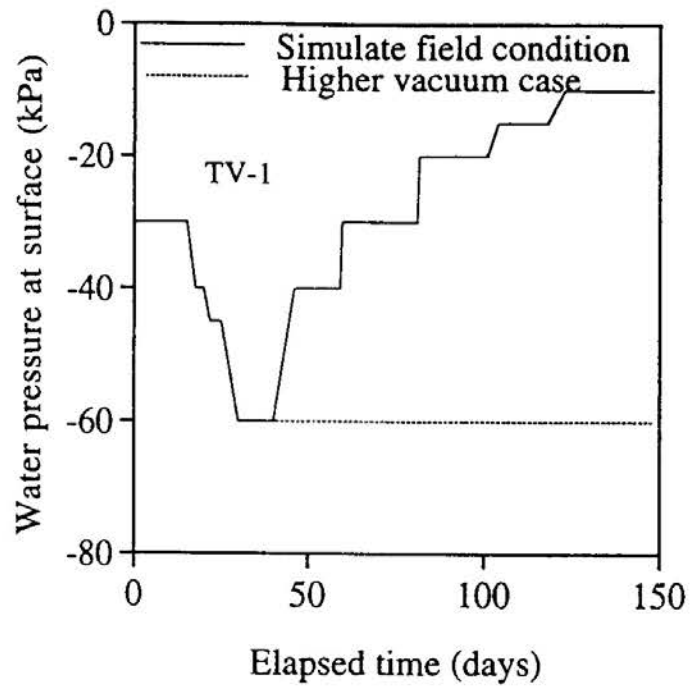
EXCESS PORE PRESSURES

Figures 16(a) and 16(b) show the contours of simulated excess pore pressures for both embankment foundations at the end of high vacuum application (45 days after pumping started). For Embankment 1, the vacuum pressure affected down to 15.0 m depth (depth of PVD installation). However, the vacuum pressure at 15.0 m depth is only -15 kPa which is quite small compared to -60 kPa vacuum pressure at the ground surface. For Embankment 2, the vacuum pressure at 12.0 m depth (depth of PVD installation) was -30 kPa. This higher value is considered to be the main reason for larger settlements in Embankment 2.

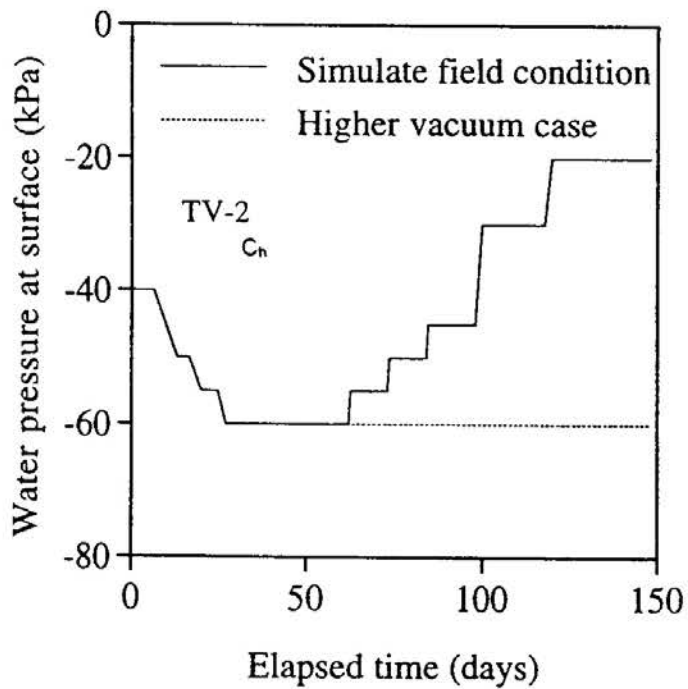
The simulated and measured excess pore pressures are compared in Figs. 17(a) and 17(b) for both embankments. At 45 days for both embankments, the lower measured excess pore pressures in the lower depths maybe explained as follows: (a) the piezometers might be close to the PVD, (b) the initial total pore pressures might be higher due to the recharge effects of PVD (Fig. 10), and (c) the effects of ground subsidence due to excessive withdrawal of groundwater which greatly reduced the excess pore pressures (piezometric drawdown) at lower depths (Fig. 10). For Embankment 2 at 140 days in Fig. 17(b), the predicted excess pore pressure is lower than the measured data. This is because to fit the measured settlements in the simulation, the surface vacuum pressure was maintained at -20 kPa.

COMPARISON WITH PREVIOUS STUDIES ON PVD

The settlement of Embankment 2 with PVD spaced at 1.0 m in triangular pattern and 12.0 m long with vacuum preloading was compared with the results of previous studies with conventional sand surcharge. Embankment TS3 in the previous test embankment had PVD spaced at 1.0 m in triangular pattern and 12.0 m long preloaded with conventional sand embankment. Figure 18 shows the loading and settlement records of both embankments. Embankment TS3 indicated a total settlement of 1.60 m after 400 days under a maximum sandfill surcharge of 4.2 m high. However, under a sandfill height of 2.5 m surcharge, greater settlements were indicated for Embankment 2 with vacuum preloading than Embankment TS3. Moreover, an acceleration in the rate of settlement of 60% was recorded. Furthermore, under vacuum pressure, the preloading period to obtain the same amount of settlement is also reduced by 4 months.



(a)



(b)

Fig. 9 Vacuum Pressure Preloading at the Ground Surface for (a) Embankment 1 (TV-1) and (b) Embankment 2 (TV-2)

PVD IMPROVEMENT OF SOFT BANGKOK CLAY

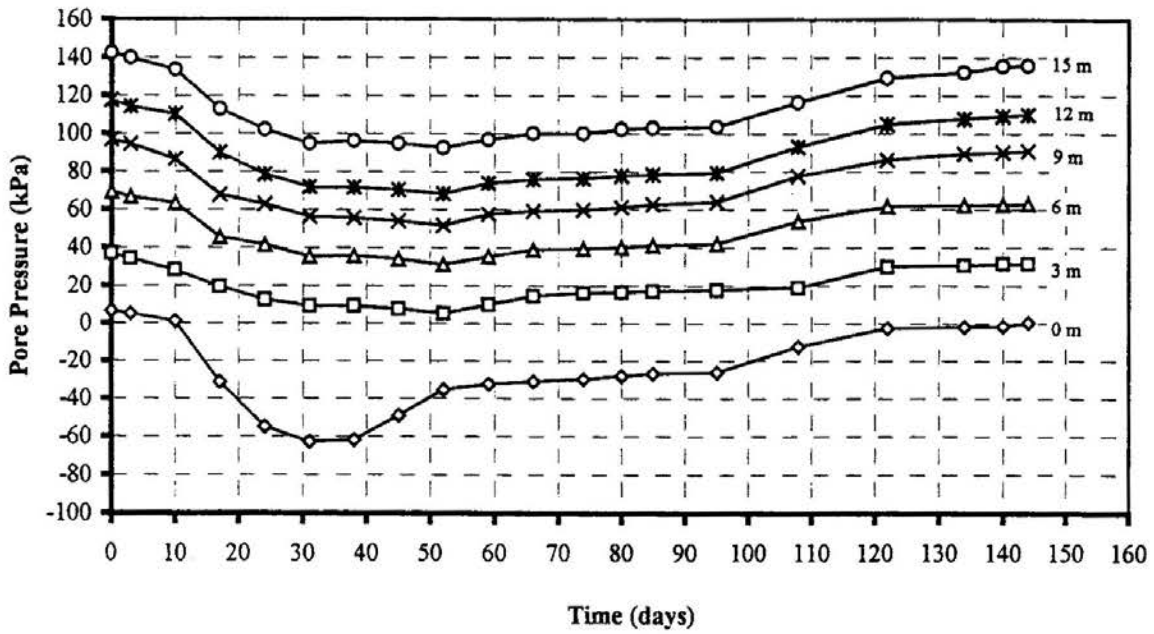


Fig. 10(a) Pore Pressure of Embankment 2 at Different Depths with Time from Vibrating Wire Piezometers

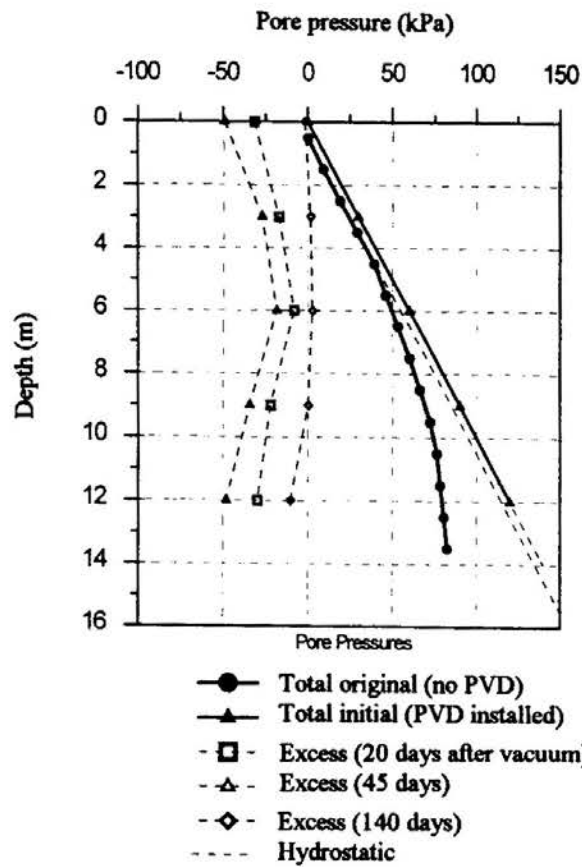


Fig. 10(b) Pore Pressures with Depth at Embankment 2

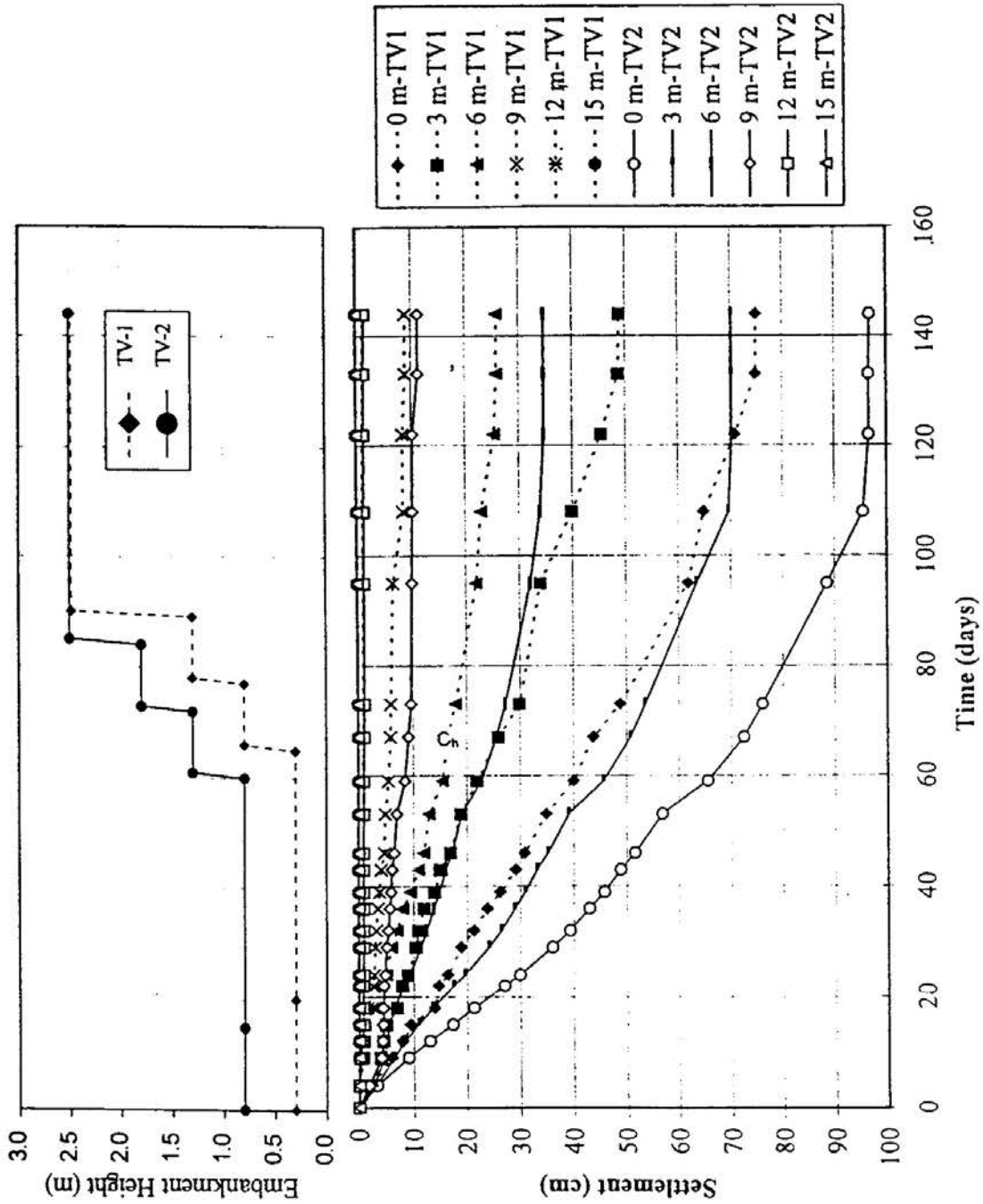
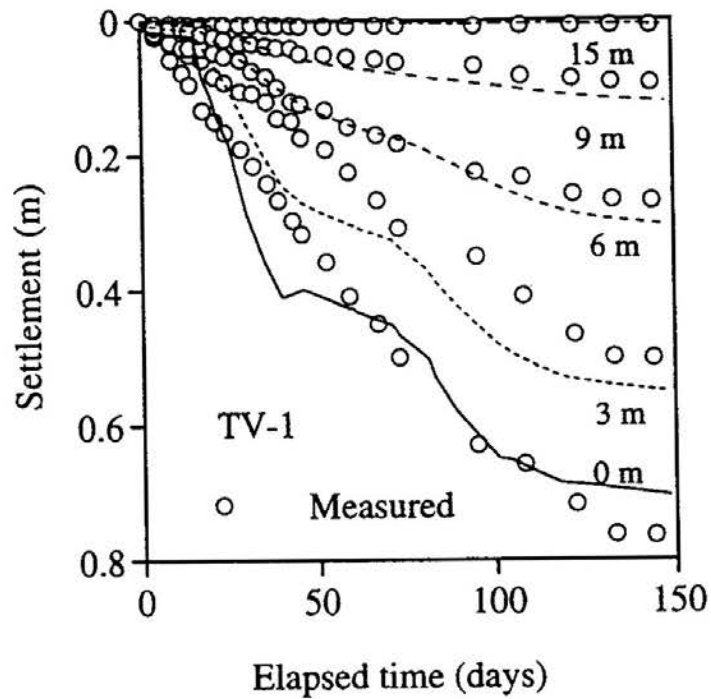
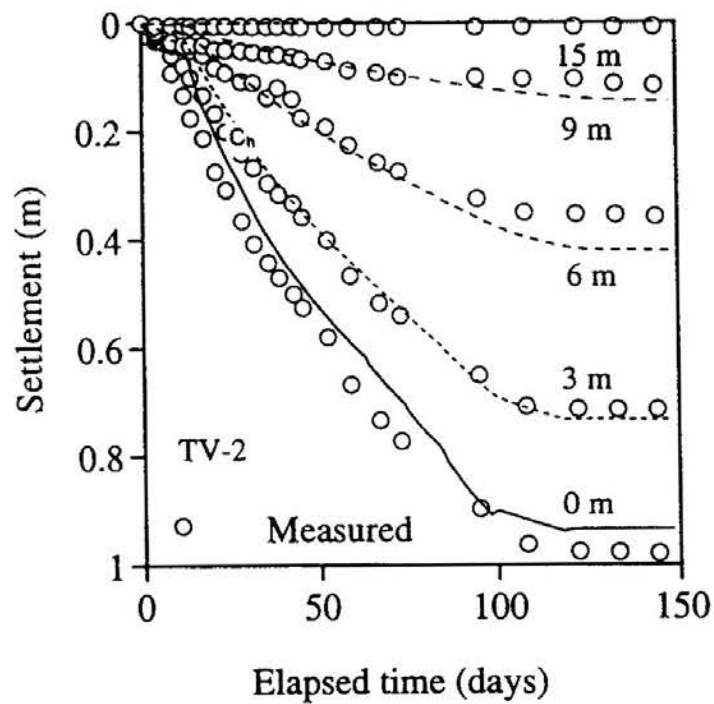


Fig. 11 Stage Loading and Settlements with Time for Embankment 1 (TV-1) and Embankment 2 (TV-2)

PVD IMPROVEMENT OF SOFT BANGKOK CLAY



(a)



(b)

Fig. 12 Calculated and Measured Settlements for (a) Embankment 1 (TV-1) and (b) Embankment 2 (TV-2)

Table 2 Soil Parameters

Depth m	e_o	λ	κ	ν	M	K_h 10^{-4} m/day	K_v 10^{-4} m/day	γ kN/m ³
0-1.0	1.8	0.3	0.03	0.3	1.2	26	26	16.0
1.0-8.5	2.8	0.73	0.08	0.3	1.0	11	5.5	14.5
8.5-10.5	2.4	0.5	0.05	0.25	1.2	5.2	2.6	15.0
10.5-13.0	1.8	0.3	0.03	0.25	1.4	2.2	1.1	16.0
13.0-18.0	1.2	0.1	0.01	0.25	1.4	0.52	0.26	18.0

Table 3 Initial Stresses

Depth m	σ_{ho} kPa	σ_{vo} kPa	μ_o kPa	Size of Yield, Locus (ρ_o') kPa
0.0	5.0	5.0	-5.0	57.5
0.5	8.0	8.0	0.0	52.7
1.0	11.7	11.0	5.0	42.0
2.0	13.2	15.5	15.0	40.0
3.0	15.6	20.75	25.0	39.7
8.5	35.3	54.75	70.0	75.0
10.5	39.9	79.75	75.0	80.0
13.0	49.3	114.75	80.0	105.5
18.0	88.0	204.75	80.0	188.3

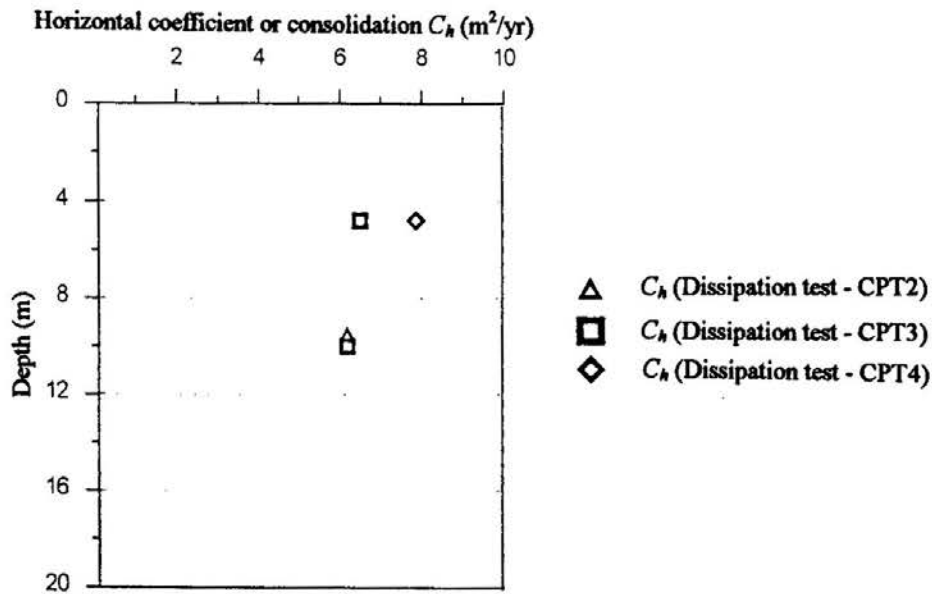
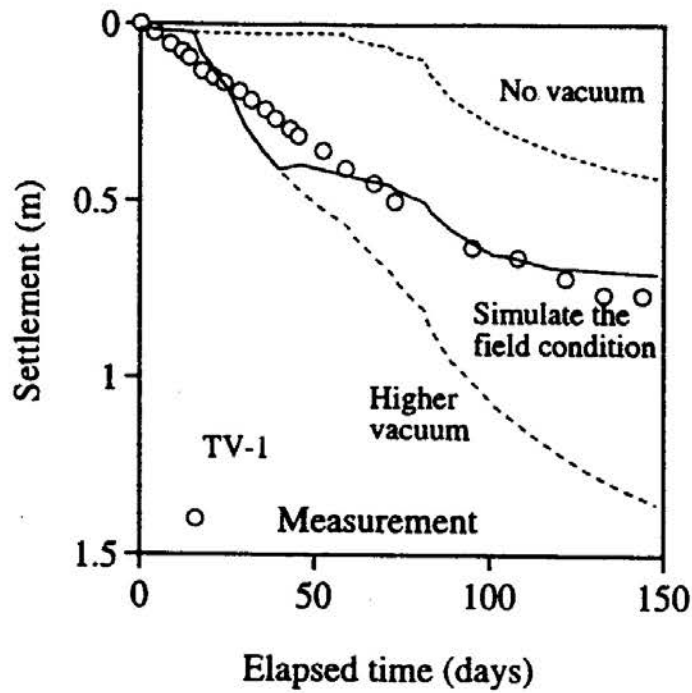
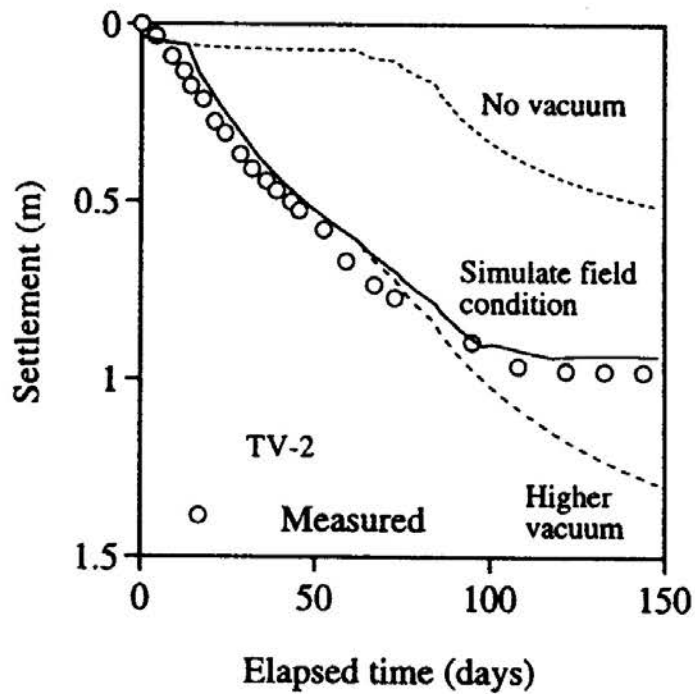


Fig. 13 Measured C_h Values from Piezocome Tests (Hanh, et al., 1998)

PVD IMPROVEMENT OF SOFT BANGKOK CLAY

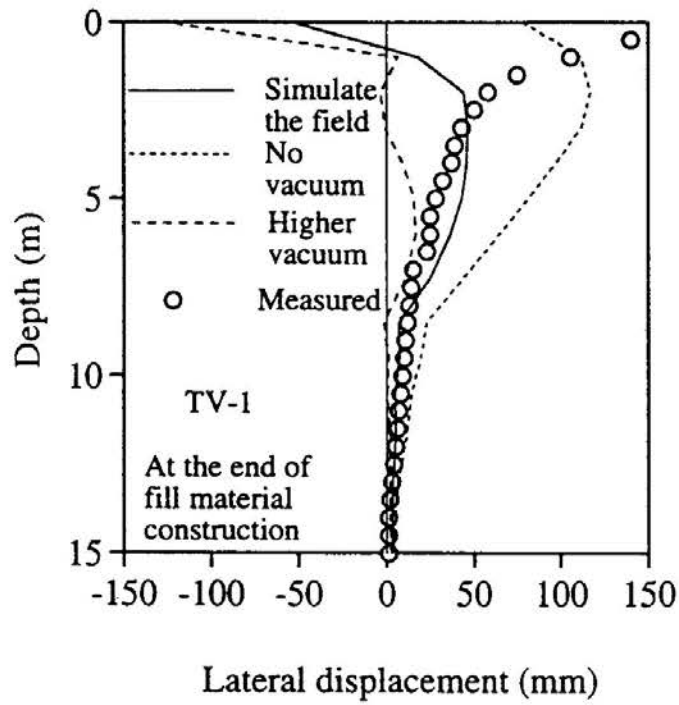


(a)

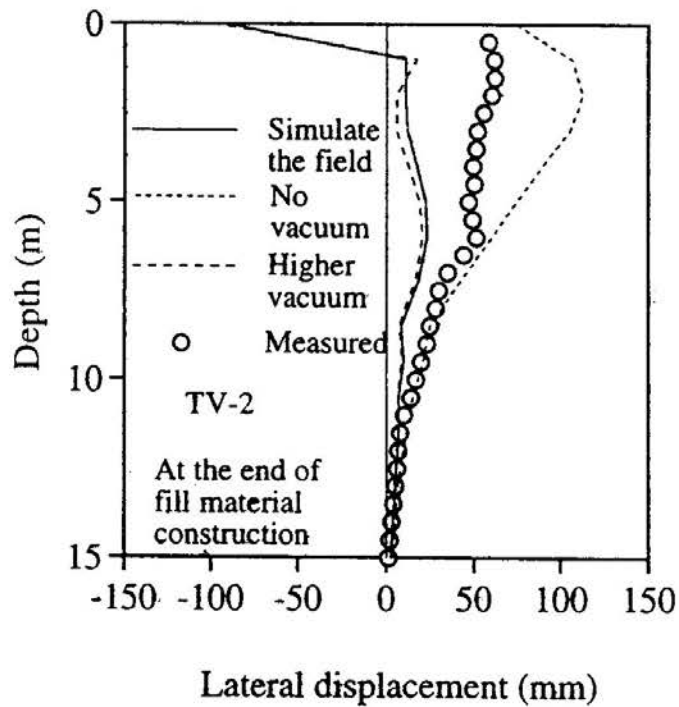


(b)

Fig. 14 Comparison of Simulated and Measured Settlements for (a) Embankment 1 (TV-1) and (b) Embankment 2 (TV-2)



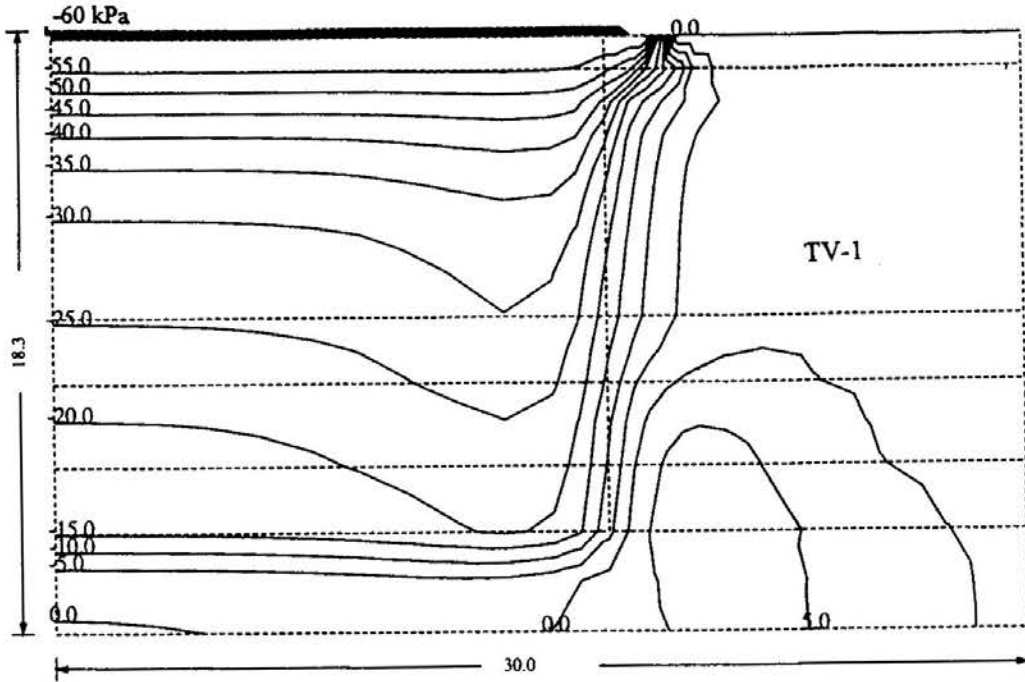
(a)



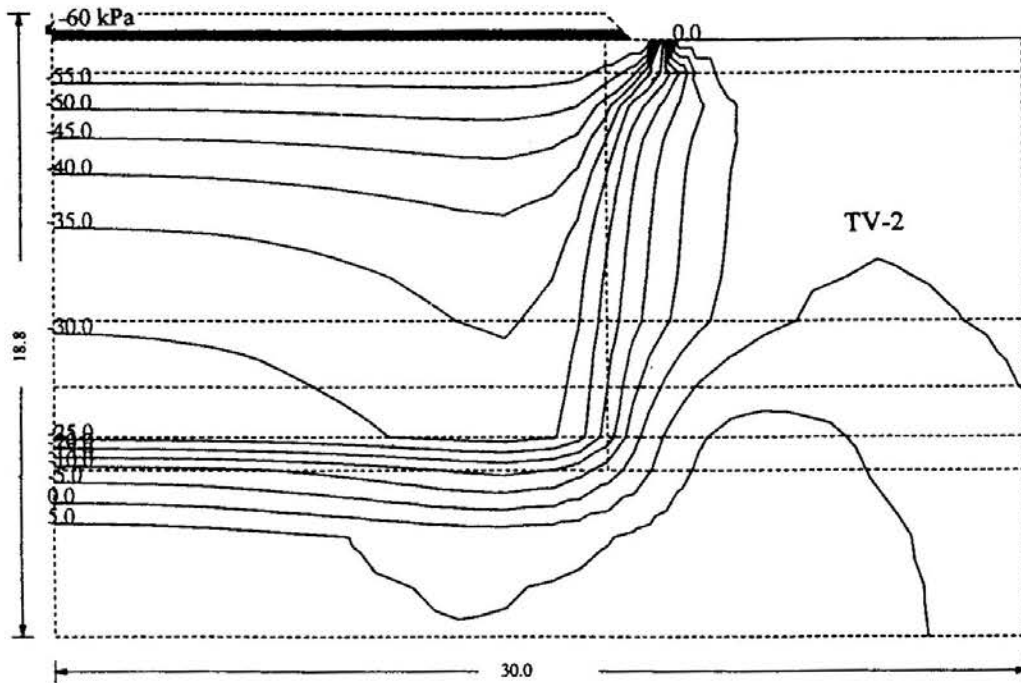
(b)

Fig. 15 Calculated and Measured Lateral Displacements at (a) Embankment 1 (TV-1) and (b) Embankment 2 (TV-2)

PVD IMPROVEMENT OF SOFT BANGKOK CLAY



(a)



(b)

**Fig. 16 Simulated Contours of Excess Pore Pressures for
(a) Embankment 1 (TV-1) and (b) Embankment 2 (TV-2)**

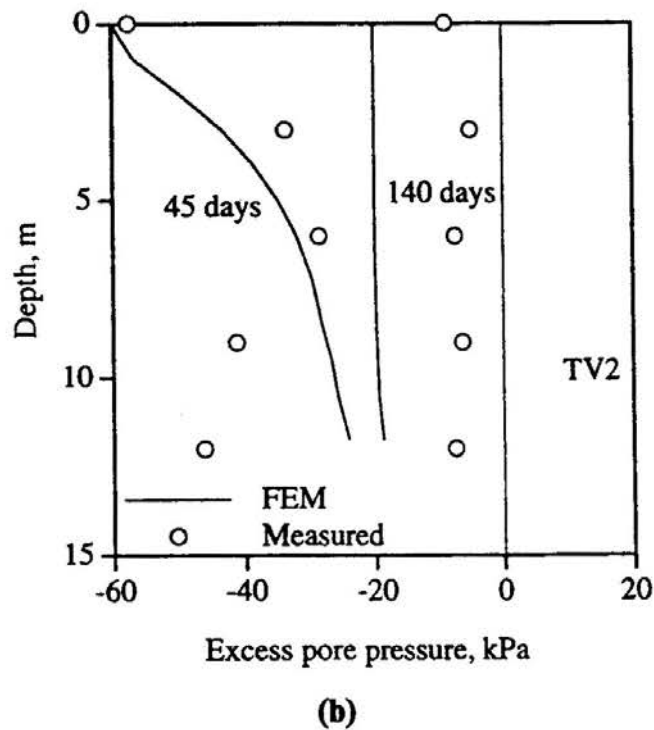
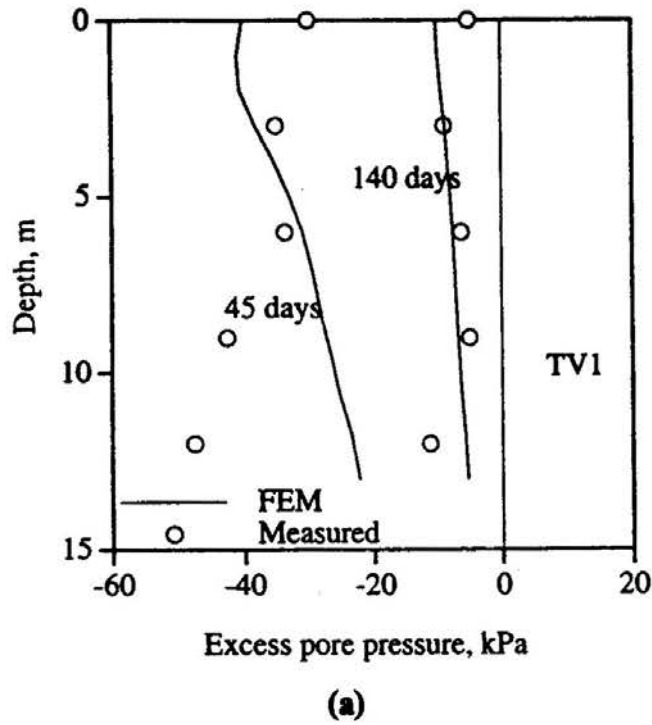


Fig. 17 Comparison of Predicted and Measured Excess Pore Pressures for (a) Embankment 1 (TV-1) and (b) Embankment 2(TV-2)

PVD IMPROVEMENT OF SOFT BANGKOK CLAY

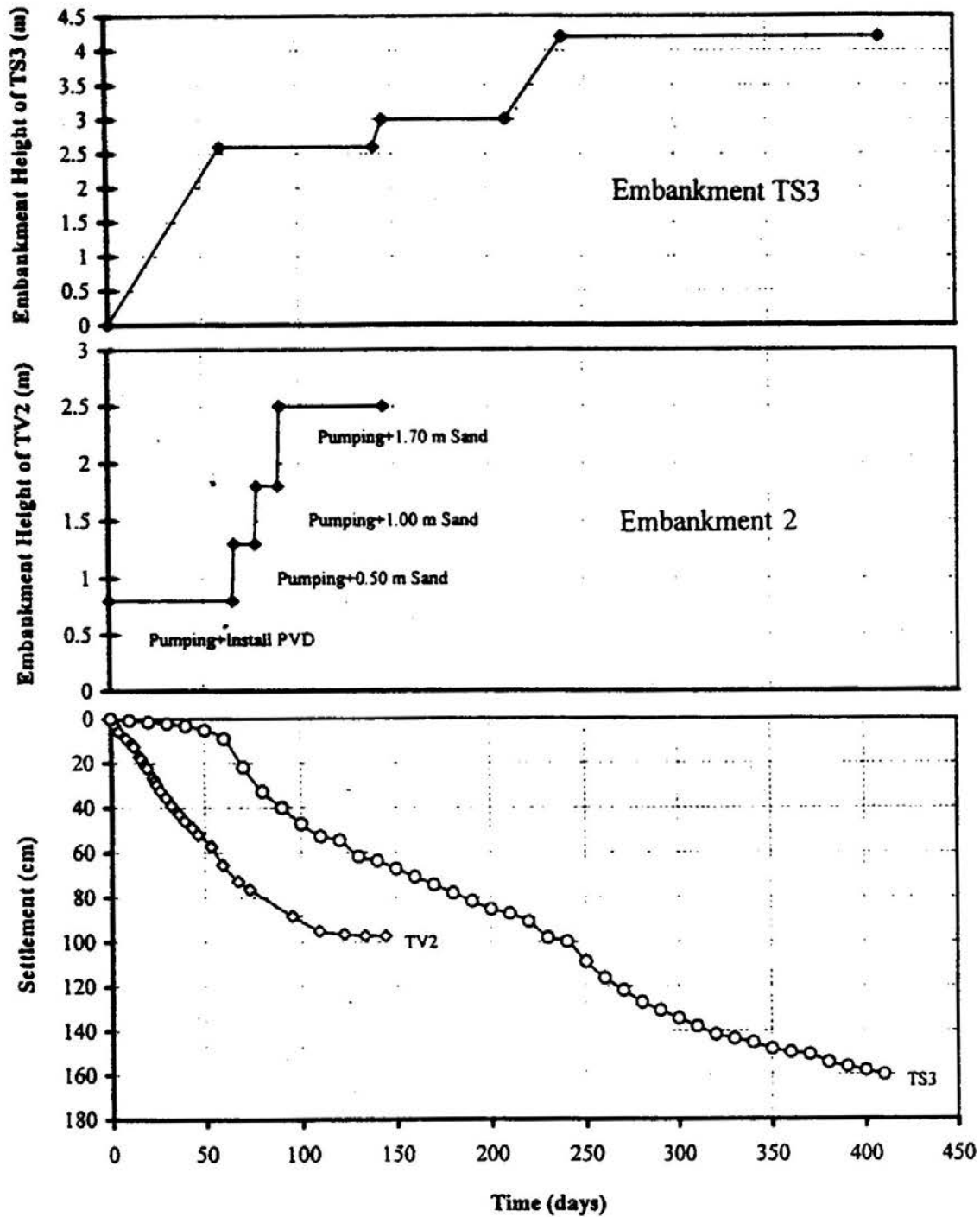


Fig. 18 Comparison of Maximum Surface Settlement Between Embankment 2 and Previous Embankment TS3

If leakages did not occur, the combined 2.50 m high sandfill and vacuum preloading for Embankment 2 is supposed to have the same level of surcharge as that using conventional surcharging in Embankment TS3 with 4.2 m high sandfill. However, the final settlement of 0.97 m for Embankment 2 is lower than the settlement of 1.60 m for Embankment TS3. For the high vacuum case, the numerical results yielded a settlement of 1.30 m at 145 days which is much larger than the corresponding value of TS3. In addition, under vacuum pressure, the lateral deformations near the ground surface can be less than the corresponding values when subjected to sand fill loading. The lower lateral movements can reduce the settlements.

CONCLUSIONS

At the proposed site of the Second Bangkok International Airport (SBIA), two full scale and fully instrumented test embankments, each with 40 m by 40 m base area, was constructed on 16 m thick soft Bangkok clay improved with prefabricated vertical drain (PVD). In this site, ground improvement with PVD subjected to conventional sand surcharging has already been studied successfully. Vacuum assisted consolidation with reduced sand surcharging provides cheaper and faster alternative. In this study, vacuum preloading in combination with reduced amount of sand surcharging were applied. The performances of the 2 test embankments with different drainage systems are described and analyzed. In Embankment 1, hypernet (geonet) drainage system combined with 15.0 m PVD length were used as drainage system with 0.3 m thick sand blanket. In Embankment 2, perforated corrugated pipes combined with nonwoven geotextiles were used as drainage system in combination with 0.8 m thick sand blanket at the top of 12 m long PVDs with spacing of 1.0 m in triangular pattern. After 45 days of vacuum loading, the sand surcharge was raised to 2.5 m high. Finally, finite element method (FEM) was utilized to investigate the efficiency of the field study. Based on the measurements and subsequent analyses, the following conclusions can be made:

1. The final settlement of Embankment 1 and Embankment 2 amounted to 0.74 m and 0.96 m, respectively. Although some leakages occurred, the effectiveness of vacuum-assisted consolidation has been demonstrated.
2. The finite element method (FEM) illustrated the beneficial effects of vacuum preloading combined with reduced sand surcharging by comparison of the simulated results using the (a) actual field loading conditions, (b) by maintaining higher vacuum loading, and (c) by no vacuum loading. The numerical results indicated that even with PVD, the vacuum pressure needs to be maintained for more than 4 to 5 months in order to achieve higher degree of consolidation.

PVD IMPROVEMENT OF SOFT BANGKOK CLAY

3. The performance of Embankment 2 with vacuum preloading, when compared to previous studies using conventional sand surcharging showed an acceleration in the rate of settlement by about 60% and a reduction in the period of preloading by about 4 months.

ACKNOWLEDGEMENTS

Heartfelt thanks are due to COFRA (Thailand) Co. Ltd. and Geotechnics Holland B.V. for sponsoring the research project. The cooperation of the Airports Authority of Thailand (AAT) and the New Bangkok International Airport (NBIA) are highly appreciated. Lastly, Mr. Santi Sangmala, Mr. Pongkrit Eakthamasuth, Ms. L.T. Hanh who are former graduate students of AIT, as well as Ms. Aries Patawaran, Research Associate, are also commended for their valuable contributions and hard works.

REFERENCES

- ASIAN INSTITUTE OF TECHNOLOGY. (1995). The Full Scale Field Test of Prefabricated Vertical Drains for the Second Bangkok International Airport: Final Report, Vol. 1, Asian Institute of Technology, Bangkok, Thailand.
- BERGADO, D.T.; BALASUBRAMANIAM, A.S.; FANNIN, R.J.; ANDERSON, L.R. and HOLTZ, R.D. (1997). Full scale field test of prefabricated vertical drain (PVD) on soft Bangkok clay and subsiding environment. *ASCE Geotechnical Publication No. 69 (Geo-Logan '97)*, pp. 373-393.
- CHAI, J.C.; BERGADO, D.T.; MIURA, N. and SAKAJO, S. (1996). Back-calculated field effects of vertical drain. *Proceedings of the Second International Conference on Soft Engineering*, Vol. 1, pp. 270-275.
- CHAI, J.C., and MIURA, N. (1997). Method of modeling vertical drain-improved subsoil. *Proceedings of the China-Japan Joint Symposium on Recent Developments of Theory and Practice in Geotechnology*, Shanghai, China, pp. 1-8.
- CHOA, V. (1989). Drains and vacuum preloading pilot test. *Proceedings of the Twelfth International Conference on Soil Mechanics and Foundation Engineering*, Rio de Janeiro, Brazil, pp. 1347-1350.
- COGNON, J.M.; JURAN, I.; and THEVANAYAGAM, S. (1994). Vacuum consolidation technology-principles and field experience. *Proceedings of Vertical and Horizontal Deformation of Embankments (Settlement '94)*, ASCE Special Publication No. 40, Vol. 2, pp. 1237-1248.

BERGADO, CHAI, MIURA, and BALASUBRAMANIAM

- HANH, L.T.; BERGADO, D.T.; and SHIBUYA, S. (1998). Engineering properties of soft Bangkok clay improved using PVD with surcharge and vacuum preloading. *Proceedings of the International Symposium on Problematic Soils, IS-Tohoku '98, Japan.*
- HANSBO, S. (1979). Consolidation of clay by band-shaped prefabricated drains, *Ground Engineering*, Vol. 12, No. 5, pp. 16-25.
- HOLTZ, R.D. (1975). Preloading by vacuum: Current prospects. *Transportation Research Record No. 548*, pp. 26-69.
- JACOB, A.; THEVANAYAGAM, S.; and KAVANZANJIAN, E. (1994). Vacuum-assisted consolidation of hydraulic fill. *Proceedings of Vertical and Horizontal Deformation of Embankments (Settlement '94)*, ASCE Special Publication No. 40, pp. 1249-1261.
- KJELLMANN, W. (1952). Consolidation of clay soil by means of atmospheric pressure. *Proceedings of Soil Stabilization Conference, Boston, U.S.A.*
- ROSCOE, K.H., and BURLAND, J.B. (1968). On the generalized stress-strain behavior of wet clay. *Engineering Plasticity*, pp. 535-609.
- SCOTT, R.F. (1963). *Principles of Soil Mechanics*. Reading, Massachusetts: Addison-Wesley Publishing Company.